

Role of MicroRNAs in Human Skeletal Muscle

Tissue Engineering *In Vitro*

by

Cindy Sue Cheng

Department of Biomedical Engineering
Duke University

Date: _____

Approved:

George A. Truskey, Supervisor

Andrew Billin

Nenad Bursac

William E. Kraus

William M. Reichert

Dissertation submitted in partial fulfillment of
the requirements for the
degree of Doctor of Philosophy in the
Department of Biomedical Engineering in the
Graduate School of Duke University

2014

ABSTRACT

Role of MicroRNAs in Human Skeletal Muscle

Tissue Engineering *In Vitro*

by

Cindy Sue Cheng

Department of Biomedical Engineering
Duke University

Date: _____

Approved:

George A. Truskey, Supervisor

Andrew Billin

Nenad Bursac

William E. Kraus

William M. Reichert

An abstract of a dissertation submitted in partial
fulfillment of the requirements for the
degree of Doctor of Philosophy in the
Department of Biomedical Engineering in the
Graduate School of Duke University

2014

Copyright by
Cindy Sue Cheng
2014

Abstract

The development of a functional tissue-engineered human skeletal muscle model *in vitro* would provide an excellent platform on which to study the process of myogenesis, various musculoskeletal disease states, and drugs for muscle toxicity. The global hypothesis that motivated this research was that joint inhibition of microRNA (miR)-133a and miR-696 in isolated primary human skeletal myoblasts (HSkM) leads to accelerated differentiation of tissue-engineered muscle constructs with higher proportion of Type I myofibers and that are capable of significantly increased active contractile forces when subjected to electrical stimulus. The proposed research tested the following specific hypotheses: (1) HSkM require different culture conditions than those optimal for C2C12 culture, as measured by differentiation and microRNA expression, (2) in 2D culture, joint inhibition of miR-133a and miR-696 accelerates, (3) inhibition of miR-133a and/or miR-696 in 3D human skeletal muscle model results in active contractile forces significantly higher than control, and finally (4) co-culture of human cord blood-derived endothelial cells (ECs) on the surface of 3D HSkM bundles is capable of active contraction, as measured by isometric force testing and immunofluorescence.

Culture conditions of 100 $\mu\text{g}/\text{mL}$ growth factor reduced-Matrigel-coated substrates and 2% equine serum in differentiation medium improve HSkM culture, compared to conditions optimal for C2C12 cell culture (uncoated substrates and 8% equine serum media). Liposomal transfection of HSkM with anti-miR-133a and anti-miR-696 led to increased presence of sarcomeric α -actinin and PGC-1 α proteins when cells were cultured in 2D for 2 weeks. Presence of mitochondria and distribution of fiber type did not change with microRNA transfection in a 2D culture. Joint inhibition also resulted in increased PPARGC1A gene expression after 2 weeks of 2D culture. For muscle bundles in 3D, there exists a myoblast seeding density threshold for the production of functional muscle. 5×10^6 HSkM/mL did not produce active contraction, while 10×10^6 HSkM/mL and above were successful. Of the seeding densities studied, 15×10^6 HSkM/mL produced constructs that exerted the highest twitch and tetanus forces. Treatment of human skeletal muscle with anti-miR-133a and anti-miR-696 led to significant increases in force amplitude when both anti-miRs were added together compared to negative control (transfection with scrambled sequence). Joint inhibition in myoblasts seeded into 3D constructs led to decreased presence of slow myosin heavy chain and increased fast myosin heavy chain. Finally, co-

culture of functional HSkM with ECs is possible in 3.3% FBS in DMEM culture conditions, with significant increases in force amplitudes after 48 of co-culture. These results suggest the potential of delivering more than one microRNA for therapy and the feasibility of developing a functional HSkM-EC co-culture model.

Dedication

This dissertation is dedicated to my grandfather, Chen-Ho Wang, whose curiosity was infectious. We miss you dearly.

Contents

Abstract.....	iv
List of Tables	xiv
List of Figures.....	xv
Acknowledgements.....	xviii
CHAPTER 1. INTRODUCTION.....	1
1.1. Research Overview	1
1.2. Skeletal Muscle Development.....	4
1.2.1. Satellite Cells and Muscle Repair.....	4
1.2.2. Structure and Function of Skeletal Muscle.....	6
1.3. Considerations for Skeletal Muscle Tissue Engineering.....	17
1.3.1. Satellite Cells.....	18
1.3.2. Scaffold	19
1.3.3. Metabolism and Myofiber Types.....	22
1.3.4. Contractile Forces.....	24
1.4. Methods to Increase Muscle Maturity and Force Production.....	26
1.4.1. Mechanical and Electrical Stimulation.....	26
1.4.2. MicroRNA's	28
1.5. Motivation and Significance.....	34
1.6. Hypothesis & Specific Aims.....	35

CHAPTER 2. Optimization and Characterization of Primary Human Skeletal Myoblasts (HSkM) (Specific Aim 1).....	38
2.1. Introduction.....	38
2.2. Materials and Methods	40
2.2.1. Primary Human Skeletal Myoblast Isolation.....	40
2.2.2. Cell Culture.....	41
2.2.3. Myoblast Size and Growth Rate.....	42
2.2.4. Immunofluorescence	42
2.2.5. MicroRNA/RNA Isolation and Quantitative Real-Time PCR.....	44
2.2.6. Cyclic Mechanical Stretch	46
2.2.7. Statistical Analysis	47
2.3. Results	47
2.3.1. Comparison of C2C12 and HSkM growth, size, and differentiation under conditions optimal for C2C12 myofiber maturation	47
2.3.2. Culture Conditions for HSkM.....	53
2.3.3. Effect of culture conditions on C2C12 and HSkM microRNA and MEF-2C expression.....	54
2.3.4. Effect of stretch on HSkM differentiation.....	59
2.3.5. Comparison of microRNA levels in fresh muscle explants and culture HSkM.....	61
2.4. Discussion	62
2.5. Chapter Acknowledgements.....	68

CHAPTER 3: Joint Inhibition of miR-133a and miR-696 for Accelerated Type I Human Myofiber Differentiation <i>In Vitro</i> (Specific Aims 2 & 3)	69
3.1. Introduction	69
3.2. Materials and Methods	71
3.2.1. Primary HSkM Isolation.....	71
3.2.2. Cell Culture	72
3.2.3. MicroRNA Transient Transfection	73
3.2.4. Mold Preparation and Sterilization	74
3.2.5. Engineered 3D Human Muscle Bundle Construction	75
3.2.6. Immunofluorescence	76
3.2.7. Quantitative Real-Time PCR of Mef-2C and PPARGC1A.....	77
3.2.8. Western Blot.....	77
3.2.9. Measurement of Contractile Force.....	79
3.2.10. Statistical Analysis	80
3.3. Results	80
3.3.1. Transient Transfection Efficiency and Lifetime of MicroRNA's	80
3.3.2. MiR-133a and MiR-696 Inhibition in 2D Cultures Accelerates Myogenesis and Affects PGC-1 α	81
3.3.3. Functional Three-Dimensional Human Skeletal Muscle Bundles.....	87
3.3.4. Effect of MicroRNA-133a and/or -696 Inhibitors upon 3D Human Skeletal Muscle Bundles.....	92

3.4. Discussion	107
3.5. Chapter Acknowledgements.....	117
CHAPTER 4. Endothelialization of Human Skeletal Muscle Bundles (Specific Aim 4).....	118
4.1. Introduction.....	118
4.2. Materials and Methods	120
4.2.1. Endothelial Progenitor Cell Isolation and Culture.....	120
4.2.2. Human Skeletal Muscle and Endothelial Progenitor Cell Co-Culture in 2D.....	121
4.2.3. Human Skeletal Muscle and Endothelial Progenitor Cell Co-Culture in 3D.....	122
4.2.4. Isometric Force Testing.....	122
4.2.5 Immunofluorescence	123
4.2.6. Statistical Analysis	124
4.3. Results	124
4.3.1. Endothelial Cell Coverage of Fused Skeletal Muscle in 2D Studies	124
4.3.2. Identification of Co-culture Media for Retention of HSkM Bundle Functionality	128
4.3.3. Co-culture Bundle Functionality is Retained in 3.3% FBS in DMEM ...	130
4.3.4. Endothelial Cell Coverage of Muscle Bundle in 3.3% FBS in DMEM ..	132
4.4. Discussion	136
4.5. Acknowledgements.....	140

CHAPTER 5. Dissertation Summary & Future Work	141
5.1. Dissertation Summary.....	141
5.2. Strengths & Weaknesses of Work.....	145
5.3. Implications for Tissue Engineering	149
APPENDICES	152
APPENDIX A. Antibodies.....	153
APPENDIX B. Primer Sequences for Quantitative Real Time RT-PCR.....	154
APPENDIX C. MATLAB Code for Force Measurements	155
APPENDIX D. HSkM Culture Media Recipes	156
APPENDIX E. Matrigel Coating Protocol.....	158
APPENDIX F. HSkM Isolation Protocol	159
APPENDIX G. HSkM Muscle Bundle Protocol.....	164
APPENDIX H. Immunostaining Protocol.....	166
APPENDIX I. HSkM miR Transfection Protocol	167
APPENDIX J. miR Isolation Protocol	168
APPENDIX K. TAQMAN qRT-PCR for miR Expression.....	170
APPENDIX L. SYBR Green qRT-PCR Protocol.....	174
APPENDIX M. Western Blot Protocol.....	177
APPENDIX N. Copyright Releases.....	184

REFERENCES	185
BIOGRAPHY.....	210

List of Tables

Table 1: Z- and M-line widths for humans [43].....	16
Table 2. MicroRNA Levels in Explant, C2C12, and HSkM. [1].....	62

List of Figures

Figure 1. Schematic of satellite cell myogenesis and markers typical of each stage. [17]	7
Figure 2: Components of sarcomere.	8
Figure 3: Skeletal muscle force-length relationship.....	16
Figure 4. MicroRNA Pathway for Proliferation and Differentiation of Skeletal Muscle.	31
Figure 5. MicroRNA Pathway for Energy Metabolism in Skeletal Muscle.....	33
Figure 6. C2C12 vs. HSkM Cell Area.....	49
Figure 7. C2C12 vs. HSkM Growth Rates.	49
Figure 8. Effect of DM on Cell Proliferation.	50
Figure 9. C2C12 vs. HSkM Myofiber Morphology.....	52
Figure 10. Effect of serum and Matrigel coating on formation of striated human muscle fibers 14 days after shifting to differentiation medium (DM) with the indicated level of serum.	54
Figure 11. Comparison of microRNA and Mef-2C mRNA levels in mouse C2C12 (reference) and HSkM cells.	58
Figure 12. Effect of culture conditions on expression of microRNAs.....	59
Figure 13. Cyclic Stretch Affects microRNA Levels.	61
Figure 14. Preparation of PDMS Molds for Engineered 3D human skeletal muscle bundle construction.	75
Figure 15: Schmatic of isometric force testing setup.	79
Figure 16: Transfection efficiency and lifetime of exogenous microRNA.....	81

Figure 17: Sarcomeric α -actinin and mitochondria presence in 2D cultures.	84
Figure 18: Expression of PPARGC1A gene at Day 14 post-differentiation.....	85
Figure 19: Fiber Type in 2D Engineered Human Skeletal Muscle.....	87
Figure 20: Engineered human skeletal muscle bundles with 5×10^6 cell/mL.	88
Figure 21: Human skeletal muscle bundle ultrastructure in 3D cultures seeded with 10×10^6 cells/mL.....	89
Figure 22: HSkM seeding density for muscle bundles.....	90
Figure 23: Human skeletal muscle bundle ultrastructure in 3D cultures.....	91
Figure 24: Bundle diameters and fiber density.	94
Figure 25: Active and passive forces generated by engineered human skeletal muscle.	96
Figure 26. Isometric force testing of muscle bundles..	98
Figure 27: Specific force per muscle fiber area.	101
Figure 28. Half Relaxation Time.	102
Figure 29: Myosin heavy chain presence..	104
Figure 30: Immunofluorescence for slow and fast fibers.....	106
Figure 31: Mef-2C expression of engineered human skeletal muscle.....	107
Figure 32: Role of Mef-2 in development of fiber type.	116
Figure 33: 2D Co-Culture Media Studies.	126
Figure 34: Percent Coverage of EC and HSkM.	127
Figure 35: Testing co-culture media in muscle-only engineered constructs.....	129

Figure 36: Ultrastructure of muscle-only bundles in tested co-culture media. ..	130
Figure 37: Twitch and tetanus force amplitude for co-culture bundles.	131
Figure 38: Endothelial cell coverage on engineered muscle bundles.....	134
Figure 39: Orthogonal views of co-culture bundles.	135

Acknowledgements

I would like to acknowledge my advisor Dr. Truskey for his guidance and encouragement through this process. As an advisor who has mentored me through my undergraduate and graduate time at Duke, he has truly shaped me as a researcher. I am hugely grateful for his time, dedication, and faith in my abilities. I would also like to thank my committee members for their invaluable insight and feedback. I truly believe that with their help my project has become more complete and cohesive.

Next, I would like to thank my friend and graduate mentor Caroline Rhim for her constant guidance in lab and also in life. Thank you for agreeing to mentor me – otherwise, I would likely not be where I am now! Thank you for being such a caring colleague and friend. I also extend my most heartfelt thanks to the ladies of the Truskey Lab: Tracy Cheung, Alexandra Jantzen, and Brittany Davis. You all made coming to work such an enjoyable time. I could not have asked for a better support system through the stresses of graduate school and for that I am hugely grateful.

Many individuals contributed to the success of this project, and without them, this would not be possible. I would like to thank: Yasheng Gao for his expertise and guidance with confocal microscopy, Mark Juhas for his knowledge and guidance for tissue-engineered skeletal muscle, Chris Jackman for his help with the force transducer setup, Lauran Madden for her contribution to the isolated human skeletal myoblast cell stock, and Lydia Ran for her tremendous work ethic and dedication to the co-culture project. Thank you all for your help and contributions to the project; this is truly a collaborative effort!

I would like to thank my parents, Chann and Yingya, and my sister Faye for their support. Thank you for understanding that some holidays needed to be sacrificed in the pursuit of experiments. And thank you for your constant reassurance that I was almost there!

Finally, I would like to thank Mehran Chowdhury, my rock through my entire graduate school career. Your support and reassurance kept me going through the tough times, and your company during late-night and weekend experiments was extremely touching and appreciated! You inspire me to go after my dreams, and with your unwavering support and love, I know I can achieve them. Thank you (and fuzzy puppy Winston!) for always standing by me and believing in me.

CHAPTER 1. INTRODUCTION

1.1. Research Overview

Skeletal muscle is a major target for tissue engineering given that it comprises over 40% of human body mass [2] and can require up to 80% of cardiac output during heavy exercise [3]. Additionally, skeletal muscle plays a key role in energy metabolism and diabetes. Muscular diseases, such as muscular dystrophy and muscle wasting with age (sarcopenia), are debilitating and greatly affect one's quality of life; therefore, the need for therapies targeting musculoskeletal diseases is tremendous. Tissue-engineered skeletal muscle has been largely studied using murine and rat models. However, human primary skeletal myoblasts provide a more physiologically-relevant model for testing drugs and therapies. The development of a functional human skeletal muscle model is important to the study of drug interactions within the body, as all drugs must pass through and may accumulate within the musculature. Additionally, having a human model of skeletal muscle holds great translational potential as it would give insight into interactions of human cells with various drugs and therapies. However, the dearth of knowledge and experience with culturing human skeletal muscle *in vitro* presents many challenges. Requirements for functional engineered muscle include comparable gene expression, micromorphology, and contractile forces to those found in native muscle tissue.

The major goal of this research was to develop a protocol for engineering human skeletal muscle capable of active functional force output when stimulated. We hypothesized that joint inhibition of proliferation-promoting miR-133a and oxidative metabolism-repressing miR-696 will lead to accelerated differentiation and directed myofiber type development of functional tissue-engineered 3D human skeletal muscle. Thus far, a model that produces contractile human skeletal muscle without added stimuli and cultured in a static fashion has not been reported.

The specific aims for this project are to (1) identify culture conditions for efficient human skeletal myoblast growth and differentiation and establish a temporal profile of microRNA expression during differentiation, (2) assess the effects of miR-133a and miR-696 inhibition on gene and protein expression in human muscle cultured in 2D and on contractile forces and ultrastructure of human muscle cultured in 3D, and (3) identify co-culture conditions to support HSkM and EC together and retain active contractile function *in vitro*.

In **Chapter 2**, we addressed specific aim 1 and identified conditions for effective culture of HSkM in 2D culture. We measured myogenic microRNAs at the onset and through the progression of differentiation in C2C12 murine myoblasts and primary isolated human myoblasts (HSkM). HSkM expressed low levels of all measured microRNAs compared to C2C12, so culture conditions were tailored to increase these microRNA levels significantly compared to initial culture conditions (those optimal for C2C12 culture). Cyclic stretch and miR-133a inhibition were

explored as methods for improving myoblast differentiation. Using the Flexcell Tension System, we used a stretch regimen of $\pm 10\%$ at 1 Hz for 1 hour alternating with 5 hours of rest to promote differentiation of myoblasts [4] over a two-week period. Quantitative real-time PCR and immunostaining were utilized to measure gene expression and observe muscle morphology, respectively. While proper culture conditions for HSkM increased microRNA expression by over 20-times compared to baseline expression in C2C12 culture conditions, microRNA levels were still far removed from native human explant tissue.

In **Chapter 3**, we addressed specific aims 2 and 3 and assessed the effects of joint miR-133a and miR-696 inhibition on human skeletal muscle differentiation and fiber type development. Joint inhibition was performed in 2D and 3D conformations – 2D served as proof of principle for 3D studies. We developed a protocol to culture functional 3D HSkM constructs in a fibrin hydrogel capable of active contraction. Proof of principle in 2D provided the basis for joint microRNA inhibition of functional skeletal muscle constructs cultured in 3D. In 2D, Western blots, qRT-PCR, and immunostaining were used to assess extent of HSkM differentiation and myofiber type. In 3D, isometric force testing, immunostaining, and qRT-PCR were used to demonstrate function, differentiation, and myofiber type.

In **Chapter 4**, we addressed specific aim 4 and identified co-culture conditions to successfully endothelialize human muscle bundles while retaining active contractile function. In order to successfully co-culture HSkM with EC, a

common culture media was developed in order to maintain and support both cell types and allow functionality of engineered skeletal muscle. Functional force testing and immunostaining were used to observe differentiation and retention/spreading of EC on HSkM bundle, respectively.

In **Chapter 5**, we summarize our main results and present conclusions from our work. We also present future directions and translational implications of this work.

1.2. Skeletal Muscle Development

1.2.1. Satellite Cells and Muscle Repair

Satellite cells are a progenitor population of cells that are essential to skeletal muscle development and repair [5-7]. The regenerative potential of skeletal muscle fibers relies on this pool of undifferentiated myogenic progenitor cells [8], satellite cells, be found between the myofiber plasma membrane and basal lamina. They are characterized by expression of Pax7, which is important for self-renewal [9-11], but do not express muscle-specific transcription factors, making their characterization difficult. Under normal conditions, satellite cells remain quiescent in the periphery of the myofiber; while in this quiescent state, they exhibit limited gene expression and protein synthesis [5].

Satellite cells become activated in response to stresses that result from myotrauma and/or weight bearing [5, 7]. After injury, activation cues (i.e. growth factors, cytokines, etc.) released from injured myofibers signal satellite cells to leave

their niche and move outside the basal lamina. Here, they begin to proliferate [7, 12]; at this point in time, the cells are known as myoblasts and coexpress Pax7 and MyoD [5].

As myoblasts continue to proliferate, they downregulate Pax7 and express MyoD and myogenin – a myogenic transcription factor that pushes cells towards differentiation [5-7]. As Pax7 expression decreases and myogenin is upregulated, myoblasts fuse to form multinucleated myotubes that either repair muscle damage (if fused to existing fibers) or reinforce muscle fibers (if fused to form new fibers). As sarcomeres develop, the new myotubes appear striated and are capable of contraction. *In vivo*, a fraction of myoblasts maintains their Pax7 expression and loses their myogenic marker expression. These cells ultimately leave the cell cycle and return to a self-renewing, quiescent satellite cell state. The renewed satellite cell pool, if activated, can reenter a new cycle of repair and regeneration [13].

Interestingly, not all myoblasts in culture fuse to form fibers and the extent of myofiber formation declines with continued satellite cell subculture [14]. To counter this decline and form high density myofiber cultures, forskolin, which activates cyclic AMP, can be added in culture to promote satellite cell proliferation without compromising the ability to form myotubes [15]. Other subpopulations of muscle stem cells can form myofibers but these stem cells are rare [16]. Induced pluripotent stem cells are another cell source that can differentiate into muscle cells hold the promise of providing a ready source of satellite cells and myoblasts, but further

work is needed to produce sufficient numbers of cells [15] and address potential safety concerns [16].

1.2.2. Structure and Function of Skeletal Muscle

Skeletal muscle comprises over 40% of the human body's total muscle mass. Abnormalities and diseases affecting skeletal muscle have profound systemic effects; therefore, it is important to understand the structure and function of this tissue organ system. Skeletal muscle is composed of bundles of myofibers running in parallel. This particular structure allows for the effective transmission of contraction and cumulative peak force generation. Myofibers are bound together by connective tissue that houses blood vessels and nerves. Within each myofiber, there are numerous mitochondria for energy production and many peripherally-located nuclei.

Myofibers arise from the fusion and maturation of skeletal myoblasts. This process is guided by the selective and sequential expression of various myogenic cell markers, including CD34, Pax7, Myf5, MyoD, myogenin, and MLC3F-tg (Figure 1) [17]. CD34 and Pax7 are expressed during the satellite cell stage: from the change from quiescence to activation. Once the cells start to proliferation and become myoblasts, Myf5 and MyoD are expressed and CD34 and Pax7 are downregulated. As the myoblasts begin to fuse to myotubes and mature into myofibers, expression of myogenin and MLC3F-tg occur.

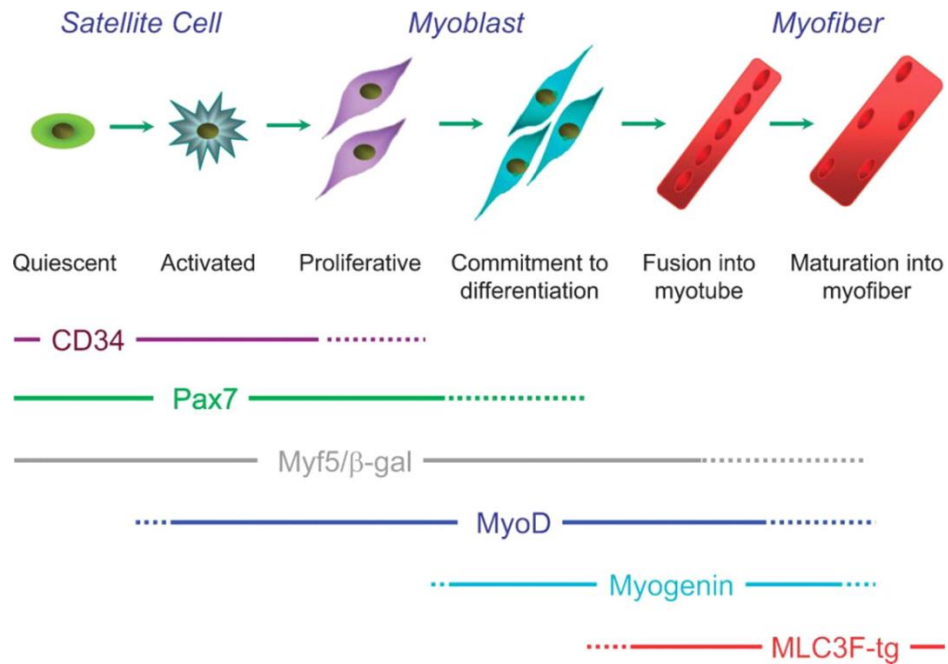


Figure 1. Schematic of satellite cell myogenesis and markers typical of each stage. [17]

Sarcomeres are the basic functional units of muscle. They are separated by Z-lines, and they contain myofibrillar proteins that allow muscles to contract, including myosin (the thick filament) and actin (the thin filament) [18]. Myosin has 6 polypeptides: 2 heavy chains and 4 light chains. The heavy chains contain the myosin heads that interact with actin and allow muscle to contract (Fig. 2); this same area of the myosin heavy chain also binds ATP and converts it to ADP, providing the energy necessary for muscle contraction [18]. The thin filament is composed of actin and the regulatory proteins troponin and tropomyosin. When the myofiber receives a stimulus, Ca^{2+} is released from the sarcoplasmic reticulum and binds to troponin. This binding then causes tropomyosin to expose a myosin-binding site on the actin filament. When ATP is present, the myosin head pulls the actin along the myosin – which allows the sarcomere to shorten in contraction. The process of

myosin head attachment to actin, pulling, release, and reattachment is known as cross-bridge cycling. This process occurs at different speeds depending on the rate of ATP hydrolysis, which is in turn limited by the rate that the ATPase of the myosin head can hydrolyze ATP. [18]

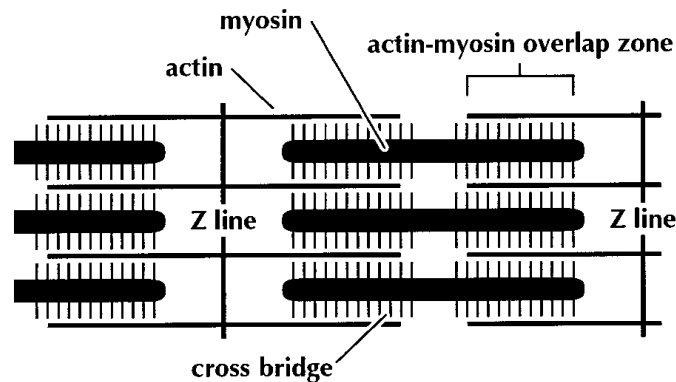


Figure 2: Components of sarcomere. Sarcomeres are composed of myosin and actin proteins. The actin-myosin overlap zone allows for generation of contractions. Cross bridges are the several actin-myosin overlap zones contained within a sarcomere. Each sarcomere is separated by Z-lines. [19]

Skeletal muscle fibers are surrounded by the sarcolemma, which limits the entry and exit of ions into the intracellular environment. This selective permeability allows for the careful control of the electrical potential and membrane excitability of a skeletal muscle fiber. Action potentials are initiated by depolarization of the sarcolemma resulting from binding of acetylcholine (ACh) to acetylcholine receptors (AChR) at the neuromuscular junction. The binding of 2 ACh molecules to each AChR induces a conformational change in the AChR, which leads to opening of the central pore, allowing cations to flow into or from the muscle cell. Due to the electrochemical gradient, generally more Na^+ flows into the cell than K^+ out, resulting in depolarization of the muscle fiber. [20, 21]

Depolarization of the muscle fiber leads to opening of L-type voltage-gated Ca^{2+} channels in the t-tubule of the membrane. T-tubules (or transverse tubules) are invaginations in the sarcolemma that run transverse to the length of the muscle fiber. T-tubules allow for the depolarization of the membrane to travel quickly to the interior of the cell (7 cm/sec [21]). The opening of the voltage-gated Ca^{2+} channels in the t-tubules induces conformational changes in adjacent Ca^{2+} -release channels located in the membrane of the sarcoplasmic reticulum. This causes the Ca^{2+} -release channels in the sarcoplasmic reticulum to open, resulting in an efflux of sequestered Ca^{2+} into the cytoplasm. The Ca^{2+} then binds to troponin C on the actin myofilament and leads to initiation of cross-bridge cycling of the muscle, also known as excitation-contraction coupling. [20, 21] Once bound to calcium, troponin undergoes a conformational change allowing the myosin head group to bind to the active site on actin. The subsequent bending of the bound myosin initiates a power stroke in which myosin pulls the actin about 10 nm; this is also known as a cross-bridge cycle. After the power stroke, ATP binds to myosin, enabling the myosin head group to dissociate from actin; this also energizes the cross bridges and places myosin in the position to bind to actin for the next cycle. The bound ATP is hydrolyzed to ADP releasing energy and detaching from myosin. Calcium ions are pumped back into the sarcoplasmic reticulum, causing dissociation from troponin. Troponin then covers the myosin binding site on actin and the sarcomere returns to its initial condition.

Skeletal muscle is comprised of various types of myofibers that allow for the fast or slow contractions displayed by human muscle. There are several methods in which fiber types are classified, including protein myosin heavy chain (MHC) content, fiber metabolism, and presence of various ion channels. First, human muscle fiber types can be defined with the contractile protein MHC and the ATPase activity associated with each MHC classification [22]. The presence of various MHC isoforms as well as the temporally and spatially regulated expression of these isoforms is important for defining of specific muscle properties and functions [23]. Specifically, the ATPase activity of various MHC isoforms dictates the speed of shortening or contraction – thus, giving the fiber types their characteristic names: “fast” and “slow” [18, 24, 25]. The isoforms of MHC present in human skeletal muscle include 1, 2A, and 2X, corresponding to Type I (slow), Type IIA (fast), and Type IIX (fast), respectively. Mouse and rat muscle contain these MHC isoforms and the additional 2B isoform. Human skeletal muscle also differs from mouse skeletal muscle by the proportions of each fiber type in its musculature. Mouse muscle are composed primarily of MHC-2B and MHC-2X fibers, with very little MHC-2A and MHC-1 fibers [26]. Human skeletal muscle contain mostly MHC-1 and MHC-2A in fibers, and less MHC-2X [26]. Given this important difference between mouse and human skeletal muscle, mouse skeletal muscle is not the best model for studying human skeletal muscle.

Metabolism is another method commonly used for classifying skeletal muscle fibers. Type I fibers are termed “slow twitch” due to the slow contraction speed of fibers utilizing oxidative metabolism. In close relation to the metabolism of fiber type is the content of myoglobin and mitochondria within each fiber: slow twitch fibers contain more myoglobin and mitochondria (giving the fibers their characteristic red hue), machinery necessary for the process of oxidative metabolism [26]. Human muscle fibers range in diameter from 10-100 μm [27], with Type I fibers being thinner to adapt for sustained activity, as slow fibers are fatigue “resistant.” [27]. Slow myosin cross-bridge cycling and a combination of both low abundance and activity of energy-consuming calcium pumps in the sarcoplasmic reticulum reduce the energy demands of Type I fibers [28]. Type I fibers sustain aerobic activity using fats and carbohydrates as fuel, and although oxidative phosphorylation is a slower process (1 mole of ATP per min), ATP synthesis is significantly more efficient, producing 36 molecules of ATP per molecule of glucose [29]. Type II fibers are generally classified as “fast twitch” due to the rapid contraction resulting from rapid calcium release and uptake during the contraction-relaxation cycle of these fibers utilizing glycolysis [26]. Type II fibers contain high levels of glycolytic enzymes, allowing for rapid firing of fibers. However, Type II fibers can further be classified into IIA and IIX based on the metabolism used, similar to the presence of different MHC isoforms presented above. Type IIA fibers are also known as fast-twitch oxidative glycolytic fibers, and IIX are called fast-twitch glycolytic fibers [29]. Type

IIA fibers contain more myoglobin and mitochondria than IIX fibers. Functionally, fast fibers are utilized for short bursts of near-maximal activity, but they do require more energy and fatigue quickly [30]. Rapid cross-bridge cycling and significant calcium fluxes are hallmarks in the fast twitch Type II fibers, resulting in much higher energy demands [28]. During anaerobic glycolysis, glucose is broken down to pyruvate and converted to lactic acid [31], producing 2.5 moles of ATP per minute [32]. Fibers utilizing glycolysis fatigue quickly because anaerobic metabolism is limited to the amount of glucose or glycogen accessible within muscle.

Physiologically, Type II fibers are thicker, allowing for higher force amplitude generation than slow fibers. Since these fibers do not contain high levels of myoglobin and mitochondria, Type IIA and IIX fibers appear more white/pale in color compared to Type I fibers.

Slow and fast twitch fibers can also be classified by their electrophysiological properties as well. Fast fibers have resting membrane potentials that are more negative than slow fibers (-90 to -95 mV compared -80 to -85 mV, respectively) [29]. Chloride ions play an important role in the stabilization of resting membrane potential in skeletal muscle cells: approximately 70% of the conductance of a muscle fiber membrane at rest relies on Cl^- and 30% relies on K^+ . Fast fibers contain 3-5-times more L-type voltage-gated Ca^{2+} channels per volume than slow twitch fibers [29], which helps for the rapid firing that is characteristic of fast twitch fibers. Studies have shown that Cl^- conductance is higher in fast fibers compared to slow fibers [29].

K^+ currents out of the skeletal muscle fibers are relatively small, resulting in their lower contribution to overall resting membrane potential. There exist many types of K^+ channels in the human body; however, ATP-sensitive K^+ are the most abundant within skeletal muscle. The density of K-ATP current is higher in fast twitch muscle fibers compared to slow twitch muscle fibers. [29] The excitability of the muscle fiber membrane is dependent on the number of Na^+ channels and the proportion of these channels that are not inactivated [29]. Similar to Ca^{2+} channels, Na^+ channels have higher densities in fast fibers than slow fibers. This greater density of Na^+ channels leads to the rapid response and short-lasting contraction that are characteristic of fast fibers over their counterpart [29]. While there is no singular way to classify skeletal muscle fiber type, it is clear that these methods are all in agreement. The specific MHC isoforms, metabolism utilized, and ion channels present in muscle fibers all contribute to either the slow, sustained contraction or fast, maximal contraction phenotypes.

Adult skeletal muscle may exhibit plasticity in response to sustained stimuli, including resistance exercise or immobilization. Reinnervation has been demonstrated to induce fast-to-slow transformations in the contractile properties of rabbit skeletal muscle [33, 34], and chronic low-frequency stimulation have been shown to change fast muscles towards slow muscles in various animal model studies [35]. However, such studies have not had as much success in human muscle tissue. Human skeletal muscle studies that have applied electrical stimulation protocols

similar to those in animal studies have not reported an increase in MHC-1 composition within the tissue [36, 37]. Andersen et al. electrically stimulated skeletal muscle from spinal cord injury patients for 30 min/day 3 times per week for 1 year, but saw a reduction in MHC-2X isoforms and no change in MHC-1 isoforms [38]. In contrast, immobilization and disuse of human skeletal muscle leads to a slow-to-fast transition in MHC content. Individuals with spinal cord injuries showed almost no MHC-1 isoforms in the *vastus lateralis*, while healthy individuals express approximately 50% MHC-1 [39]. Their muscles are, instead, predominantly composed of MHC-2 isoforms, with over half being MHC-2X. Although the reason for slow-to-fast transition in conditions of muscle disuse is unclear, there is evidence suggesting that MHC-2X may be the default protein isoform [40]. Additionally, muscle fibers containing more than one MHC isoform have been reported, which may represent fibers that are in transition from one type to another. However, these hybrid muscle fibers are most commonly found in the muscle of older people [39]. While there is some evidence that human fiber type plasticity is possible, there still remains a large gap between what has been demonstrated in animal models and what can be done with human skeletal muscle. This presents further reason for human-specific studies of skeletal muscle to better understand its physiology and dynamic development.

The ability of skeletal muscle to contract is a hallmark of this tissue.

However, the magnitude of contraction is dependent on the muscle length at

relaxation – this phenomenon is known as the force-length relationship: the force produced increases with the extent of stretch of sarcomeres at rest (Fig. 3, note this Figure considers frog muscle). Minimal stretch of sarcomeres leads to low force production due to minimal length of contraction. Within the optimal range of actin-myosin overlap, as the sarcomeres are stretched, there will be increased force production due to optimal overlap between actin and myosin and adequate length of contraction to exert force. Finally, if the sarcomere is stretched too far and there exist no actin-myosin overlap, the force falls to zero. Therefore, there exists an optimal range in which force produced is greatest. In human skeletal muscle, actin and myosin lengths are approximately 1.30 μm and 1.66 μm , respectively [41]. Z-line widths range from 69-95 nm and M-line (midzone of the myosin filament that does not contain cross-bridges) widths range from 60-89 nm, depending on myofiber type [42]. Lengths of Z-lines and M-lines associated with each myofiber type are given in Table 1.

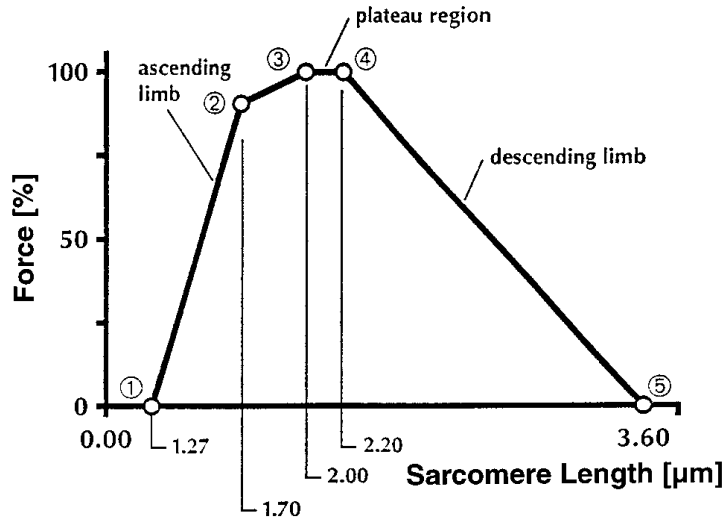


Figure 3: Skeletal muscle force-length relationship. The amount of force exerted by skeletal muscle is dependent on the length of the sarcomeres at rest. (1) Zero force is generated at complete overlap between actin and myosin. As the overlap decreases, force increases until the optimal range of overlap is reached (2). The optimal range is shown between (2) and (4). A plateau region exists between (3) and (4) since the midzone of the myosin filament does not form cross-bridges. There is a gradual decrease to zero of force from (4) to (5) as the sarcomere is stretched to an extent that cross-bridge formation declines due to separation of myosin and actin filaments. [19]

Table 1: Z- and M-line widths for humans [43]

Myofiber Type	Z-lines	M-lines
Type I	95 nm	89 nm
Type IIA	74 nm	79 nm
Type IIX	69 nm	60 nm

This phenomenon of length-tension is not a major factor for *in vivo* skeletal muscle physiology as individual sarcomeres are maintained near the optimal length within their working range [27] and, under normal conditions, are not stretched beyond the optimal working range. The surrounding extracellular matrix (ECM) not only serves to support musculature, but it also prevents the sarcomeres from being stretched beyond the optimal length for function. In fact, the extracellular matrix itself may modify the force-length curve by adding a passive force. Measurement of

active and passive forces can be used to test engineered 3D constructs for functionality and how closely the engineered muscle mimics native tissue.

1.3. Considerations for Skeletal Muscle Tissue Engineering

Three-dimensional engineered skeletal muscle tissues possess many of the important features of skeletal muscle *in vivo*, including many key functional proteins found in mature muscle, abundance of striations, contraction in response to electrical/neural stimuli and length-tension and force-frequency relationships similar to those of excised myofibers. However, there exist limitations of engineered *in vitro* muscle models that prevent complete recapitulation of native muscle – mainly that specific forces are substantially lower and fiber density and organization are not representative of native tissue.

Over the past decade, considerable advances have been made to address these challenges and produce three-dimensional engineered muscle bundles with higher myofiber density, organization, and increased functional force output. Another challenge is regulation of myofiber type - ensuring that mature fibers are produced and that conditions are developed to selectively produce Type I, IIA and IIX myofibers. Mimicking roles of innervation, either through co-culture with nerve cells or electrical stimulation and/or addition of neurotrophic factors, may be essential to producing mature human myofiber types [44, 45]. A large parameter space still needs to be explored with mechanical conditioning of engineered muscle. Finally, microRNAs provide a promising way to enhance differentiation and

function, and when expressed transiently by delivery via liposomes, could stimulate specific developmental steps.

Engineering challenges associated with culturing functional skeletal muscle *in vitro* include: (1) cell source and isolation from excised tissue, (2) selection of appropriate scaffold for maturation of cells into muscle, (3) skeletal myofiber type development, (4) generation of contractile forces, and (5) methods for stimulating construct maturation, including co-culture with other cell types and microRNA modulation of cells.

In order to utilize engineered muscle bundles for a relevant clinical drug and toxicity testing, human engineered skeletal muscle bundles need to be developed. Optimized culture conditions to efficiently expand human satellite cells and myoblasts and promote their fusion and maturation are needed.

1.3.1. Satellite Cells

To engineer skeletal muscle, the stages of cell development must be carefully controlled in order to produce organized and mature skeletal muscle. As satellite cells are removed from the native niche environment, they are activated to myoblasts capable of proliferation. Myoblast proliferation is promoted by high content of serum contained in the culture medium; the serum contains significant growth factors necessary for cell division, including IGF-1, TGF- β 1, FGF-2. Common sera used include fetal calf serum and fetal bovine serum. Myoblast differentiation and fusion are promoted by switching to media containing low growth factor serum or

serum-free medium to inhibit further proliferation. In three-dimensional skeletal muscle cultures, it is important to produce an engineered construct with high density of fused myofibers in order to allow for important cell-cell interactions and enough power to exert strong contractile forces. This necessitates expanding myoblasts to an appropriate number corresponding to the size/volume of engineered muscle to ensure the density criterion is met.

1.3.2. Scaffold

Tissue engineering involves recreating the structure and function of native tissue. This goal has been approached many ways, including layering contracting sheets of myofibers to form a muscle bundle (myoid) [46], embedding skeletal myoblasts into hydrogels [47-50], and by migration of myoblasts into a polymer or acellular tissue supporting matrix [51].

To engineer myoids, static culture of myoblasts and fibroblasts were grown on Sylgard-coated 35-mm dishes in a two-dimensional manner. At opposing sides of the dish, two anchor points were made using laminin-coated silk sutures. As the co-culture of myoblasts and fibroblasts matured, the monolayer detached from the Sylgard surface and rolled into a cylindrical three-dimensional construct anchored by the suture points. [52] Two-week culture of myoids led to 30-60% of total cross sectional area occupied by myotubes and gradual loss of ECM. However, there was significant cellular disorganization: cross sections appeared markedly different from differentiated adult mammalian skeletal muscle, visible striations were rarely

evident in myooid constructs, and myotubes in myooids contained centrally located nuclei (a sign of muscle immaturity) rather than peripherally located nuclei [52].

Myoblast survival and formation of organized, aligned myotubes in culture requires the generation of tension by fixing the ends of engineered constructs and allowing passive contraction of the cells; co-culture conditions have utilized fibroblasts or smooth muscle cells to serve as the tension-generating entity [53]. Engineered myooid constructs did not apply tension to myoblasts until after differentiation had occurred, as differentiation was induced by change in culture medium approximately 2-3 weeks prior to monolayer detachment from the substrate [52]. Other methods for establishing a more mature myofiber phenotype include incorporating specific peptide sequences of extracellular matrix proteins or signaling molecules in the scaffold, application of electrical or mechanical stimulation, and suspension of cells within a 3D matrix.

Many groups have chosen to seed myoblasts into a three-dimensional scaffold prior to differentiation so that tension of the 2 anchor points can direct cell alignment and fusion. Important considerations when choosing an appropriate scaffold and supporting matrix hydrogel include material biocompatibility, degradation over time, rigidity, and cell to scaffold ratio (cell seeding density). Biocompatibility of material is important to prevent cell toxicity within culture; additionally, it is a vital criterion for research aiming to develop implantable tissues [54]. Many hydrogel and ECM materials degrade over time, and it is important to be

able to tune the degradation rate to allow enough time for skeletal myoblasts to fuse and mature into robust muscle tissue and form connection with surrounding ECM proteins. Many have cited the importance of fibroblasts for secretion of ECM [55]. Differentiation medium supplemented with 1 mg/mL 6-aminocaproic acid (ACA) has been used to inhibit rapid fibrin gel degradation by serum in the culture medium; the concentration of ACA in media dictates the degradation rate of the fibrin gel [47]. The rigidity of a hydrogel can also influence myoblast fusion and differentiation. Myoblast differentiation has been found to be enhanced on surfaces with elasticity of 8-12 kPa [56], which modulates integrin engagement with the cytoskeleton [57].

Engineered skeletal muscle bundles in hydrogels have been produced using fibrin, Matrigel, and collagen-based hydrogels [47-50, 58]. Collagen hydrogels are stiffer and tend to rupture more easily at high cell densities which limit the contractile forces that can be produced [46, 47]. Fibrin gels assemble into a network of branching fibers [59], enabling them to withstand higher contractile forces. Engineered muscle bundles made with collagen or fibrin hydrogels can survive for several weeks, whereas myooids prepared with primary myoblasts and fibroblasts and without a hydrogel or extracellular matrix can survive as long as 100 days [46]. Myooids exhibit a similar force length-relationship to that found *in vivo* and show insulin-stimulated glucose uptake [60], but take over one month to produce [61]. Relatively mature three-dimensional engineered fibrin hydrogel muscle bundles can

be produced in 10-12 days and also produce a physiological force-length relationship [47].

1.3.3. Metabolism and Myofiber Types

Under resting conditions *in vivo*, skeletal muscle energy needs are met by fatty acid breakdown. Muscle has limited permeability to glucose due to low levels of the primary glucose transporter, GLUT4, on the cell membrane. When plasma insulin levels rise, insulin binds to its receptor, activating a series of signaling molecules that cause GLUT4 to move from intracellular vesicles to the plasma membrane [62] enabling glucose to enter into myofibers. Glucose is then stored as glycogen to meet long-term energy needs and fatty acid metabolism is reduced. While skeletal muscle accounts for little glucose uptake in the absence of insulin, skeletal muscle is responsible for about 75% of whole body insulin-stimulated glucose uptake. Moderate to heavy exercise can cause GLUT4 translocation to the cell membrane independent of insulin, thereby increasing glucose uptake [63].

Skeletal muscle energy metabolism is regulated by the peroxisome proliferator-activated receptor γ (PPAR γ) coactivator-1 α (PGC-1 α), which interacts with a wide range of transcription factors involved in mitochondrial biogenesis, glucose and fatty acid metabolism as well as fiber type switching [64, 65]. Peroxisome proliferator-activated receptors (PPARs) are a family of nuclear transcription factors that regulate the expression of genes important to myofiber development. In skeletal muscle, PPAR δ is more abundant than PPAR α or PPAR γ [64] and is also more abundant in

type I [65] than Type II myofibers, while PPAR α induces metabolic changes in muscle and regulates the expression of muscle-specific markers, including myocyte enhancer factor 2A (MEF2A) [66].

PGC-1 α increases mitochondrial biogenesis and respiration rates and regulates the expression of many genes involved in metabolism [67]; PGC-1 α directly co-activates nuclear receptors (e.g. – thyroid hormone receptor, glucocorticoid receptors, estrogen receptors) and nonnuclear transcription factors (e.g. Mef-2 and the family of forkhead O-box (FOXO) transcription factors [68, 69]) to quickly and effectively manipulate cellular energy metabolism. As a potent co-activator, it regulates metabolic events indirectly. PGC-1 α overexpression in skeletal muscle enhances the proportion of oxidative Type IIA and Type I myofibers [69, 70]. Lin et al. reported that PGC-1 α is a principal factor regulating muscle fiber type determination [69].

Much of skeletal muscle tissue engineering has been achieved by using murine and rodent myoblast sources. Although myosin heavy chain isoforms expressed by myotubes derived from rodent myoblasts reflect the distribution found in the muscle from which the cells were derived, cultured human myotubes express MYH1, MYH2 and MYH7 in ratios that differ from those found in the muscle of origin [14]. Limited studies with human myoblasts have shown that after seven days, embryonic (MYH3), perinatal (MYH8), Type I (MYH7), Type IIA (MYH2) and

Type IIX (MYH1) mRNA are expressed [71]. After three weeks, adult MHC I was the major isoform [71], suggesting maturation of myofibers *in vitro*.

1.3.4. Contractile Forces

Muscle is composed of multinucleated myofibers that are 100 μm or less in diameter and can span the muscle length. Each myofiber contains thousands of myofilaments consisting of repeating functional units (sarcomeres). Muscle contractile forces can be generated under conditions of constant force or tension (isotonic) or constant length (isometric). During isometric contraction the sarcomeres act in series with elastic elements in the muscle, and sarcomere contraction is balanced by extension of elastic elements. Typically, the twitch contraction times range from 10 ms to 40 ms *in vivo* [29]. Lewis and Chamberlain found that a 50:50 mixture of fast and slow fibers *in vitro* had a time to peak force of about 19 ms [72]. *In vitro*, contraction of aneural myotubes can be induced by electrical stimulation or alteration of extracellular ion concentrations. Contractile forces have been measured with myotubes attached to a cantilever [73], small engineered muscle bundles attached to elastic posts [74], and cell sheets cultured on deformable polymer sheets [75]. Forces as high as 1.68 ± 0.32 mN for twitch and 2.84 ± 0.5 mN for tetanus have been obtained for a fibrin-Matrigel hydrogel system seeded with neonatal rat myoblasts [47]. Corresponding specific forces (force/cross-sectional area) were 5.5 ± 0.6 kPa and 9.4 ± 0.7 kPa, respectively [47]. By preparing fibrin hydrogels with

rodent primary myoblasts that were cast around posts of different sizes, the contractile force of the sheet increased due to increased myofiber alignment, increased numbers of nuclei per fiber and increased total volume occupied by myofibers [76]. Myoblasts seeded into fibrin gels led to contractile forces as high as 36.3 ± 4.2 kPa were produced [61]. Engineered muscle derived from primary cells produce higher specific forces than those derived from cell lines [46].

Specific forces produced by engineered rodent or human muscle are 10-100 times less than values measured for individual myofibers *in vivo*. A number of factors may be responsible for the lower contractile forces *in vitro*: myofiber density and orientation, presence of fetal forms of myosin, and/or inadequate force transmission from myofibers to extracellular matrix. As noted above, increasing the alignment of the myoblasts and using higher initial cell densities may enhance the fusion of myofibers and increase the specific force [76]. The inadequate differentiation of myotubes is probably the major factor contributing to lower specific forces *in vitro* than *in vivo*. The low specific force of individual myotubes estimated from studies with small bundles of rodent muscle cells (0.69 ± 0.13 kPa) [74], individual myotubes on cantilevers (0.94 kPa) [73], and from three-dimensional aligned muscle bundles (0.80 ± 0.15 kPa) [76] suggests that cultured myotubes are not fully reproducing the differentiated state found *in vivo*.

1.4. Methods to Increase Muscle Maturity and Force Production

While engineered muscle bundles with mouse and rat cells spontaneously contract and produce significant contractile forces, the application of electrical stimulation, mechanical stimulation or innervation with cultured neurons may be needed to generate active contraction of three-dimensional engineered human muscle bundles [44, 51]. Studies have found that denervation reduces the contractility of muscles *in vivo* [77]. Conversely, contractile force is increased by the co-culture of muscle with nerve fibers to form neuromuscular junctions [78] or addition of a recombinant form of agrin, a proteoglycan found in neuromuscular junctions [79].

1.4.1. Mechanical and Electrical Stimulation

Mechanical and electrical stimulation have both been found to enhance differentiation of skeletal muscle *in vitro* through the mimicking of exercise; however, the mechanisms are very different. Skeletal muscle contraction is initiated by the depolarization of the membrane potential. *In vitro*, skeletal muscle fibers require the need for external stimulation for the generation of an action potential since muscle *in vivo* activation of contraction is caused by cues from the central nervous system via motor neurons [80]. Mechanical stimulation simply stretches engineered muscle at preset parameters of percent stretch and frequency, but does not elicit action potentials and engage the machinery for contraction. Electrical stimulation, though, does provide the required stimulus for membrane

depolarization and has been shown to promote the transition toward adult myofibers in engineered skeletal muscle [80].

Cyclic mechanical stimulation of engineered three-dimensional human muscle bundles in collagen increases the construct elasticity and myofiber diameter [50]. After mechanical stimulation, human muscle bundles generate passive forces between 500-1000 $\mu\text{N}/10^6$ cells, 2-4 times greater than unstretched samples [50]. Passive forces in collagen-based human muscle constructs without Matrigel or mechanical stimulation are much lower with a peak force of 43 $\mu\text{N}/10^6$ cells [81]. Mechanical preconditioning of acellular porcine bladder repopulated with human skeletal myoblasts and collagen improved tissue organization and fiber orientation [51]. Applying 17% stretch at 1 Hz on murine myoblasts [82] or 10% stretch at 0.5 Hz for 1 hour on bovine myoblasts inhibited differentiation and promoted proliferation, while 10% strain at 0.5 Hz for 1 hour alternated with 5 hours of relaxation enhanced expression of integrin β_{1D} , which activates RhoA, thereby regulating myofiber formation, differentiation and nitric oxide release [83]. Human skeletal muscle constructs exhibited KCl induced contraction after three weeks of mechanical conditioning [51], although this must be interpreted cautiously since myofibroblasts also contract in response to KCl. After implantation in the mouse *latissimus dorsi* for 2 or 3 weeks, mechanically conditioned engineered human muscle exhibited tetanus, although the specific forces were far below those in the native mouse muscles, and

the contribution of host vs. donor cells to generated force of explanted muscle constructs was not determined [51].

Low frequency electrical stimulation induced spontaneous contraction of human skeletal myofibers in two-dimensional cultures [84]. Like exercise, low frequency stimulation of human myofibers in vitro increased glucose uptake independent of insulin and increased mitochondrial content and PGC-1 α gene expression [84]. Mechanical or electrical stimulation produces more mature sarcomeres [85] resulting in a greater percentage of myotubes in three-dimensional muscle bundles expressing adult forms of MHC than fetal forms [86]. Electrical stimulation also promotes GLUT4 transport to the cell membrane, but does not alter the levels of GLUT1 and GLUT4 [85]. GLUT4 activity has been associated with type I fibers that utilize oxidative metabolism compared to glycolysis [87].

1.4.2. *MicroRNA's*

MicroRNAs are short (~22nt), highly conserved, non-coding RNAs [49, 88, 89] that act by negatively regulating gene expression, and are usually repressors of repressors [89]. Currently, their known functions include inhibiting protein translation by directly blocking translation or enhancing messenger RNA degradation [90]. MicroRNAs are initially transcribed in the cell nucleus as a long strand of primary microRNA, or pri-microRNA, that contains the mature microRNA as a hairpin. Inside the nucleus, Drosha (an RNase III endonuclease) cleaves the pri-microRNA into an intermediate (~60-70nt) precursor microRNA, or pre-microRNA.

Exportin-5 (XPO5) transports the pre-microRNA from the nucleus and into the cytoplasm where further processing occurs: a second RNase III endonuclease called Dicer1 excises the pre-microRNA into a ~22nt microRNA duplex. One strand is degraded, leaving the mature single-stranded microRNA [90]. This mature microRNA is then incorporated into the RNA-induced silencing complex (RISC), a ribonucleoprotein complex. This enables the RISC to target specific portions of the 3' untranslated region (UTR) of the target mRNA by base-pairing across the “seed sequence” – the 7-8nt sequence of the mature microRNA that dictates the microRNA:microRNA binding. This binding results in repression of protein translation [89].

The role of microRNAs is essential to many important cell processes, such as proliferation, differentiation, and apoptosis [89]. Three muscle-specific microRNAs are essential to the proliferation and differentiation of skeletal myoblasts: miR-1, miR-133a, and miR-206 [49, 88, 89, 91]. In the human and mouse genomes, miR-1 and miR-206 are located on different genetic loci, but are both known to promote myoblast differentiation, while miR-133a is located near miR-1, but promotes proliferation [89]. Since microRNAs are repressors of repressors, they effectively upregulate certain processes. For example, miR-133 represses serum response factor (SRF), which represses proliferation – therefore, miR-133a promotes myoblast proliferation (Figure 4). Since miR-1 and miR-133a are located on the same genetic locus, their expression is coupled. MiR-1 blocks histone deacetylase-4 (HDAC4), an

inhibitor of myocyte enhancer factor-2 (Mef-2). Mef-2 is a family of transcription factors that encode for proteins to promote differentiation at various stages of development. The expression of Mef-2 is linked strongly to the onset of skeletal muscle differentiation. Mef-2C, a member of the Mef-2 family is particularly sensitive to mechanical stretch in skeletal muscle [92, 93]. This transcription factor is also implicated in a wide variety of muscle-specific developmental processes [94], including control of myoblast differentiation and function [95, 96], maintenance of myofiber integrity [94], and regulation of mitochondrial biogenesis [97, 98]. MiR-206 negatively affects Pax7, discussed previously as the important factor for cell renewal and maintenance of “stemness.” The inhibition of Pax7 by miR-206 leads to the promotion of MyoD, another transcription factor important to the onset and succession of muscle differentiation.

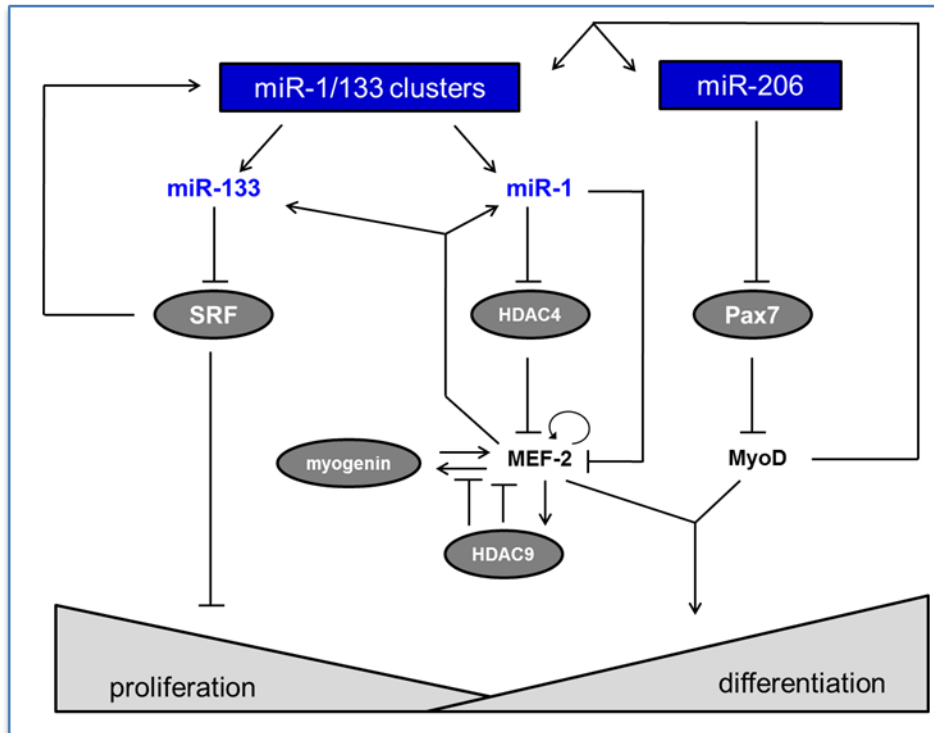


Figure 4. MicroRNA Pathway for Proliferation and Differentiation of Skeletal Muscle. MiR-133a represses serum response factor (SRF), which represses myoblast proliferation. MiR-1 represses histone deacetylase 4 (HDAC4), which represses myoblast differentiation. MiR-206 represses Pax7, which represses MyoD, an important transcription factor for myoblast differentiation.

Our lab has shown that transfection of C2C12 myoblasts with miR-133a inhibitor successfully enhanced differentiation of myofibers in 3D muscle bundles [49]. Since miR-133a promotes proliferation, inhibiting it forced cells down the differentiation pathway and led to enhanced differentiation of *in vitro* muscle. Engineered muscle bundles seeded with anti-miR-133a C2C12 cells exhibited 20% higher forces than those transfected with a scrambled microRNA sequence [49]. Additionally, Mef-2C expression was used to assess extent of differentiation between anti-miR-133a and negative control (scrambled sequence) transfected cells.

Myoblasts transfected with anti-miR-133a exhibited heightened Mef-2C expression compared to the negative control as assessed by intensity of fluorescence stain [49].

Aside from affecting muscle maturation and differentiation, microRNAs also play important roles in muscle cell metabolism [99, 100] (Figure 5). MiR-696 plays a critical role in regulating myoblast response to mechanical stretch [101] and affecting the downstream metabolism co-activator PGC-1 α . PGC-1 α is a powerful transcriptional co-activator protein that binds to the activators of many transcription factors that influence in metabolism and energy expenditure [68, 101]. PGC-1 α works by increasing mitochondrial biogenesis and respiration rates and the utilization of cues from the microenvironment, including oxidative stress or exercise, for energy production. This co-activator is recognized as a “master controller” of many genes involved in metabolic regulation [67]; PGC-1 α directly co-activates a plethora of transcription factors, including nuclear receptors – thyroid hormone receptor, glucocorticoid receptors, estrogen receptors, etc. – and nonnuclear receptor transcription factors – Mef-2 and the family of forkhead O-box (FOXO) transcription factors [68]. PGC-1 α affects various tissues, including adipose tissue, liver, cardiac muscle, and skeletal muscle [67]. Through these multiple pathways, PGC-1 α is able to quickly and effectively manipulate cellular energy metabolism.

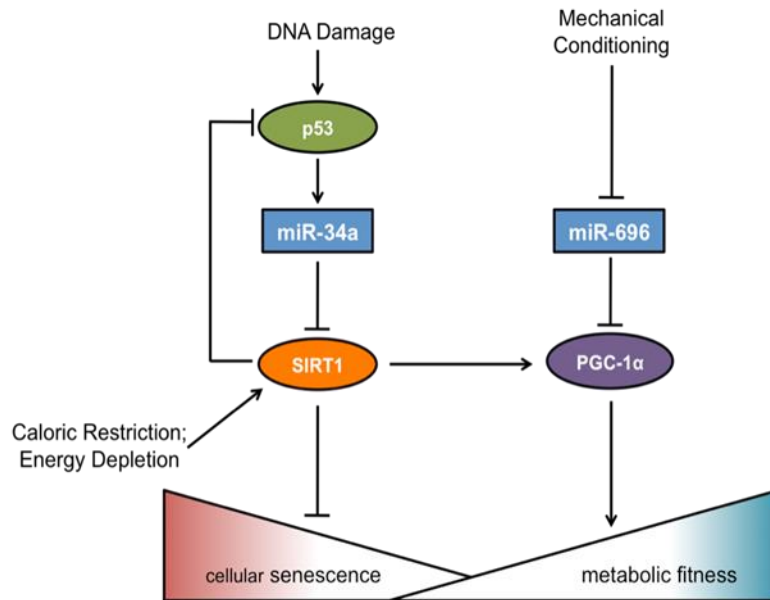


Figure 5. MicroRNA Pathway for Energy Metabolism in Skeletal Muscle. MiR-34a represses sirtuin 1 (SIRT1), which represses cellular senescence. MiR-696 represses PGC-1 α , an important metabolism co-activator that has been shown to increase metabolic fitness and oxidative metabolism in skeletal muscle.

PGC-1 α is present in a wide variety of tissues, but it is highly expressed in tissues requiring high-energy oxidative capacity, like the heart and skeletal muscle [68, 102]. Transgenic animals with increased PGC-1 α exhibit increased mitochondrial number and function compared to wild-type, while those with deletions of PGC-1 α demonstrated abnormal glucose homeostasis, decreased endurance capacity and mitochondrial gene expression [68]. Due to the importance and overarching metabolic function of PGC-1 α , even minor disturbances in the co-activator's activity may lead to severe metabolic syndromes and/or low of whole-body homeostasis [68, 103]. While the biology of PGC-1 α and its regulation is still largely unknown, it is agreed that this co-activator is essential to maintaining balanced energy metabolism.

Recently, links between PGC-1 α and myofiber composition have been reported [65, 69, 104, 105]; specifically, increased PGC-1 α expression has been reported as a factor leading to the development of slow-twitch type I myofibers [69].

1.5. Motivation and Significance

In order to utilize engineered muscle bundles for a tissue engineering applications and relevant clinical drug and toxicity testing, human engineered skeletal muscle bundles must be developed. Optimized culture conditions to efficiently expand human satellite cells and myoblasts and promote their fusion and maturation are needed. Additionally, while the source of human muscle cells can be primary muscle biopsies, developing robust protocols for induction of satellite cells and myoblasts from human induced pluripotent stem cells will be needed to examine a range of physiological and pathological conditions.

While considerable work has been done with murine skeletal myoblasts to study skeletal muscle *in vitro*, there is a dearth of knowledge about the differentiation and maturation of primary isolated human skeletal myoblasts in the same environment. This project aims to develop a three-dimensional human skeletal muscle construct that will demonstrate contraction under electrical stimulus. Such a construct would be instrumental to the pharmaceutical industry for pre-clinical testing of drugs, whether musculature-targeting or not [106]. Since skeletal muscle is the largest tissue organ system in the human body, it is important to study the effects

of any drug on its development and function. Treatments that may adversely affect the skeletal muscle could potentially be life altering.

This project was conducted in conjunction with the Tissue Chip Award for Model Systems given by the National Institutes of Health (NIH) to develop microphysiological systems to test drugs in a pre-clinical setting.

1.6. Hypothesis & Specific Aims

This research aimed to evaluate primary human skeletal myoblast differentiation *in vitro* and the effect of microRNA modulation on the progression of differentiation and fiber type development. We hypothesized that joint inhibition of proliferation-promoting miR-133a and oxidative metabolism-repressing miR-696 will lead to accelerated differentiation and directed myofiber type development of functional tissue-engineered 3D human skeletal muscle. The work presented here was approached by means of 3 specific aims:

- 1. Specific Aim 1: Identify culture conditions for efficient HSkM growth and differentiation and establish a temporal profile of microRNA expression during differentiation.**

The goal of this aim was to identify proper culture conditions for the efficient differentiation of HSkM *in vitro*. Most research for skeletal muscle has been completed using the immortalized C2C12 mouse myoblast line due to accessibility and cost. However, it is important to study human tissue as there may be distinct differences. We hypothesized that HSkM would require

different culture conditions than those optimal for C2C12 culture (8% equine serum in differentiation medium on uncoated substrates). To test this hypothesis, immunofluorescence for sarcomeric α -actinin and microRNA expression was used to assess differentiation of muscle cultures. [92]

2. **Specific Aim 2: Assess the effects of miR-133a and miR-696 inhibition on gene and protein expression in HSkM cultured in 2D.**

The goal of this aim was to test the hypothesis that joint inhibition of miR-133a and miR-696 would result in 2D human skeletal muscle cultures with accelerated differentiation and increased Type I muscle fibers compared to control and individual inhibition of each microRNA. To test this hypothesis, expression of genes and proteins important to the process of myogenesis and fiber type development were assessed.

3. **Specific Aim 3: Develop a 3D functional model for human skeletal muscle *in vitro* to assess effect of miR-133a and miR-696 inhibition on active contractile forces and ultrastructure.**

The goal of this aim was to develop a 3D human skeletal muscle model capable of active contraction. The second goal of this aim was to test the hypothesis that joint inhibition of miR-133a and miR-696 in this functional 3D human skeletal muscle model would result in active contraction significantly higher than control and individual inhibition by each microRNA. To test this hypothesis, isometric force testing was used to measure functionality of

engineered muscle bundles and compare forces between microRNA treatments. Additionally, immunofluorescence was used to visualize ultrastructural organization of bundles and identify myofiber type distribution as result of microRNA treatment.

4. Specific Aim 4: Endothelialize 3D muscle bundle to model capillary-muscle interface *in vitro*.

The goal of this aim was to identify culture conditions to support a lamellar co-culture model in 3D of human cord blood-derived endothelial cells (hCB-ECs) and HSkM capable of active contraction. To identify these conditions, immunofluorescence was used to visualize confluent layer of endothelium on fused human skeletal muscle and isometric force testing was used to test construct functionality.

CHAPTER 2. Optimization and Characterization of Primary Human Skeletal Myoblasts (HskM) (Specific Aim 1)

2.1. Introduction

The use of murine models for the study of human diseases is a widely practiced phenomenon in biomedical research [107, 108]. This stems from the accessibility of mice and our shared organ systems and genetic material. Mice provide an easily genetically manipulated mammalian system and the rapid procreation necessary for efficient data collection. However, the question remains: how relevant are these results to human biology in phenotype and function [109]? Some recent studies have begun to study the similarities and differences between these two cell types; Harrison et al. found that in mouse and human skeletal muscle, myosin heavy chain IIB/X isoform (MyHC-IIB/X) genes have significantly different basal transcriptional activities despite highly conserved upstream regulatory regions [110]. Many groups have also delved into the characterization and use of human myoblasts *in vitro*; Stern-Straeter et al. measured the relative expression of various well-defined differentiation markers, including myogenic factor 5 (MYF5), myogenin, skeletal muscle α -actin1 (ACTA1), and adult myosin heavy chain (MYH1) [111]. This study saw a decrease of MYF5, an early differentiation marker, from day 1-16 post-differentiation; there was a steady increase of expression in myogenin and ACTA1 post-differentiation; there was a rise and fall around day 12 post-differentiation in MYH1 expression [111].

Others have clearly demonstrated the importance of microRNA involvement in the successful proliferation and differentiation of human skeletal myoblasts to mature skeletal muscle; however, a detailed time course of microRNA dynamic expression during differentiation in human cells has not yet been shown. Koning et al. report significant downregulation in miR-106b, miR-25, miR-29c, and miR-320c levels between quiescent satellite cells and fused myotubes [112]; additionally, they showed miR-1 and miR-206 relative expression at four points throughout *in vitro* muscle growth: proliferation, confluency, differentiation, and muscle [113]. Chen et al. used a mouse model to show, both *in vivo* and *in vitro*, the expression of miR-351 immediately after induced cardiotoxin (CTX) injury; in both cases, a peak and fall of miR-351 expression was seen post-CTX injury [114].

Here, we attempted to fill this gap by measuring levels of miR-1, miR-133a, and miR-206 at various days post-differentiation. We began the study with a comparison of microRNA levels between isolated HSkM and immortalized C2C12 cells. Next, brief characterization studies were conducted comparing the two as well: cell proliferation/growth rates, cell size/area, myoblast response to differentiation medium (DM), and rates of fusion and striation. Finally, we optimized the culture conditions for *in vitro* proliferation and differentiation of HSkM to use in future studies. This is the first study showing a detailed timeline of microRNA levels after the onset of differentiation.

2.2. Materials and Methods

2.2.1. Primary Human Skeletal Myoblast Isolation

Primary human skeletal myoblasts (HskM) were isolated from biopsies of the *vastus lateralis* of healthy middle-aged volunteers (male and female) under conditions of informed consent and approval of the Duke Investigational Review Board. Biopsies were placed in growth medium for human skeletal myoblasts (hGM) containing low glucose (1 g/L D-Glucose) Dulbecco's Modified Eagles' Medium (DMEM; Gibco/Invitrogen), 8% heat-inactivated fetal bovine serum (HyClone), and SkGM Singlequots (Lonza/Clonetics) with insulin removed and kept on ice until ready for isolation. The muscle biopsy (30-50mg) was placed in Ca⁺⁺ and Mg⁺⁺-free HBSS (Gibco/Invitrogen) and minced into fine pieces. After removal of HBSS, minced tissue was placed in warmed solution containing 0.25% trypsin, 0.1% collagenase, 0.1% BSA, and 0.05% EDTA for 30 minutes. The action of the trypsin and collagenase were halted with addition of 10% fetal bovine serum in medium to tissue. Tissue was placed onto uncoated T25 flask to eliminate undesired cells (i.e. fibroblasts, nerve cells, blood cells) by adhesion to plastic. An adhesion time of 3 hours was optimal for adhesion of other cell types but without significant adhesion of skeletal myoblasts. After 3 hours, tissue was transferred to collagen-coated T25 flask (BD Biosciences) to allow migration of skeletal myoblasts from tissue. The hGM was changed every 5 days until the flask was 75% confluent, approximately 1-2 weeks. Once 75% confluent, HskM were split into dishes for expansion. After about

one week, when the cells were 85-90% confluent, cells were trypsinized and plated for studies or frozen. One 30-50mg biopsy yielded 15-20 million cells.

Primary isolated HSkM were assessed for purity by staining for desmin, a muscle-specific intermediate filament protein that has been widely used in measuring primary skeletal myoblast purity [109, 115, 116]. Cultures were fixed with ice-cold 100% methanol and rinsed twice with PBS. Fixed samples were blocked in 10% goat serum for 30 minutes at 37°C. The primary antibody against desmin (Sigma) was diluted 1:100 in 10% goat serum and incubated at 37°C for 30 minutes. After rinsing with PBS, samples were incubated at 37°C with secondary Alexa Fluor-546 goat anti-mouse antibody (1:250, Invitrogen) for 30 minutes. Finally, Hoechst 33342 nuclear stain (1:1000, Invitrogen) was added for 15 minutes at 37°C. Samples were thoroughly rinsed with PBS and viewed on a Nikon Eclipse TE2000-U fluorescent microscope. Images were analyzed using ImageJ software for percentage of desmin-positive cells per field of view.

2.2.2. Cell Culture

Primary HSkM cultures were expanded from 1,500 cells/cm² in uncoated standard tissue culture plastic flasks at passages 3 to 6 (split 1:4 in flasks) at 37°C and 5% CO₂/95% air. Cells were fed every other day with hGM until confluent. Myoblasts were plated onto tissue culture plastic 6-well plates coated with either 100 µg/mL growth factor reduced Matrigel (GFR-MG, BD Biosciences) or left uncoated. To promote differentiation of confluent myoblasts to myotubes after 2-3 days, hGM

was changed to differentiation medium (DM), consisting of high glucose DMEM (Gibco/Invitrogen) supplemented with 2% or 8% equine serum (ES, HyClone) and 0.1% gentamicin (Gibco/Invitrogen).

Immortalized murine C2C12 myoblasts (ATCC), originally derived from C3H mouse leg muscle, were expanded and cultured on uncoated standard tissue culture plastic at passages 3 to 7 in conditions of 37°C and 5% CO₂; each passage was split 1:4. Cells were fed every other day with mGM consisting of high glucose (4.5 g/L D-Glucose) DMEM, 8% calf serum (HyClone), 8% fetal bovine serum (HyClone), 0.5% chicken embryo extract (Accurate Chemicals), and 0.1% gentamicin. Similar to HSkM cultures, mGM was changed to DM to promote myoblast fusion upon confluency, about 2-3 days.

2.2.3. Myoblast Size and Growth Rate

Four hours post-plating, brightfield images were taken of HSkM and C2C12 cultures. Areas of observation were marked on culture flasks and reexamined after 28 and 48 hours. Cell growth rate was observed in the same manner as cell size; images were taken at 4, 12, 24, 36, 48, and 72 hours. Images were assessed using ImageJ software for cell size and cell number.

2.2.4. Immunofluorescence

Cellular proliferation was measured with the Click-iT EdU Imaging Kit (Invitrogen) following the manufacturer's protocol. Briefly, cultures of myoblasts were incubated for 2 hours at 37°C with hGM or mGM containing 1mM EdU

solution. EdU (5-ethynyl-2'-deoxyuridine) is a nucleoside analog of thymidine and is incorporated into DNA during active DNA synthesis, and therefore, preferentially stains the nucleus of proliferating cells. Detection of EdU occurs through a click reaction: a copper-catalyzed covalent reaction between an azide and an alkyne [117]. The cells were fixed with ice-cold 100% methanol and rinsed with PBS. Fixed cultures were incubated for 30 minutes at room temperature with EdU reaction cocktail. The labeled cells were then incubated for 30 minutes at room temperature with Hoechst 33342. Cultures were rinsed with PBS and imaged using a Nikon Eclipse TE2000-U fluorescent microscope. EdU stained cells were counted with ImageJ software and quantified as fraction of total number of cells present in the field of view. Four fields of view were taken per well in a 6-well plate.

To assess the timeline of differentiation for primary HSkM and C2C12 cells, samples were fixed every other day, starting from the day on which the media was changed from growth media to differentiation media at 80% confluence, denoted as Day 0, until Day 14 post-differentiation. Cultures were fixed with 100% ice-cold methanol and stained for sarcomeric α -actinin (1:800, Sigma) and nuclei (Hoechst 33342, Invitrogen). At each time examined, the proportion of nuclei contained within α -actinin-positive fibers was calculated to find the rate of fusion during myoblast differentiation.

To identify optimal level of serum for differentiation medium, HSkM were cultured in 2% and 8% equine serum-supplemented differentiation medium and on

100 μ g/mL GFR-MG coated surfaces and uncoated tissue-treated polystyrene surfaces in both normoxic (21% O₂) and hypoxic (2% O₂, physiologic) conditions. Samples were fixed at 10 days post-differentiation with 100% ice-cold methanol and stained for sarcomeric α -actinin and nuclei. Briefly, fixed samples were blocked in 10% goat serum for 30 minutes at 37°C. The primary antibody against sarcomeric α -actinin (Sigma) was diluted 1:800 in 10% goat serum and incubated at 37°C for 30 minutes. After rinsing with PBS, samples were incubated at 37°C with secondary Alexa Fluor-488 goat anti-mouse antibody (1:250, Invitrogen) for 30 minutes. Finally, Hoechst nuclear stain was added for 15 minutes at 37°C. Samples were thoroughly rinsed with PBS and viewed via Nikon Eclipse TE2000-U fluorescent microscope. At each time, the proportion of myofibers containing striations was calculated and compared to total number of fibers per field of view to assess development of striations and muscle maturation.

2.2.5. MicroRNA/RNA Isolation and Quantitative Real-Time PCR

Samples from static, stretched, and transfected studies were gathered at denoted days to track microRNA and RNA expression changes over time. MicroRNAs were isolated using the mirVANA microRNA Isolation Kit (Applied Biosystems). Total mRNA was isolated using the Aurum Total RNA Mini Kit (Bio-Rad).

To assess microRNA levels in mature human muscle tissue, fresh human muscle explants (from the *vastus lateralis*) were also used for microRNA isolation.

Tissue was minced in a glass petri dish using sterile forceps and scalpels. MicroRNA isolation was completed with the mirVANA microRNA Isolation Kit (Applied Biosystems).

Quantitative RT-PCR (qRT-PCR) was used to assess microRNA and RNA expression from collected samples. MicroRNA/RNA concentration and quality were measured using the NanoDrop ND-1000 spectrophotometer (NanoDrop, Wilmington, DE). For microRNA expression, cDNA was prepared using the MicroRNA Reverse Transcriptase kit (Applied Biosystems) and the MyiQ Single Color Real-Time PCR Detection System (Bio-Rad) per manufacturer instructions. Hairpin primers for microRNAs of interest were purchased (Applied Biosystems): hsa-miR-1, hsa-miR-133a, and hsa-miR-206. Small nucleolar RNA RNU6B was used as an endogenous control (Applied Biosystems). All primers were tested and approved by the manufacturer for use with mouse and human cell samples. TaqMan Universal PCR Master Mix (Applied Biosystems) and hairpin primers were added to the cDNA samples per manufacturer instructions and placed back into the MyiQ Single Color Real-Time PCR Detection System for PCR analysis. For RNA expression, cDNA was prepared using the iScript cDNA Synthesis Kit (Bio-Rad) following manufacturer instructions. Primers for Mef-2C and GAPDH (endogenous control) were custom ordered (IDT) for the following sequences: Mef-2C Forward ACTTCCTGGAGAAGCAGAAAGGCA, Mef-2C Reverse AACACGTTTCCTTCTTCAGCACGC, GAPDH Forward

TCAACAGCAACTCCCCTCTTCCA, GAPDH Reverse

ACCCTGTTGCTGTAGCCGTATTCA. These primers have been previously used to measure GAPDH and Mef-2C mRNA levels [118, 119]. IQ SYBR Green Supermix (Bio-Rad) and primers were combined with cDNA and placed into the MyiQ Single Color Real-Time PCR Detection System for PCR analysis. The $2^{-\Delta\Delta C_T}$ method was used to assess the real-time mRNA and microRNA expression data. Total RNA from 11-day-old mouse embryo was used as the calibrator (Clontech).

PCR results were normalized to account for variability among the levels initially present in the different biological replicates. Data from all experiments, regardless of conditions, were averaged to obtain a “global average.” To identify the variability between experiments, data from each experiment were then averaged. To decrease inter-experiment variability while maintaining the relation between conditions within each experiment, a normalization factor was calculated by dividing the global average by the average of each experiment. New normalized values were calculated for each experiment by scaling each data point by the normalization factor of the experiment. This data was used to calculate statistical significance.

2.2.6. Cyclic Mechanical Stretch

Primary HSkM and C2C12 cells were cultured until 80% confluent. At this point, hGM and GM were shifted to 2% ES-DM and 8% ES-DM, respectively. This timepoint was denoted as Day 0. Mechanical stretching of myoblast cultures was

applied via the Flexcell FX-5000T Tension System (Flexcell International, Inc.) onto flexible silastic membranes; unstretched silastic membranes served as the control. Previous work on our lab with C2C12 optimized parameters for stretch studies to be 10% stretch at 0.5Hz for 1 hour alternating with 5 hours of rest for differentiation [83].

2.2.7. Statistical Analysis

Data are presented as mean \pm standard error (SEM) unless otherwise noted. ANOVA and Fisher's PLSD post-hoc tests were performed using the STATVIEW 5.0 statistical analysis package. A value of $p < 0.05$ was considered significant. HSkM isolated from separate individuals were considered distinct n 's whereas for C2C12 cells, the value n represents separate cultures of the same cell line.

2.3. Results

2.3.1. Comparison of C2C12 and HSkM growth, size, and differentiation under conditions optimal for C2C12 myofiber maturation

The purity of subconfluent primary HSkM myoblasts was assessed at passage 3. Using the percent of desmin-positive cells as a measure of purity, $90.4\% \pm 4.2\%$ (mean \pm SEM, $n=3$) of subconfluent myoblasts were positive for desmin.

When grown on uncoated tissue culture plastic in 8% serum, primary HSkM were significantly larger in cell size at 8, 28, and 48 hours post-plating than C2C12 cells ($n = 3$, P4 all cells, Figure 6). Over 72 hours, both cell types exhibited the characteristic exponential growth; however, the primary HSkM had a lag phase

(typically 18-20 hours compared to none for C2C12) before reaching exponential growth (Figure 7). Using a linear fit to the log of the exponential growth phase, C2C12 doubling time was 19.7 ± 0.5 hours ($R^2 = 0.994$, $n = 3$) and primary HSkM doubling time was 41.4 ± 3.3 hours ($R^2 = 0.912$, $n = 4$).

To assess proliferation at 0 and 24 hours in various culture media, an EdU cellular proliferation assay was used. Time zero ($t = 0$ hours) was designated when the cells reached 40% confluency; a sub-confluent time point was used to prevent a change in growth rate due to contact inhibition. Cell numbers were normalized to values at time zero for individual studies to allow for comparison between studies ($n = 3$, Figure 8). As assessed by ANOVA analysis of EdU levels on the different culture days, there was a significant drop in proliferation when DM was added at time zero for 24 hours compared to cultures kept in GM for 24 hours ($p < 0.05$): C2C12 proliferation dropped from $16.9 \pm 3.8\%$ in mGM to $7.3 \pm 0.8\%$ in DM, and HSkM

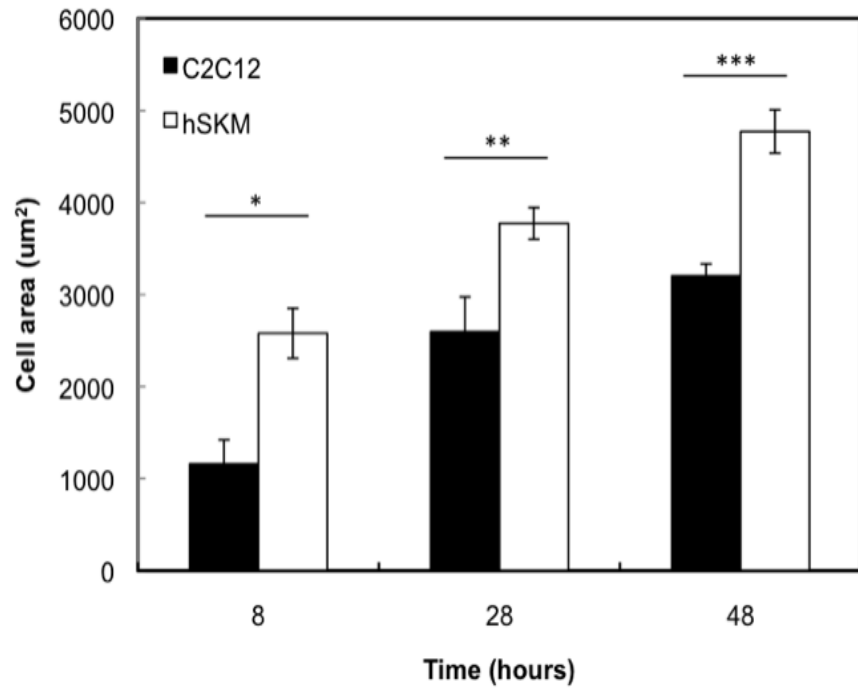


Figure 6. C2C12 vs. HSkM Cell Area. HSkM are larger than C2C12 at 8 (*p<0.03), 28 (**p<0.05), and 48 (**p<0.005) hours post-plating. Error bars are S

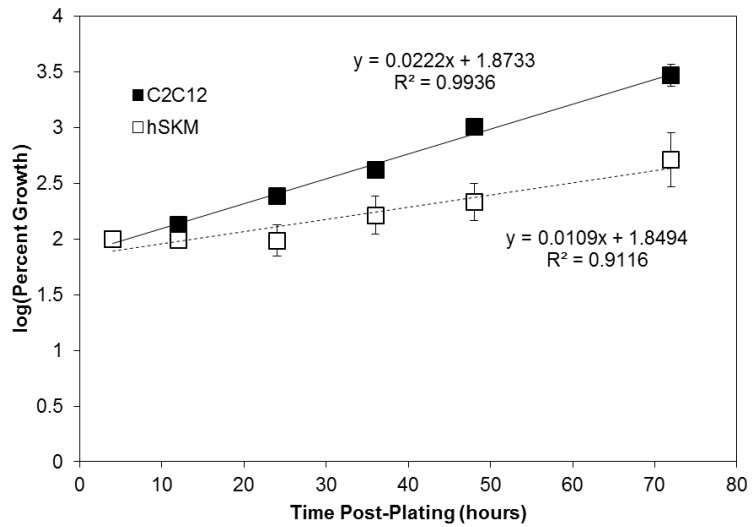


Figure 7. C2C12 vs. HSkM Growth Rates. Cell count values were normalized to counts on day 1 “percent growth.” C2C12 doubled in 19 hours and HSkM doubled in 35 hours. Error bars denote SEM.

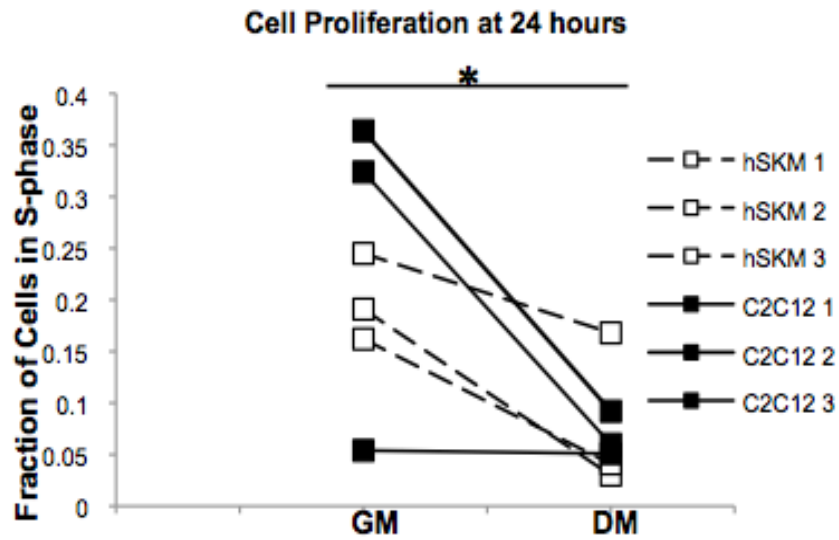


Figure 8. Effect of DM on Cell Proliferation. Cultures were split into 2 groups: cultures in GM and cultures shifted to DM at time zero. Time zero was determined to be 80% confluency. With repeated measured ANOVA analysis, the drop in proliferation at 24 hours post-differentiation was significant (* $p < 0.02$).

proliferation dropped from $18.8 \pm 0.9\%$ in hGM to $10.5 \pm 3.3\%$ in DM. HSKM EdU levels were similar to that of C2C12 under both conditions of GM and DM after 24 hours.

The extent of differentiation was first investigated by means of myotube formation and maturation to myofibers under conditions that were optimal for C2C12 differentiation (no protein coating, 8% serum in differentiation medium). Myoblasts fused and the resulting myofibers become striated as skeletal muscle matures [120]. The lag in development of striated HSKM relative to C2C12 is apparent by immunofluorescence for α -actinin, paralleling previous findings for growth rate (Fig. 9A-B) [121]. Using a linear fit, the rate of fusion was calculated over the linear portion of the data shown in Figure 9C. C2C12 fused at a rate of $11.13 \pm$

1.6% nuclei per field of view per day ($R^2 = 0.990$) from Days 0-6, which was not different than the fusion rate of HSkM ($6.92 \pm 2.9\%$ nuclei per field of view per day ($R^2 = 0.997$)) from Days 0-10. HSkM had a significantly slower rate of developing striations compared to C2C12, an important indicator of muscle maturity: $3.25 \pm 0.78\%$ vs. $8.65 \pm 2.79\%$ striations per field of view per day, respectively (Fig. 9D, ANCOVA $p < 0.05$). As skeletal muscle differentiated, HSkM fibers decreased in diameter, while C2C12 fibers increased in diameter. For Day 8 and earlier, the fiber diameters were similar. Then they diverged with diameter increasing for C2C12 and decreasing for HSkM; at Day 10, HSkM fiber widths were significantly thinner ($54.0 \pm 4.4\mu\text{m}$, $n = 3$) than C2C12 ($105.8 \pm 14.5\mu\text{m}$, $n = 3$) ($p < 0.05$) (Fig. 9E). At Day 8, C2C12 cultures showed prominent striations while the HSkM cultures took two weeks post-differentiation (Day 14) to reach a comparable maturation point. Based on these results, subsequent studies for HSkM were conducted to Day 14 to allow for appropriate development and muscle maturation.

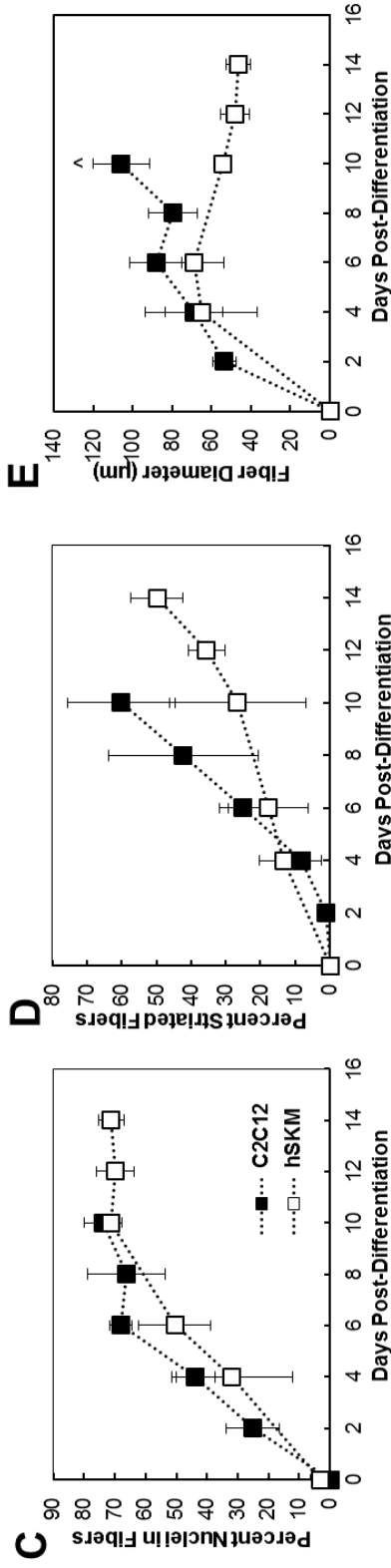
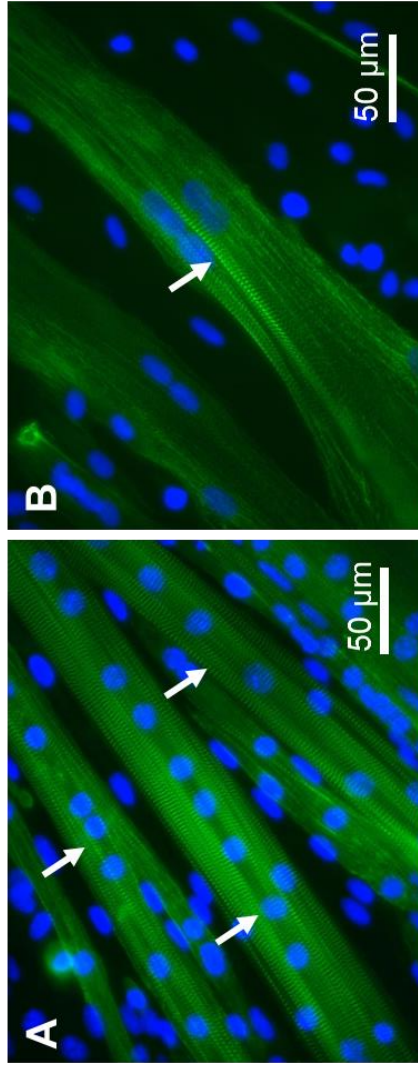


Figure 9. C2C12 vs. HSkM Myofiber Morphology. Myoblast fusion and striation of C2C12 and HSkM at passage 3. (A) C2C12 cultures stained for sarcomeric α -actinin (green) and DAPI (blue) at day 8 post-differentiation. (B) HSkM cultures stained for sarcomeric α -actinin and Hoechst at day 14 post-differentiation. (A-B) Both cell types exhibit multinucleation and clear striations at terminal differentiation day. Scale bars are 50 μ m, images taken at 40X magnification. (C) Fusion of myoblasts into myotubes. Using a linear fit, the rate of fusion was calculated: C2C12 fused at a rate of 11.13 \pm 1.6% nuclei per field of view per day ($R^2 = 0.990$) from Day 0-6, and HSkM fused at a rate of 6.92 \pm 2.9% nuclei per field of view per day ($R^2 = 0.997$) from Day 0-10. (D) C2C12 develop striations more quickly than HSkM cells; slopes of C2C12 and HSkM regression lines are significantly different by ANCOVA ($p < 0.05$). (E) C2C12 myofibers are thicker than HSkM myofibers at Day 10 ($\wedge p < 0.05$). All error bars are SEM. [1]

2.3.2. Culture Conditions for HSkM

When HSkM myoblasts were cultured on an uncoated tissue culture polystyrene surface for 14 days after shifting to 8% equine serum, immunofluorescence for sarcomeric α -actinin showed a sparse distribution of short myofibers that lacked striations (Fig. 10A). Using MATLAB image analysis, the average sarcomeric α -actinin stained area was $29.7 \pm 3.5\%$ in each field of view (4 fields of view/experiment, $n=3$). Staining for von Willebrand factor showed $3.1 \pm 0.8\%$ positive staining for endothelial cells among the myoblast population. Unfused cells are a combination of unfused self-renewed satellite cells and other cells types that were not removed by the isolation process.

In 2% serum on uncoated surfaces, myofibers appeared longer compared to those cultured in 8% serum. However, myoblasts cultured under these conditions also lacked striations (Fig. 10B) and only $23.9 \pm 2.2\%$ of total stained areas were positively stained for sarcomeric α -actinin. The culture of myoblasts on a surface treated with $100\mu\text{g/mL}$ GFR-MG, which has been shown to maintain differentiation capacity of muscle precursor cells *in vitro* [122], showed an increase of sarcomeric α -actinin staining on Day 14 to $50.1 \pm 5.2\%$ of area. These myofibers also contained striations (Fig. 10C, arrow); however, there appeared to be scattered sarcomeric α -actinin-stained aggregates as well (Fig. 10C, asterisk). HSkM grown on $100\mu\text{g/mL}$ GFR-MG and in 2% serum showed $43.4 \pm 3.0\%$ area positive for sarcomeric α -actinin with fewer stained aggregates and more striations (Fig. 10D, arrow); this result was

not statistically different than $50.1 \pm 5.2\%$ for 8% serum on GFR-MG. When cultured on surfaces coated with $100\mu\text{g}/\text{mL}$ GFR-MG in 2% serum, HSkM exhibited greater extent of fusion and striation after 14 days ($84.0 \pm 2.0\%$ of α -actinin-positive area contained striations in 2% serum vs. $13.3 \pm 7.7\%$ striated in 8% serum, $n=2$).

Therefore, 2% equine serum in DM on GFR-MG-coated surfaces appeared to best facilitate HSkM differentiation of other tested conditions.

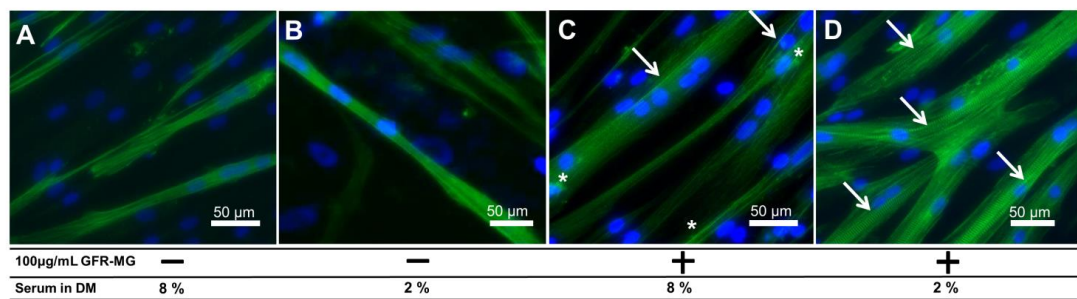


Figure 10. Effect of serum and Matrigel coating on formation of striated human muscle fibers 14 days after shifting to differentiation medium (DM) with the indicated level of serum. Differentiation was characterized by immunofluorescence for sarcomeric α -actinin (green) and DAPI (blue). (A) Few fibers were seen under uncoated, 8% equine serum in DM conditions. (B) Few fibers were present in uncoated, 2% equine serum conditions; however, myofibers were longer compared to uncoated 2% equine serum conditions. (C) Fibers were more prevalent and robust in surfaces coated with $100\mu\text{g}/\text{mL}$ GFR-MG in 8% equine serum DM. Some cell debris was also present (asterisk). Few striations were present (arrow). (D) Robust, striated fibers were seen for HSkM attached to GFR-MG-coated surfaces and differentiated in 2% equine serum-supplemented DM (arrow). All images taken at 20X magnification, scalebars are $50\mu\text{m}$. [1]

2.3.3. Effect of culture conditions on C2C12 and HSkM microRNA and MEF-2C expression

Based on the improved differentiation of HSkM on GFR-MG at low serum levels, we hypothesized that adding GFR-MG coating and decreasing media serum levels would significantly elevate the microRNA and Mef-2C gene expression of HSkM during differentiation *in vitro*. All microRNA expression was normalized to

the small nucleolar RNA RNU6B as endogenous control; Mef-2C gene levels were normalized to GAPDH as endogenous control. When cultured in 8% serum during differentiation on uncoated surfaces to reproduce typical culture conditions for C2C12, levels of miR-1, miR-133a, miR-206 and Mef-2C were at least 200% higher in C2C12 cells compared to HSkM on corresponding days (Fig. 11). C2C12 exhibited, on average, a 15-fold increase between miR-1 and miR-133a expression on Day 6 compared to Day 0 post-differentiation for both genes. In contrast, levels of these microRNAs in HSkM remained stable and very low compared to C2C12 cells (Fig. 11A-B). MiR-206 reached a plateau of 800-1000 by Day 2 in C2C12 cells, and average of 2.5-times greater expression than HSkM on Day 0. However, in HSkM, miR-206 showed a maximum expression above 350 on Day 4 and declined to less than 70 on Day 8 (Fig. 11C).

MiR-1 represses histone deacetylase 4 (HDAC4), which is a repressor of Mef-2C. Therefore, increases in miR-1 levels promote skeletal muscle differentiation [123]. The levels of the Mef-2C gene in C2C12 increased 14.5-times between Day 0 and Day 4, but remained consistently below 1 in HSkM (Fig. 11D). MiR-1 and Mef-2C gene expression in C2C12 cells were over 40-times higher than in HSkM at all times. Overall, the lower levels of key muscle microRNAs and Mef-2C in HSkM were consistent with reduced levels of differentiation in HSkM relative to C212 cells.

Relative to HSkM cultured on uncoated surfaces in 8% equine serum (Fig. 12, filled squares), HSkM plated onto GFR-MG surfaces in 8% serum (Fig. 12, gray

squares) produced average increases in the levels of miR-1, miR-133a, and miR-206 of at least 14-times compared to uncoated surfaces in 8% serum. MiR-1 levels peaked at Day 6, with levels 26-times that of Day 0, followed by a plateau between 10-20 from Days 6-14; similarly, miR-133a expression peaked at Day 4, with levels 29-times that of Day 0, followed by a plateau in expression around 40 from Days 6-14. MiR-206 levels peaked at Day 4 with expression 28-times that of Day 0, then plateaued at 400 from Day 6-14. Mef-2C did not change much in 8% serum with the addition of GFR-MG coating: levels at Day 14 with and without GFR-MG averaged between 26-27. Overall, GFR-MG presence increased Mef-2C expression an average of 67% that of uncoated HSkM in 8% equine serum-supplemented differentiation medium.

While maintaining 100 µg/mL GFR-MG coating, differentiation medium was changed from 8% to 2% serum. With this change, microRNA levels in the HSkM cultures were compared to GFR-MG in 8% serum (Fig. 12, white squares). For all times, expression increased an average of over 220% between GFR-MG in 2% serum compared to GFR-MG in 8% serum for miR-1, miR-133a, and miR-206. Similar to the previous condition, microRNA expression also exhibited dynamic changes over the measured time of 2 weeks in GFR-MG and 2% serum. MiR-1 showed a 5-fold increase between expression at Day 0 and 6, followed by a drop of 35% at Day 14 compared to Day 6. MiR-133a also peaked at Day 6, followed by a 24% drop in expression from Day 6 to Day 14. MiR-206 increased more than 6-times from Day 0 to Day 10, followed by a 38% drop between Day 10 and 14. Mef-2C increased 6.5-

times between Days 4 and 6, with a sharp 75% decline from Day 6 to 14. For all times studied, Mef-2C levels were an average of 4-fold higher when cultured on GFR-MG and 2% serum compared to the levels for GFR-MG in 8% serum.

To assess whether the serum level also influenced the increased microRNA levels observed with HSkM cultured on GFR-MG, we measured miR-1, miR-133a, and miR-206 expression at Day 8 post-differentiation for HSkM cultured in 2% serum on uncoated tissue treated polystyrene. This condition led to increases in expression for miR-1, miR-133a and miR-206 compared to the uncoated condition in 8% serum: miR-1 increased 4.4-times, miR-133a increased 9.0-times, and miR-206 increased 90.6-times. However, these cells showed markedly lower expression of all three microRNAs compared to conditions with HSkM cultured on GFR-MG and in 2% serum. Due to the elevated levels of miR-1, miR-133a, miR-206, and Mef-2C, subsequent studies with HSkM were conducted using a 100 µg/mL GFR-MG-coated substrate and 2% serum DM.

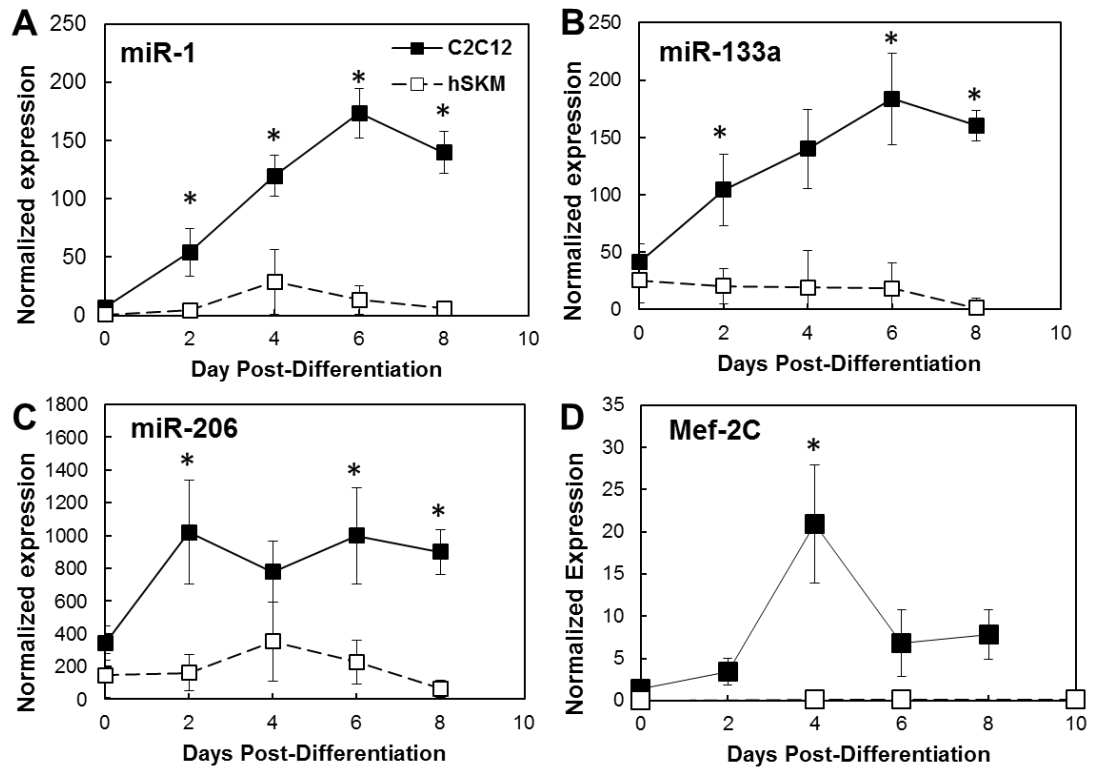


Figure 11. Comparison of microRNA and Mef-2C mRNA levels in mouse C2C12 (reference) and hSKM cells. Under optimal conditions to promote C2C12 differentiation (8% serum and no Matrigel coating of plastic surface), developing C2C12 myotubes had significantly higher expression of miR-1, -133a and 206. Dynamic expression of miR-1 (A), miR-133a (B) and miR-206 (C) from day 0 to day 8 post-differentiation. C2C12 cultures exhibited significantly higher expression of MEF-2C gene at all timepoints than hSKM samples. All error bars denote SEM (n=4); *p<0.05 C2C12 compared to hSKM.[1]

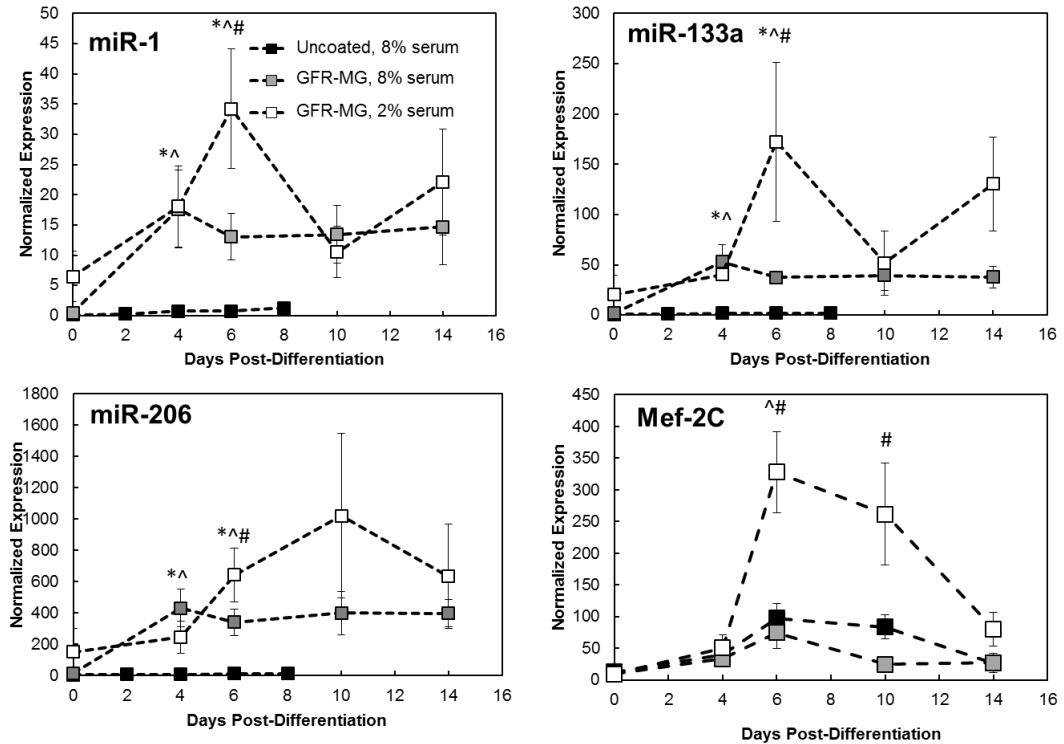


Figure 12. Effect of culture conditions on expression of microRNAs. HSkM cultures were grown on plastic that was either uncoated or incubated with 100 $\mu\text{g}/\text{mL}$ growth factor reduced-Matrigel (GFR-MG) in 2% or 8% equine serum. For all microRNAs, levels were higher under GFR-MG and 2% equine serum conditions (white squares) compared to uncoated, 8% equine serum conditions (black squares) at terminal day ($n=3$). * $p<0.05$ for uncoated, 8% equine serum compared to GFR-MG, 8% equine serum; $\wedge p<0.05$ for uncoated, 8% equine serum compared to GFR-MG, 2% equine serum; # $p<0.05$ for GFR-MG, 8% equine serum compared to GFR-MG, 2% equine serum. [1]

2.3.4. Effect of stretch on HSkM differentiation

We previously found that $\pm 10\%$ cyclic mechanical stretch at 0.5Hz for 1 hour followed by 5 hours of rest for 1 week significantly accelerated C2C12 differentiation [4] and hypothesized that this mechanical stimulation regimen would also enhance HSkM differentiation when applied for 2 weeks (to account for slower differentiation) to confluent monolayers. Cyclic sinusoidal stretch was applied continuously for 14 days after differentiation in both 8% and 2% serum. To facilitate stretch, C2C12 and HSkM were cultured on softer, flexible silastic membranes coated

with 100 $\mu\text{g}/\text{mL}$ GFR-MG (for both static and stretched samples). The decreased substrate rigidity compared to tissue culture plastic can account for differences in microRNA expression of HSkM shown in Fig. 13 relative to Fig. 12. After 14 days of cyclic stretch, HSkM cultures in 8% serum showed an increase of 40% for miR-1 expression and 128% for miR-133a expression ($*p < 0.05$, $n = 6$) compared to HSkM grown statically on GFR-MG-coated membranes in 8% serum. MiR-206 levels increased 20% after stretch in 8% serum (Fig. 13) compared to static control in 8% serum. In 2% serum, all microRNAs showed decreased expression after 14 days of cyclic stretch compared to static controls cultured in 2% serum: miR-1 decreased 36%, miR-133a decreased 55% ($*p < 0.05$, $n = 3$) and miR-206 decreased 53% ($^{\wedge}p < 0.01$, $n = 3$).

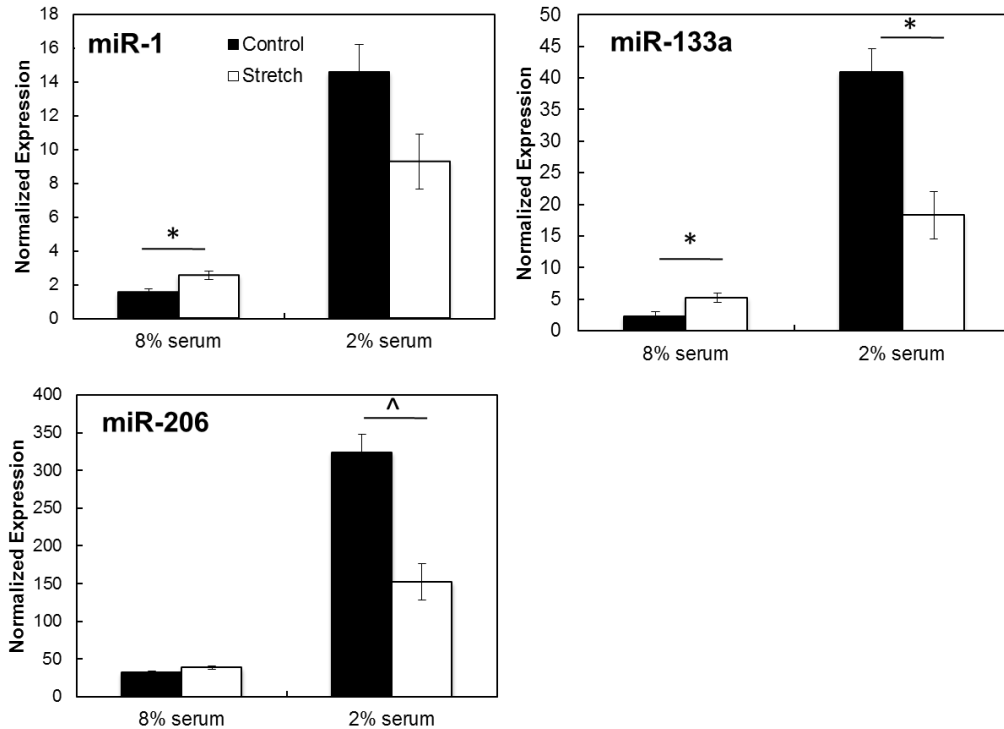


Figure 13. Cyclic Stretch Affects microRNA Levels. Cyclic stretch was applied to HSkM monolayers for 14 days post-differentiation at $\pm 10\%$ strain and 0.5Hz for 1 hour alternating with 5 hours of rest. All studies were conducted on 100 $\mu\text{g/ml}$ GFR-MG-coated flexible membranes. (A) Under conditions of 8% serum, the levels of miR-1 increased significantly ($*p < 0.05$, $n = 6$) after 14 days of stretch. In 2% serum, 14 days of stretch saw a decreasing level of miR-1 compared to static controls. (B) MiR-133a increased significantly after 14 days of stretch in 8% serum ($*p < 0.05$, $n = 6$), but decreased in 2% serum ($*p < 0.05$, $n = 3$). (C) After 14 days of stretch, HSkM cultured in 8% serum rose in miR-206 expression; those cultured in 2% serum fell significantly in miR-206 level ($^{\wedge}p < 0.01$). Error bars denote SEM. [1]

2.3.5. Comparison of microRNA levels in fresh muscle explants and culture HSkM

To assess the effect of culture on HSkM microRNA levels, microRNAs were isolated directly from mature skeletal muscle explants of the *vastus lateralis* from adult human subjects (Table 2) and compared with results obtained *in vitro* at Day 14. Measured microRNA levels from fresh explants ranged from 3-times to over 500-times greater than levels measured with no GFR-MG and 8% serum. With the

addition of a GFR-MG coating prior to culture with 8% serum during differentiation, microRNA levels *in vitro* increased drastically, but were still less than in explant tissue. Interestingly, miR-206 was most affected by the various culture conditions, with *in vitro* expression surpassing that of fresh explants by almost 6 times. In contrast, other measured microRNAs remained below levels in fresh explants. In GFR-MG and 2% serum conditions, microRNA levels further improved; however, the largest increase in expression occurred with the addition of GFR-MG coating (average 14-fold increase over uncoated) compared to a change in serum content (average 2.3-fold increase from 8% to 2% serum).

Table 2. MicroRNA Levels in Explant, C2C12, and HSkM. [1]

miRNA	Fresh Explant	HSkM Static (no MG, 8% serum)	HSkM Static (MG, 8% serum)	HSkM Static (MG, 2% serum)
miR-1	590.9 ± 154.3	1.1 ± 0.3	16.1 ± 8.3	27.2 ± 9.4
miR-133a	708.9 ± 173.8	3.6 ± 1.0	37.3 ± 9.4	130.4 ± 46.7
miR-206	64.2 ± 19.9	21.1 ± 6.1	376.6 ± 45.8	633.4 ± 331.9

2.4. Discussion

In this study, conditions were tested for improved differentiation of primary isolated HSkM myoblasts to form myofibers. The use of 100 µg/mL GFR-MG coating and 2% equine serum-supplemented differentiation media promoted human myoblast fusion and striated fiber formation while elevating levels of myogenic genes miR-1, miR-133a, miR-206, and Mef-2C in human muscle cultured *in vitro*. Further, the addition of antisense miR-133a alone accelerated differentiation in

primary HSkM shown by the increased sarcomeric α -actinin protein expression by 30%; previous studies have needed more than one microRNA to obtain a similar outcome in primary human cells [113].

Murine myoblasts differentiate well under 8% [49], 2% [104], or 1% [120] serum, and even serum-free [124, 125] differentiation media conditions on uncoated surfaces. The decreased serum content in differentiation medium is sufficient to trigger a halt in myoblast proliferation and a shift to myoblast fusion and myofiber formation. Few similar studies have been conducted with human myoblasts; Stern-Straeter et al. reported that gelatin-coated substrates induced higher rates of proliferation in primary isolated human myoblasts compared to non-coated polystyrene and used 2% horse serum in differentiation media [126]. Similar to Stern-Straeter et al., we showed the beneficial myogenic effect of decreased serum content and the addition of Matrigel coating to human skeletal myoblast culture and differentiation; however, the work presented here provides a more in-depth study of human myogenesis by way of microRNA and gene expression levels during HSkM differentiation *in vitro*.

Mouse and human skeletal muscle cell types differ drastically in growth rate, cell size, formation of sarcomeres and substrates required for growth (Figures 6 and 7). This may be due, in part, to the differences between a cell line and primary isolated cells, or due to differences in species. It has been consistently found that human cells proliferate and develop at a slower rate compared to murine cells *in vivo*

and *in vitro* [107]. The slower response of human myoblasts and myofibers may be due, in part, to the extended lifetime of humans. Human lives are, on average, 30-50 times longer than mice – this translates to about 10^5 more cell divisions in our lifetime compared to mice [107]. If human myoblasts doubled at the same rate that murine myoblasts doubled, mathematically, there would be an expected increase in incidence of cancer and other late-onset illnesses. However, on average, 30% of rodents develop cancer at the end of their lifespan (typically 2-3 years), as well as 30% of humans at 70-80 years [107]. The slowed proliferation and differentiation rates of human myoblasts compared to murine myoblasts can be partially attributed to the human body's attempt to protect from rapid ageing, cancer, and other illness.

Other groups had measured the expression levels of microRNAs during a few specific stages of human muscle development: proliferation, differentiation, and mature muscle [112, 113]; provided here is a more detailed time course of the changes in microRNA expression throughout the important process of muscle fusion and fiber formation – showing changes as large as 29-fold over a two week period of myoblast differentiation. Koning et al. report significant downregulation in miR-106b, miR-25, miR-29c, and miR-320c levels between the quiescent human satellite cell stage and fused myotube stage [112]. Additionally, they showed miR-1 and miR-206 relative expression at general points throughout *in vitro* muscle growth: proliferation, confluency, differentiation (5 days after inducing differentiation), and muscle (human biopsy tissue) [113]. The temporal trends of their miR-1 and miR-206

dynamic expression from confluency to differentiation are quite similar to our findings from Day 0-6 post-differentiation showing an increase in microRNA expression. However, they concluded that sole transfection with miR-1 or miR-206 alone was not sufficient to trigger myotube formation [113], an important step in the process of differentiation; we showed here that transfection solely with antisense miR-133a was able to achieve myotube formation.

The results presented in these studies are the first to show the effect of various culture conditions on the expression of myogenic microRNAs during differentiation. Culture conditions clearly have a significant effect on muscle growth, as miR-1, miR-133a, miR-206, and Mef-2C levels increased drastically with the introduction of protein coating and decrease in media serum content. Satellite cells are extremely sensitive to their surrounding environment [127]; we found that the presence of GFR-MG-coated substrate improved the differentiation of these cells by elevating levels of myogenic microRNAs and transcription factors. Lawson and Purslow [125] show significant mouse and rat muscle cell responses to both serum content in media and substrate extracellular matrix coating [125]. Rat L6 cells only formed myotubes in serum-containing media and exhibited higher creatine phosphokinase (CPK) activity when cultured in 2% serum media. In C2C12 cells, however, CPK activity was dependent on both the substrate coating and media serum content [125].

We found that microRNA levels in human myoblasts cyclically stretched respond differently depending on media serum content (Fig. 5). Since microRNA's work in concert to guide myoblast development, there may exist compensatory increases in differentiation signals elsewhere pushing the myoblast towards differentiation. Additionally, cells with such environmental sensitivity may, indeed, respond to stimuli conversely than expected when exposed to different conditions. Carson and Booth [128] have shown that α -actin gene expression in primary chicken myoblasts was dependent on serum availability and static mechanical stretch; cultures underwent 8-20% static stretch in either 10% or 0.5% equine serum conditions. They did not find any difference in α -actin mRNA level for stretched and static samples in 10% serum; however, the levels decreased by 26% for samples stretched in 0.5% serum [128]. Thus far, the effects of serum content on cyclically stretched primary human myoblasts had not been reported. We showed increased microRNA levels after 14 days of cyclic stretch in 8% serum, while stretch in 2% serum led to significant microRNA decreases.

We chose to study microRNAs for their potent effects on myogenesis [129], endogenous presence, and localization to the cytoplasm. The endogenous nature of microRNAs provides an available platform in which to affect myogenesis without the need to introduce foreign bodies, and the localization of microRNA's to the cytoplasm allows for easier access and manipulation than nucleic acids that predominantly reside within the cell nucleus. MicroRNA's exert their effects through

dynamic changes in expression over time, compared to transcription factors that function similar to on/off switches. Since microRNA's can be effectively delivered to the cellular cytoplasm via liposomes and have been shown to exert effects transiently [49], the potential of microRNA's to be used as therapy for individuals with muscular dystrophy or sarcopenia is large. In comparison to constitutive expression, the ability to deliver gene therapy non-virally and transiently is attractive due to lower cell cytotoxicity. However, knowledge of the microRNA expression in normal, healthy muscle tissue is necessary prior to understanding how best to treat disorders caused by their imbalances.

Prolonged increases or decreases in miR-133a expression have been implicated in energy deficit, muscular dystrophy, skeletal muscle hypertrophy, and heart failure [129-133]. This study showed, however, that transient miR-133a inhibition in primary isolated HSkM positively affects the differentiation rate of HSkM *in vitro*, consistent with past findings using C2C12 cells [49]. Transient transfection was utilized as microRNA's demonstrated long retention within HSkM ($t_{1/2} = 92.2$ hours). Overexpression of miR-1 and miR-206 in murine and human cultures [49, 113] led to increased differentiation; however, it was found that both microRNA's must be overexpressed in order to trigger myotube formation *in vitro* [88, 134]. Here, the inhibition of miR-133a alone successfully triggered formation of myotubes and increased sarcomeric α -actinin staining (a measure of differentiation) by 30%.

The delivery and application of transient myogenic microRNA's may be a viable way to enhance the growth and differentiation of engineered skeletal muscle *in vitro* for basic and translational research. The research presented here shows the importance of culture conditions and the potential of microRNA modulation for affecting human myogenesis *in vitro*.

2.5. Chapter Acknowledgements

We would like to thank Dorothy Slentz for her work in developing the primary human myoblast isolation protocol and all her guidance throughout the project, and Yasser El-Abd for being a wonderful teacher and meticulous undergraduate assistant. We also acknowledge the following students for their hard work and dedication to this project: Khanh Bui, Young-Eun Hyun, and Rebecca Harbuck Hughes. We would like to acknowledge funding from the National Institutes of Health (NIH) Pre-Doctoral Training Grant AR055195 and support from the Duke Center for Biomolecular and Tissue Engineering (CBTE).

CHAPTER 3: Joint Inhibition of miR-133a and miR-696 for Accelerated Type I Human Myofiber Differentiation *In Vitro* (Specific Aims 2 & 3)

3.1. Introduction

Engineered functional three-dimensional human skeletal muscle *in vitro* can be used as implantable tissues for diseases and injuries of muscle and serve as a platform for the pre-clinical testing of drugs [71, 135]. The fabrication and growth of three-dimensional tissue-engineered skeletal muscle constructs depends on muscle progenitor cell type, biomaterial scaffold, treatment, and geometry. Engineered three-dimensional human muscle constructs form myofibers *in vitro* [51] and human myofibers spontaneously contract in two-dimensional cultures after co-culture with human motoneurons [44] or after cyclic electrical stimulation for eight hours [136].

To date, contractile activity of three-dimensional engineered human muscle constructs has not been reported. In contrast, functional three-dimensional skeletal muscle constructs using mouse or rat myoblasts produce active contraction without the need for external or supplemental stimuli [49, 137, 138]. Rhim et al. reported statically cultured C2C12 cells in a collagen hydrogel to exert 0.33 ± 0.12 mN of force after 6-8 days of static culture [49]. Engineered 3D muscle cultured with primary rat myoblasts have found even higher forces, above 0.8 mN in peak tetanic force after 10 days of differentiation [79, 137] and even as high as 1.68 ± 0.32 mN for twitch and 2.84 ± 0.5 mN for tetanus for a fibrin-Matrigel hydrogel system seeded with neonatal rat myoblasts [47]. The addition of various stimuli (stretch, proteoglycans, gene therapy, etc.) could further aid in elevation of active contractile forces [49, 79].

Possible reasons for the lack of active force generation by human muscle *in vitro* may be the seeding density of myoblasts into 3D scaffolds or immaturity of engineered skeletal muscle [139]. In comparing seeding densities of 1×10^5 , 2×10^5 , and 4×10^5 muscle-derived cells (MDCs) onto fibrin gels, Martin et al. found that seeding 4×10^5 human myoblasts in 200 μ L exhibit the greatest myoblast fusion index and number of myotubes per microscope field [71].

Muscle maturation can also be promoted by transient regulation of the level of microRNAs. MicroRNAs are short (20-22nt), noncoding RNA strands that act through post-transcriptional regulation of genes [90, 140]. Several microRNAs are extremely important in the regulation of muscle proliferation and differentiation and their overexpression or inhibition can have profound effects on myogenesis [49, 141]. MiR-1 and miR-206 promote myoblast differentiation, and miR-133a promotes proliferation. Koning et al. demonstrated increased myoblast differentiation when miR-1 and miR-206 were transiently overexpressed in primary human skeletal myoblasts [141]. We previously showed that inhibiting miR-133a alone in C2C12 murine myoblasts and primary human skeletal myoblasts significantly accelerate differentiation [49]. Aoi et al. identified stretch-sensitive miR-696, which regulates the expression of an important and potent metabolism co-activator, PGC-1 α . Aoi et al. demonstrated heightened levels of PGC-1 α protein levels in anti-miR-696 C2C12 samples 24 hours after transfection. [101] Heightened expression of PGC-1 α , which

is encoded by the gene [142], has been linked to increased oxidative energy metabolism and type I (slow twitch) myofiber formation [65, 104, 142].

We recently reported that in 2D cultures transient inhibition of miR-133a alone accelerated myogenesis in primary human myoblasts [1], similar to what we observed with mouse myofibers [49]. In the current study, we tested the hypothesis that jointly inhibiting miR-133a and miR-696 simultaneously will lead to accelerated differentiation of 2D and 3D human skeletal muscle bundles with increased type I myofiber expression compared to negative control transfected with vehicle. 2D cultured muscle allowed for the study of proteins and gene expression without the interference of hydrogel protein. 3D engineered muscle was used to demonstrate contractile forces production after electrical stimulation and to observe detailed ultrastructure and morphology in a more native-like environment containing tension and fiber alignment.

3.2. Materials and Methods

3.2.1. Primary HSkM Isolation

Primary human skeletal myoblasts (HSkM) were isolated as presented previously [1]. Briefly, biopsies from the *vastus lateralis* of healthy, middle-aged volunteers were placed in growth medium (GM) containing low glucose (1g/L D-Glucose) Dulbecco's Modified Eagles' Medium (DMEM, Gibo/Invitrogen), 8% heat-inactivated fetal bovine serum (FBS, HyClone), and SkGM Singlequots with insulin removed (Lonza/Clonetics). The biopsy (30-50mg) was placed in Ca and Mg-free

HBSS (Gibco/Invitrogen) and minced into fine pieces. HBSS was removed and replaced with 37°C cocktail containing 0.25% trypsin, 0.1% collagenase, 0.1% BSA, and 0.05% EDTA for 30 minutes with occasional agitation. Proteolytic activity was halted with the addition of FBS in medium. Minced and partially digested tissue was then placed onto an uncoated T25 culture flask for 3 hours to eliminate fibroblasts by adhesion to plastic. Tissue was then transferred to a collagen-coated T25 flask (BD Biosciences) to allow for migration of skeletal myoblasts from tissue to surface. GM was changed every 5 days until flask reached 75% confluency, a process which took approximately 1-2 weeks. HSkM were then passaged into collagen-coated dishes for expansion and frozen or plated for studies. One 30-50mg biopsy yielded 15-20 million cells. Four isolations of HSkM from separate individuals were used for these studies with average purity of $88.0 \pm 6.1\%$ as assessed by desmin staining of 4 donors after thawing frozen cultures.

3.2.2. Cell Culture

Primary HSkM cultures were expanded from 1,500 cells/cm² in uncoated standard tissue plastic flasks at passages 3 to 6 in conditions of 37°C and 5% CO₂. GM was changed every other day until 85-90% confluent in approximately one week. Myoblasts were then trypsinized and plated onto tissue culture plastic 6-well plates coated with 100µg/ml growth factor reduced Matrigel (GFR-MG, BC Biosciences). To promote differentiation of myoblasts to myotubes when near confluence, GM was changed to differentiation medium (DM) consisting of high

glucose DMEM (Gibco/Invitrogen) supplemented with 2% equine serum (HyClone) and 0.1% gentamicin (Gibco/Invitrogen).

3.2.3. MicroRNA Transient Transfection

Single-stranded antisense microRNA molecules specific for the miR-133a (UUUGGUCCCCUUCAACCAGCUG, Applied Biosystems) and miR-696 (GCGUGUGCUUGCUGUGGG, Applied Biosystems) sequence were used with siPORT NeoFX Transfection Agent (Ambion). Anti-miR Negative Control #1 (Applied Biosystems), a single-stranded random microRNA sequence, was used as transfected control.

Transient microRNA transfection was achieved as previously described [1]. Briefly, siPORT NeoFX Agent was diluted with OptiMEM I (Gibco) and mixed with 50nM of single-stranded anti-miR (anti-miR-133a, anti-miR-696, anti-miR-negative control). The transfection mixtures were allowed to incubate in tissue culture flasks at 37°C for 10 minutes to allow for formation of liposomes. Then, HSkM cells and GM were added. Cells were transfected at 37°C and 5% CO₂ for 18 hours, after which cells were rinsed, trypsinized, and plated for studies. Day 0 was denoted at 80% confluency, in which GM was exchanged for DM.

To assess the transfection efficiency and half-life of the anti-miR, Cy3 and FAM dye-labeled anti-miR Negative Control #1 (Applied Biosystems) were used as described above. The transfected HSkM containing Cy3 or FAM labels were viewed

under fluorescence and quantified as the proportion of total cells in the field view was recorded.

3.2.4. Mold Preparation and Sterilization

Molds for Human Bioartificial Muscle (HBAM) bundles were prepared from polydimethylsiloxane (PDMS, Dow Corning Corporation) cast onto a negative mold. Molds for 165 μ l and 45 μ l bundles were prepared.

Molds were sterilized by 60 minutes of sonication in 70% ethanol. Next, they were placed into 6-well plates and allowed to dry in the biological hood under UV light for at least 2 hours. To prevent adhesion of hydrogel to mold, PDMS was soaked in 2% pluronics solution for 20-60minutes at 37C.

Stainless steel minuten pins and small pieces of Velcro were soaked in 70% ethanol for at least 1 hour and allowed to air dry in the biological hood. After aspiration of pluronics solution from PDMS molds, Velcro was pinned into the molds in preparation for muscle bundle application.

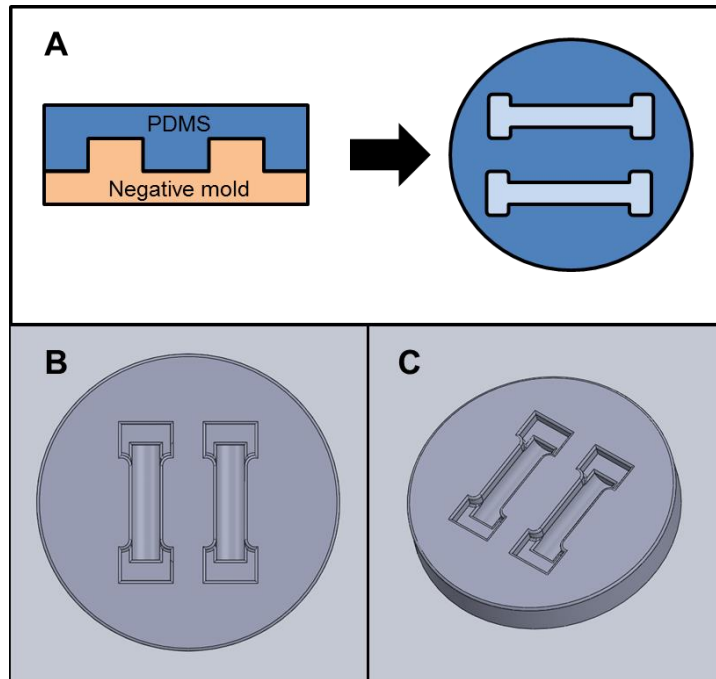


Figure 14. Preparation of PDMS Molds for Engineered 3D human skeletal muscle bundle construction. (A) PDMS was placed onto Negative Mold made of Teflon and allowed to cure. Once cured, PDMS was removed from Teflon negative. (B) Top view of PDMS mold and (C) Side view of PDMS mold.

3.2.5. Engineered 3D Human Muscle Bundle Construction

Three-dimensional human skeletal muscle bundles were constructed using sterilized 45 μ l PDMS molds. Hydrogels were comprised of 20% Matrigel (BD Biosciences), 4mg/ml final concentration of fibrinogen (Sigma), 50U/ml thrombin (Sigma), and transfected HSkM (passage 5-7) at a final density of 5, 10 or 15 $\times 10^6$ cells/ml. The solution was allowed to gel at 37C and 5% CO₂ for 1 hour before addition of GM. At 48 hours post-seeding, all gels had compacted and appeared opaque. At this time, GM was exchanged for DM (Day 0); DM was exchanged every 48 hours for the 2-week culture period.

3.2.6. Immunofluorescence

To assess for the presence of striations, as an indicator of muscle maturity, and type I and II myofibers, samples were fixed at 14 days post-differentiation with 100% ice-cold methanol for 5 minutes and then rinsed 3 times with PBS. They were then blocked in 3% BSA in 0.05% TBST/PBS overnight with gentle rocking. Primary antibodies for mouse sarcomeric α -actinin (1:800, Sigma), slow myosin heavy chain (1:300, AbCam, reacts only with human adult type I skeletal muscle fibers), and fast myosin heavy chain (1:300, AbCam, reacts with human and mouse type IIA, IIX/B skeletal muscle fibers) were diluted in 3% BSA in 0.05% TBST/PBS and incubated overnight with gentle rocking. Samples were then rinsed with PBS and incubated with secondary antibody (Alexa Fluor, 1:250, Invitrogen) and Hoechst stain (1:1000, Invitrogen) for 45 minutes at room temperature with gentle rocking. Samples were thoroughly rinsed with PBS and viewed with a Zeiss 510 inverted confocal microscope. Confocal images were taken at varying depths throughout the muscle bundles. Resulting images were assessed with ImageJ software for fiber diameter, percent of nuclei in fibers (fusion index), and myofiber type. For fiber diameter measurements, 4 measurements were taken per field of view, and 3 fields of view were taken for each condition. Images were also assessed with ImageJ for pixels stained for sarcomeric α -actinin by installing the “Color Pixel Counter” plugin. The plugin was used to quantify pixels stained, then divided by total pixels per field of

view to calculate area fraction of myofibers. This area fraction was used to quantify area containing fibers, then used to calculate specific force per fiber area.

3.2.7. Quantitative Real-Time PCR of Mef-2C and PPARGC1A

For 2D experiments at days 6 and 14 after onset of differentiation and from 3D at day 14 after onset of differentiation, total mRNA was isolated from samples using the Aurum Total RNA Mini Kit (Bio-Rad). RNA concentration and quality were measured using the NanoDrop ND-1000 spectrophotometer (NanoDrop). For RNA expression, cDNA was prepared using the iScript cDNA Synthesis Kit (Bio-Rad) following manufacturer's instructions. Primers for Mef-2C, PPARGC1A, and GAPDH (endogenous control) were custom ordered (IDT) for the following sequences: Mef-2C Forward ACTTCCTGGAGAAGCAGAAAGGCA, Mef-2C Reverse AACACGTTTCCTTCTTCAGCACGC, PPARGC1A Forward TGTGCAACTCTCTGGAAGT, PPARGC1A Reverse TGAGGACTTGCTGAGTGGTG, GAPDH Forward TCAACAGCAACTCCCCTCTTCCA, GAPDH Reverse ACCCTGTTGCTGTAGCCGTATTCA.

3.2.8. Western Blot

Western blots were performed to determine the presence of sarcomeric α -actinin and mitochondria in 2D cultures. At Day 14, cells were harvested with a cell scraper and lysed using CellLytic-M (Sigma) and Protease Inhibitor Cocktail (Sigma). Protein concentration was assessed using the BCA Protein Assay Kit (Pierce). 15 μ g

of protein was loaded into each lane on a 12% Ready Gel Tris-HCl Precast Gel (Bio-Rad) for SDS-polyacrylamide gel electrophoresis. Following, all protein was transferred from the gel onto a nitrocellulose membrane with 0.45 μm pore size (Invitrogen). The membrane was blocked for 30 minutes in 5% nonfat milk in Tris-Buffered Saline with 0.1% Tween 20 (TBST) with gentle rocking at room temperature. Primary antibodies for mouse sarcomeric α -actinin (1:2500, clone EA-53, Sigma), mouse anti-human 60 kDa glycosylated mitochondrial protein (1:2500, MTC02, AbCam), mouse PGC-1 α (1:2000, Calbiochem) and mouse β -actin (1:1000, Santa Cruz Biotechnology) were diluted in TBST solution containing 3% BSA and incubated with the membrane overnight at 4°C with gentle rocking. All antibodies reacted with the human antigens, as specified per manufacturer's protocols. After rinsing the membrane to remove unbound antibody, the membrane was incubated with goat anti-mouse HRP secondary (1:2500, Invitrogen) in TBST containing 3% BSA for 30 minutes at room temperature with gentle rocking. Residual antibody was washed and immunoreactive bands were detected by luminography using Supersignal chemiluminescent substrate (Pierce). Band density was determined by densitometry after scanning onto autoradiographic films (Kodak) and evaluated by ImageJ software. Protein expression is reported as normalized intensity of the band of interest to the band of the reference protein (β -actin).

3.2.9. Measurement of Contractile Force

At Day 14 post-differentiation, muscle bundles were removed from PDMS molds and pinned into a custom chamber and immersed in 37°C DM. Bundles were pinned to a fixed tissue anchor at one end and a PDMS holder suspended by the force transducer (custom-made by Dr. Robert Dennis, University of North Carolina, Chapel Hill, NC, USA) at the other end. Positioning of the force transducer was controlled by a motorized linear actuator (Thorlabs). A pair of parallel platinum foil electrodes applied the electrical stimuli to suspended bundles to elicit isometric muscle contractions. (Figure 15)

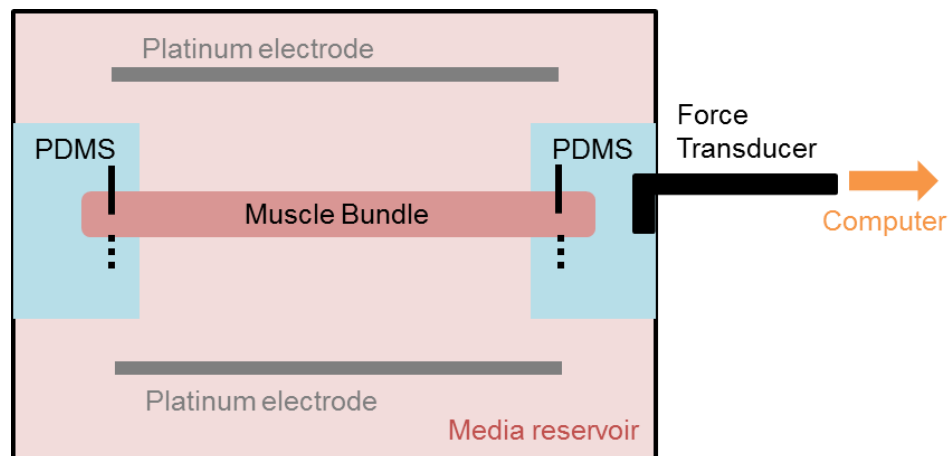


Figure 15: Schematic of isometric force testing setup. Muscle bundles were pinned into reservoir with media at 37°C. Bundles were pinned at the left to a PDMS anchor point and on the right to a force transducer. Platinum foil electrodes were used to stimulate bundles with 100V at various frequencies for 2 msec.

Using the motorized linear actuator, the initial length of the engineered muscle bundle was set to the length of culture (8 mm). Force output was recorded for electrical stimuli at 1, 5, 10, 20, and 40Hz and 100V. Measurements were repeated

for 5% increments up to 120% of initial construct length. Force traces were recorded into LabVIEW and exported to Microsoft Excel files.

For analysis, Microsoft Excel files were loaded into a custom made MATLAB program and peak forces found for each frequency and length condition. Photos taken at 100% length prior to force testing were assessed in ImageJ for muscle bundle cross-sectional area; specific forces were calculated by dividing force output (mN) by cross-sectional area (mm²).

The MATLAB code used for analysis is attached in Appendix C.

3.2.10. Statistical Analysis

Data are presented as mean \pm standard error (SEM) unless otherwise noted. ANOVA and Fisher's PLSD post-hoc tests were performed using STATVIEW 5.0 statistical analysis package. HSkM isolated from separate individuals were considered distinct *n* values. A value of $p < 0.05$ was considered significant.

3.3. Results

3.3.1. Transient Transfection Efficiency and Lifetime of MicroRNA's

The transfection efficiency of HSkMs receiving Cy3- 1 and FAM-labeled negative control anti-miRs was $90.6 \pm 2.3\%$ (Figure 16) and the transfection efficiency with one microRNA was $94.4 \pm 2.9\%$. These efficiencies were not significantly different. Using a polynomial fit, single microRNA transfection had a half-life of 105.2 ± 0.7 hours (% transfected = $-5E-5(\text{hours})^2 + 0.0008(\text{hours}) + 0.9416$, $R^2 = 0.9923$, $n = 3$) and joint microRNA transfection had a half-life of 104.1 ± 0.6 hours (% transfected = $-3E-$

$5(\text{hours})^2 - 0.0014(\text{hours}) + 0.9235$, $R^2 = 0.9623$, $n = 3$). The half-lives of single and joint microRNA transfection were not significantly different.

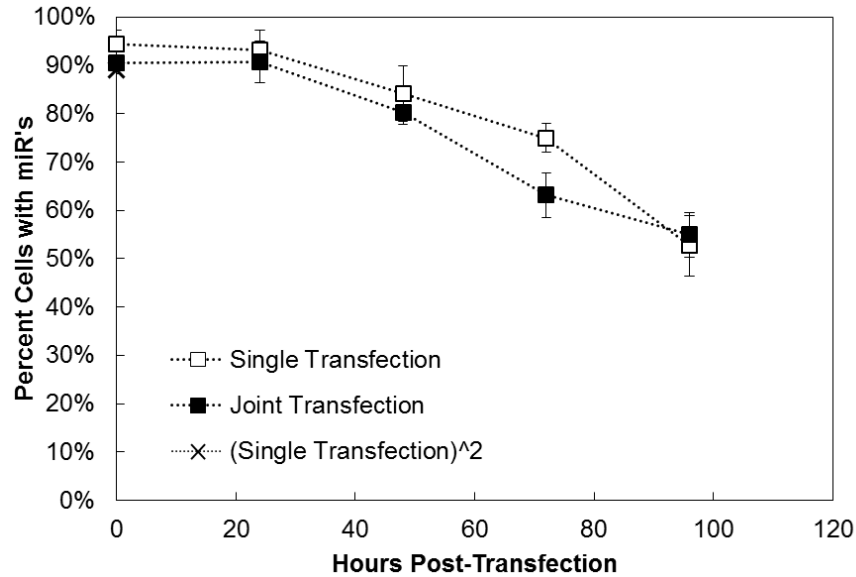


Figure 16: Transfection efficiency and lifetime of exogenous microRNA. Single transfection with one fluorescently-tagged microRNA shows $94.4 \pm 2.9\%$ initial efficiency after 18 hours of incubation of HSkM with microRNA and half-life of 102.3 ± 0.7 hours (white squares). Joint transfection with two microRNA's shows $90.6 \pm 2.3\%$ initial efficiency after 18 hours of incubation of HSkM with microRNA's and half-life of 97.7 ± 0.6 hours (black squares).

Mathematically, the efficiency of joint transfection is equal to the square of single transfection efficiency. This was calculated to be 89.1% efficiency (marked in Figure 16 with "X"), slightly lower than 94.4% efficiency with one microRNA. The measured efficiency was, in fact, very close to this value: 89.1% calculated efficiency vs. 90.6% measured efficiency.

3.3.2. *MiR-133a and MiR-696 Inhibition in 2D Cultures Accelerates Myogenesis and Affects PGC-1 α*

HSkM differentiation was examined after plating on GFR-MG and shifting to DM for 14 days, duration previously found to produce prominent striations

demonstrating tissue maturity [143]. Western blot analysis of sarcomeric α -actinin expression at day 14 post-differentiation showed significant differences between joint inhibition samples and negative control (Fig. 17A and 17B, * $p < 0.05$, $n = 4$). Joint inhibition samples presented over 55% more sarcomeric α -actinin protein normalized to reference β -actin as compared to negative control. Based on the expression of a 60 kDa non-glycosylated protein component of mitochondria, there was no significant difference in mitochondrial presence at 14 days post-differentiation between tested microRNA inhibition treatments. Consistent with our prior results in mouse and human myotubes [1, 49], inhibiting miR-133a promotes myotube maturation. These results of sarcomeric α -actinin presence indicate an interaction between miR-133a and miR-696 in the development of skeletal muscle tissue, as individual effects were not significant but joint effects were significant. Further, there may be a possible additional role of miR-133a on downstream transcription factors that affect the oxidative metabolism pathway.

Since miR-696 negatively regulates expression of PGC-1 α protein [101], Western blots were performed for PGC-1 α , which should increase with the inhibition of miR-696. Relative to negative control anti-miR-133a, anti-miR-696, and joint inhibition conditions all showed significantly increased protein expression of PGC-1 α (Figure 17C). Treatment of myoblasts with anti-miR-133a caused over 65% increase in PGC-1 α expression, anti-miR-696 showed over 80% increase in expression, and joint inhibition showed over 70% increase in expression over

negative control PGC-1 α expression (Fig. 17D, * $p < 0.05$, # $p < 0.005$, $n = 3$). While treatment of myoblasts with either anti-miR-133a or anti-miR-696 did not affect the levels of PPARGC1A gene relative to negative control, joint inhibition of anti-miR-133a or anti-miR-696 caused PPARGC1A levels to increase over 2-times the levels found in negative control samples ($p < 0.05$, $n = 3$, Figure 18), suggesting an interaction between anti-miRs that affects not only the protein, but also the gene that encodes PGC-1 α .

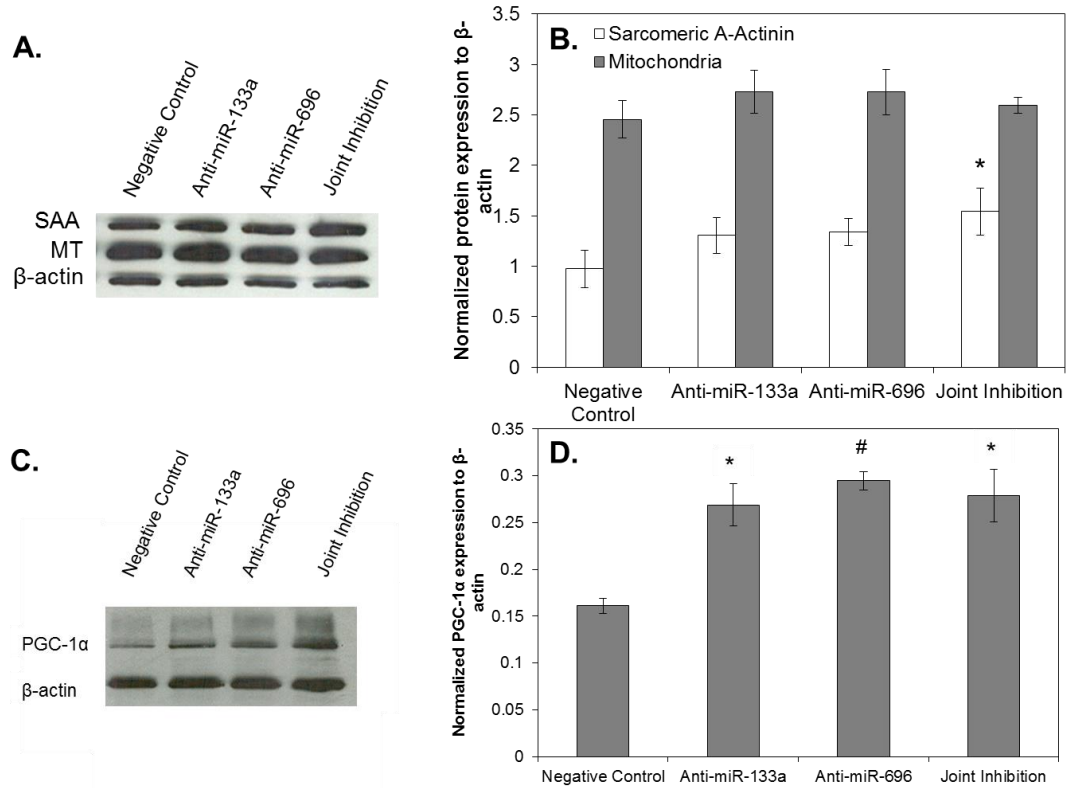


Figure 17: Sarcomeric α -actinin and mitochondria presence in 2D cultures. (A) Western blot for sarcomeric α -actinin (SAA) and mitochondrial protein showed significant increase in SAA with joint inhibition of miR-133a and miR-696 compared to negative control. There was no difference in mitochondrial protein expression between transfection conditions. β -actin was used as reference for normalization of protein expression. (B) Densitometry of SAA and MT normalized to β -actin showed significantly higher SAA in joint inhibition compared to negative control ($n=4$, $*p<0.05$) and no change for MT. (C) Western blot for PGC-1 α with β -actin as reference protein. (D) Densitometry of PGC-1 α protein normalized to β -actin and negative control showed significant increases in expression for anti-miR-133a, Anti-miR-696, and Joint Inhibition, compared to negative control. ($*p<0.05$, $\#p<0.005$, $n=3$)

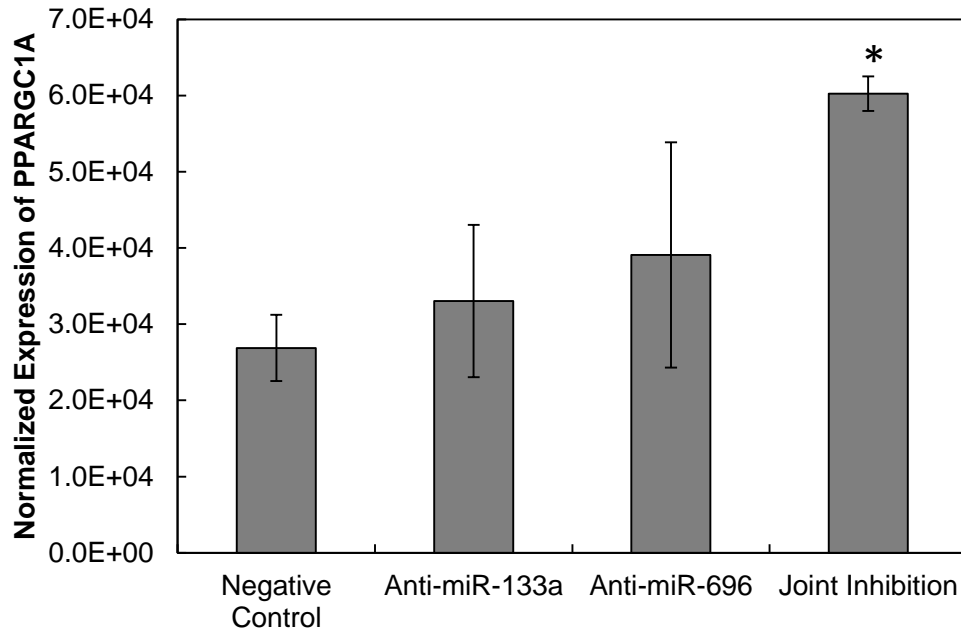


Figure 18: Expression of PPARGC1A gene at Day 14 post-differentiation. Joint transfection samples showed significantly increased expression of PPARGC1A gene compared to negative control. Results were normalized to housekeeping gene GAPDH (* $p < 0.05$, $n = 3$). Error bars denote SEM.

Due to the observed increases in PGC-1 α expression with anti-miR transfection, immunofluorescence for slow and fast myosin heavy chain, corresponding to Type I and Type II fibers, respectively, was used to visualize the distribution of fibers within 2D human skeletal muscle culture 14 days post-differentiation to see downstream effects of this elevated metabolism co-activator. There was no apparent difference between the staining of slow and fast myosin in both proportion of fibers stained as well as intensity of staining at day 14 post-differentiation (Figure 19). Proportion of fibers positive for fast myosin heavy averaged $91.9 \pm 2.9\%$, and proportion of fibers positive for slow myosin heavy

averaged $86.9 \pm 3.9\%$ between all conditions, including negative control. Most human skeletal muscle fibers co-expressed both slow and fast myosin protein isoforms, consistent with previously reported *in vitro* [144-146] and *in vivo* [18, 29] findings. Edom et al. found similar distribution of culture human skeletal myofibers isolated from the masseter: 94.4% of fibers expressed fast myosin heavy chain and 95% expressed slow myosin heavy chain after 4 days of differentiation [146]. Similarly, studies using satellite cells isolated from human quadriceps found 95.2% positive for fast myosin heavy chain and 91% positive for slow myosin heavy chain after 4 days of differentiation [146]. There was no significant difference between myofiber density and nuclei in fibers between all conditions.

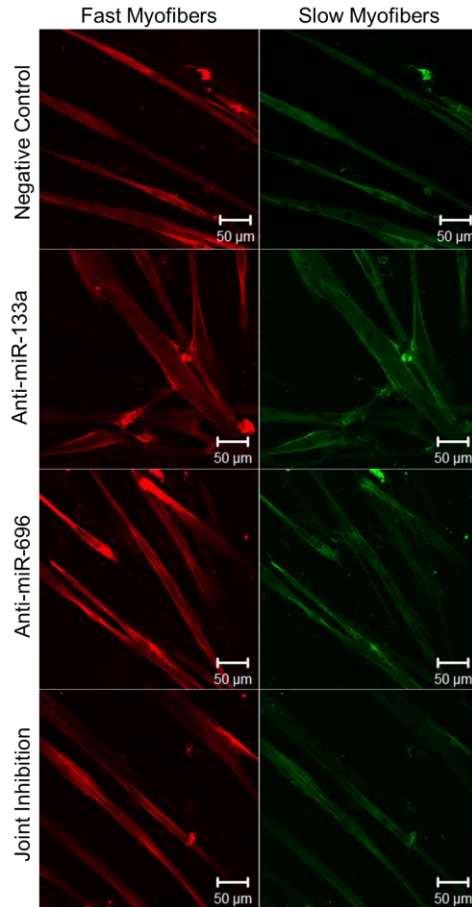


Figure 19: Fiber Type in 2D Engineered Human Skeletal Muscle. Immunofluorescence for fast (red) and slow (green) myofibers did not show any difference in intensity or proportion of image stained. Scalebars at 50 μm .

3.3.3. Functional Three-Dimensional Human Skeletal Muscle Bundles

Results with human myotubes in 2D culture suggest that miR-133a and miR-696 inhibition of myogenesis should affect skeletal muscle *function*. We hypothesized that a 3D tissue engineered human skeletal muscle bundle seeded with anti-miR-treated HSkM and cultured in a fibrin-based hydrogel under static conditions could exert active contraction forces under isometric force testing. Since the seeding density of skeletal myoblasts into a 3D scaffold or hydrogel affects maturation of muscle and generation of force [71, 147, 148], we examined seeding densities from 5×10^6 HSkM myoblasts/mL 15×10^6 HSkM/mL. While a seeding density of 5×10^6

C2C12/mL was sufficient to produce contractile forces after electrical stimulation in a collagen-based gel [48], HSkM muscle bundles with 5×10^6 cells/mL repeatedly did not elicit forces when subjected to electrical stimulation at various frequencies (Figure 19A). Consistent with this result, confocal imaging of immunostained bundles showed negligible myoblast fusion and little organization (Figure 20).

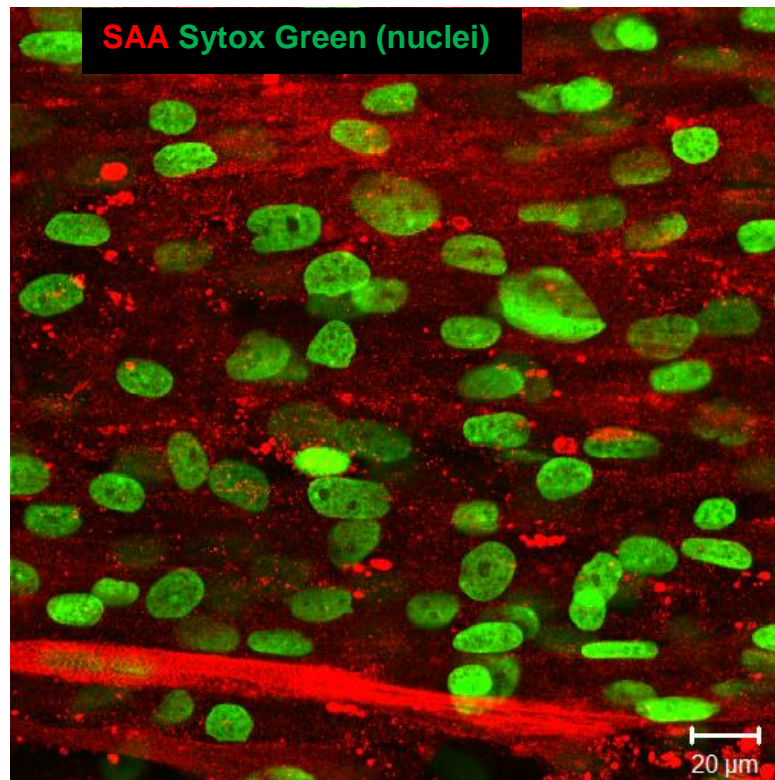


Figure 20: Engineered human skeletal muscle bundles with 5×10^6 cell/mL. Constructs seeded with 5×10^6 HSkM/mL consistently showed little fusion and organization. Sarcomeric α -actinin shown in red and nuclei shown in green.

Bundles seeded with 10×10^6 HSkM/mL exhibited fusion and striations of myofibers when subjected to immunofluorescence (Figure 21). Furthermore, these muscle bundles produced contractile forces after electrical stimulation (Fig. 22A-B). Muscle bundles containing 15×10^6 HSkM/mL generated 33.2% and 15.8% greater

forces compared to 10×10^6 HSkM/mL bundles at 10 and 20 Hz frequencies, respectively (Fig. 22B, $*p < 0.05$, $n = 3$). Furthermore, engineered human muscle exhibited the characteristic force-length relationship of native muscle: magnitude of force output increased with percent length of engineered constructs (Fig. 22C). We observed little decline in force after the peak, which may be attributed to the low level of force generated in our engineered constructs. Subsequent studies were conducted with 15×10^6 HSkM/mL in fibrin/Matrigel bundle system. Thus, there appears to be a threshold of HSkM seeding density into fibrin-based muscle constructs that allows for functional force output by engineered muscle.

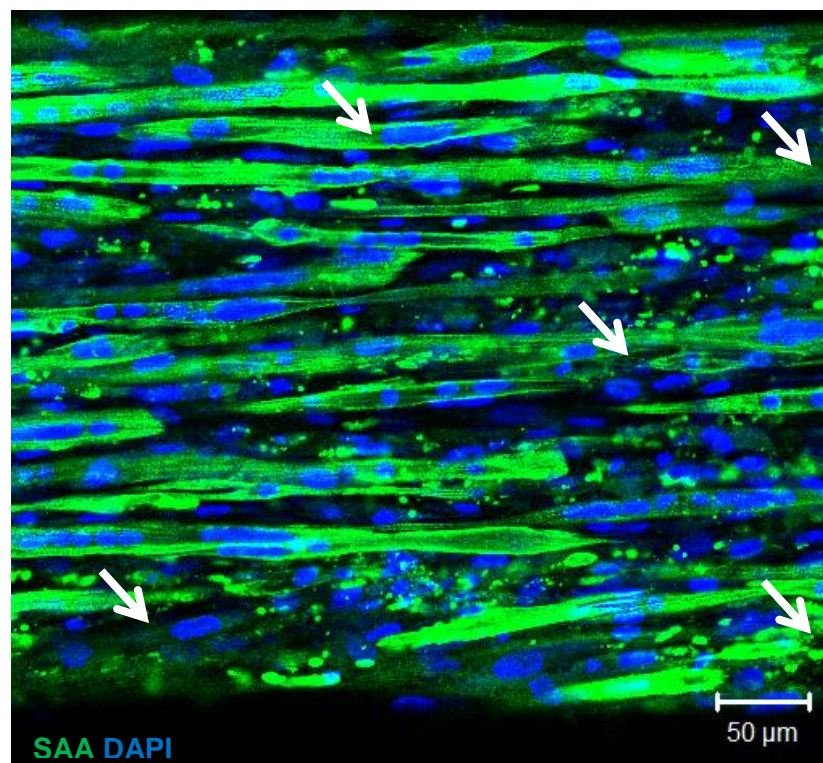


Figure 21: Human skeletal muscle bundle ultrastructure in 3D cultures seeded with 10×10^6 cells/mL. Immunofluorescence for sarcomeric α -actinin (SAA, green) and Hoechst (blue) show myofibers aligned to the direction of tension with striations (arrows). Image taken at 40X magnification.

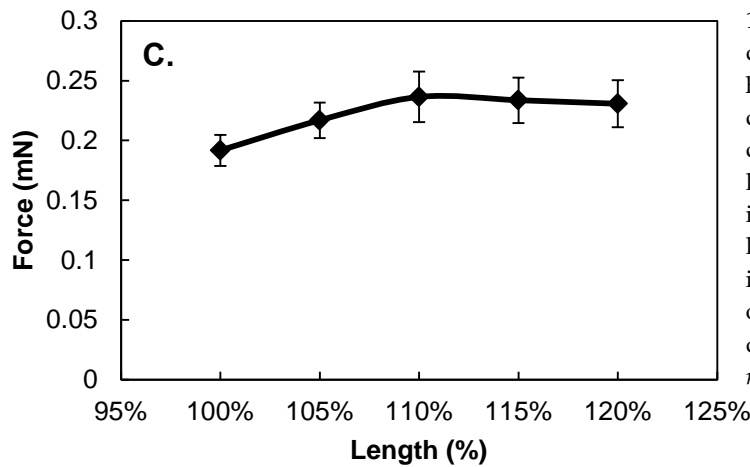
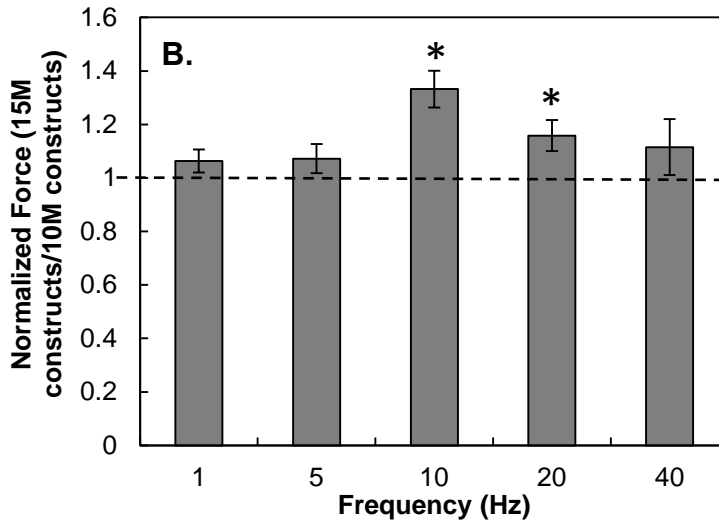
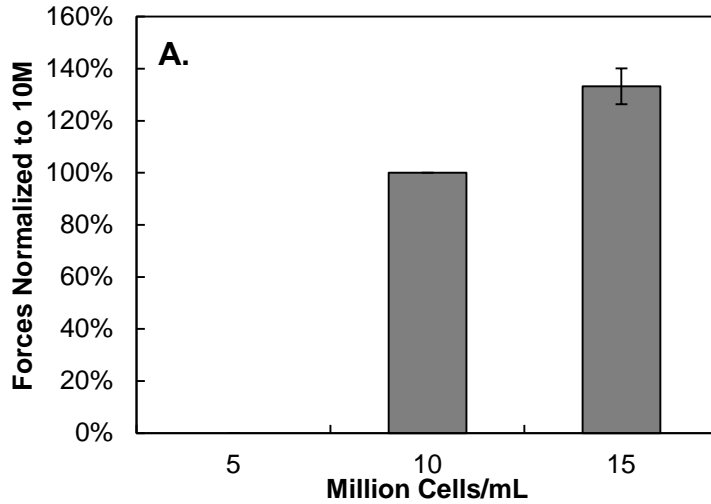


Figure 22: HSkM seeding density for muscle bundles.

Bundles were seeded with 5×10^6 HSkM/mL, 10×10^6 HSkM/mL, and 15×10^6 HSkM/mL and cultured statically for 2 weeks. (A) Bundles seeded at 5×10^6 HSkM/mL did not return forces. Bundles seeded with 10×10^6 HSkM/mL and 15×10^6 HSkM/mL did exhibit force output at 10 Hz and 100V, with forces at 15×10^6 HSkM/mL significantly higher than those at 10×10^6 HSkM/mL ($n=3$, $p<0.05$). (B) Functional force testing showed significantly higher specific force output at both 10 Hz and 20 Hz for constructs seeded with 15×10^6 HSkM/mL. All frequencies measured showed increased specific forces with 15×10^6 HSkM/mL seeding density. (C) Engineered human skeletal muscle construct exhibit characteristic force-length curves, with increasing length leading to slight increases in force output. All error bars denote SEM. (* $p<0.05$, $n=3$)

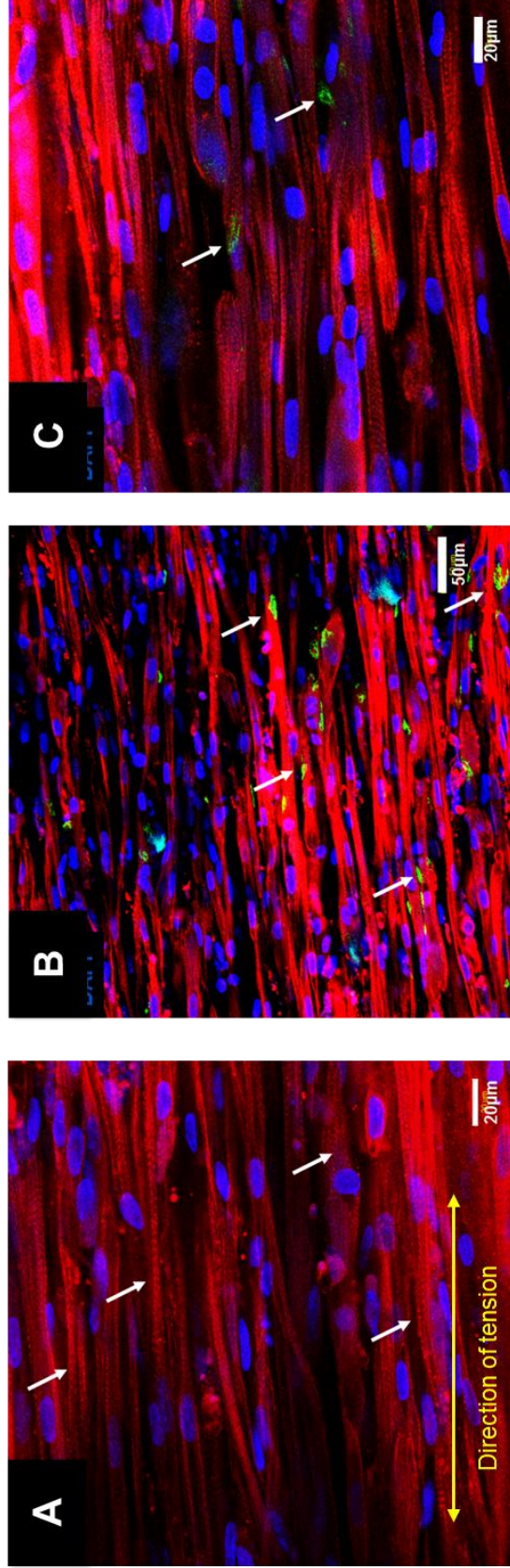


Figure 23: Human skeletal muscle bundle ultrastructure in 3D cultures. (A) Immunofluorescence for sarcomeric α -actinin (SAA, red) and Hoechst (blue) show myofibers aligned to the direction of tension with striations (arrows). Image taken at 40X magnification. (B-C) Immunofluorescence for SAA and α -bungarotoxin (BTX, green, arrows) for acetylcholine receptors (AChR) show presence of AChR and aligned, striated myofibers (red). (B) Image taken at 20X magnification. (C) Image taken at 40X magnification

To assess the maturation of engineered skeletal muscle, bundles were fixed and stained for sarcomeric α -actinin, acetylcholine receptors, and nuclei. Constructs showed high density of aligned myofibers containing striations (Fig. 23A-C, striations denoted by arrows). Myofibers were aligned with the direction of tension, which was generated through attachment to Velcro anchor points at each end of the PDMS mold. Functional force output in innervated tissue necessitates the presence of machinery for the propagation of an action potential, notably acetylcholine receptors (AChR) [149, 150]. Although the engineered muscle is not innervated, the formation of AChR *in vitro* is a sign of muscle proper development and maturity. In native tissue, AChR are clustered in mature muscle fibers in the postsynaptic membrane at the neuromuscular junction [151]; here, the presence of these receptors *in vitro* indicates myofiber maturity within the engineered bundles.

Immunofluorescence for acetylcholine receptors showed their presence at the periphery of myofibers within the engineered muscle; however, they appeared to occur infrequently (Fig. 23B-C, arrows).

3.3.4. Effect of MicroRNA-133a and/or -696 Inhibitors upon 3D Human Skeletal Muscle Bundles

Compaction of hydrogels is a cell-mediated process [152, 153], resulting from tension produced by cells aligned along the longitudinal axis of the construct [153, 154]. The extent of fibrin gel compaction depended upon the microRNA treatment administered to HSkM prior to bundle seeding. Anti-miR-133a constructs were 22.4

$\pm 6.1\%$ thinner than the negative control (Fig. 24A, $p < 0.05$, $n = 3$). Joint inhibition led to $36.8 \pm 3.4\%$ thinner constructs compared to negative control ($p < 0.005$, $n = 3$).

Interestingly, myofiber diameters did not differ between various microRNA conditions. While adding the anti-miR did reduce the diameter of the 3D constructs, myofibers within engineered muscle constructs did not differ in diameter based upon microRNA treatment. Constructs made with HSkM that received the negative control contained myofibers were $14.3 \pm 3.7 \mu\text{m}$ in diameter, anti-miR-133a constructs contained myofibers with a diameter of $16.0 \pm 3.4 \mu\text{m}$, anti-miR-696 constructs contained myofibers with a diameter of $13.7 \pm 4.4 \mu\text{m}$, and joint inhibition constructs contained myofibers with a diameter of $13.9 \pm 3.3 \mu\text{m}$. Myofiber diameters between all microRNA treatments were not different; however these diameters were lower than those reported in 2D most likely due to the spreading of myofibers on the substrate in 2D compared to suspension of fibers in the hydrogel in 3D.

To further assess ultrastructure of the bundles, the fusion within the bundles was quantified by counting proportion of nuclei within sarcomeric α -actinin-stained myofibers. The average percent of nuclei in fibers (fusion index) for negative control bundles was $61.9 \pm 3.5\%$ nuclei in fibers. There was no significant difference between the negative control and anti-miR treatments, as all conditions fell in the range of 60-70% nuclei in fibers ($n = 3$). Fiber density was significantly higher in anti-miR-133a constructs compared to negative control constructs ($p < 0.05$, $n = 4$, Figure 24B).

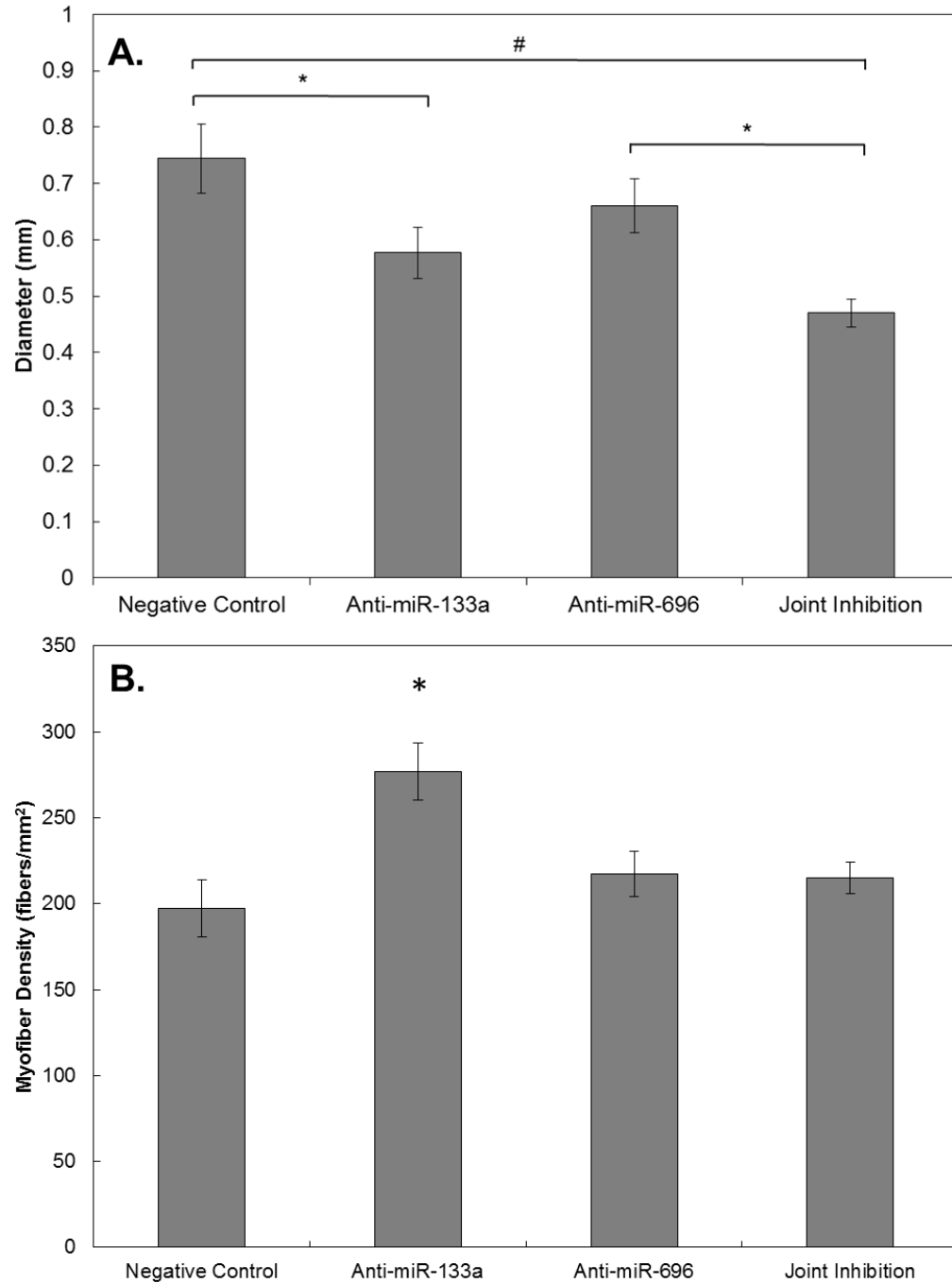


Figure 24: Bundle diameters and fiber density. (A) Engineered muscle bundles were measured for diameter at 2 weeks post-seeding. Negative control bundles were significantly thicker than Anti-miR-133a ($n=3$, $*p<0.05$) and Joint inhibition bundles ($n=3$, $\#p<0.005$). Joint inhibition bundles were significantly thinner than Negative Control and Anti-miR-696 bundles ($n=3$, $*p<0.05$). (B) Sarcomeric α -actinin-stained human skeletal muscle bundles were analyzed by ImageJ for density of fibers per area. Anti-miR-133a bundles exhibited the highest density of fibers compared to negative control ($*p<0.05$, $n=4$). All other conditions were not statistically different in fiber density.

After 2 weeks of culture, isometric force testing of twitch forces was conducted over the range of various length elongations: 100-120% in increments of 5%. This allowed us to study the force-elongation relationship of the engineered muscle bundles and verify that it is behaving similarly to native tissue. Additionally, measurements of passive force were taken to assess the contribution of ECM to the overall force production and determine whether the anti-miR treatments affected fibroblast function which might explain the different levels of compaction. Increased passive force generation has been correlated with increased ECM presence in both native and 3D engineered tissues [47, 155-158]. Active force amplitudes exhibited the characteristic force-elongation relationship in which forces increase around the optimal length elongation and decrease at shorter and longer lengths (Figure 25). Joint inhibition bundles exhibited significantly higher active forces per elongation for twitch and tetanus than negative control ($p < 0.0001$, $n=4$), anti-miR-133a ($p=0.0004$, $n=4$), and anti-miR-696 ($p=0.0002$, $n=4$). The magnitudes of active force amplitude changes, however, were not large, which may be due to the low forces generated by tissue-engineered skeletal muscle compared to native muscle.

Passive forces exhibit a characteristic force-length relationship that is exponential with increasing length elongation [159]. Our range of length elongation led to an approximately linear relation with force output due to shorter deformations of the tissue. Figure 28 shows the measured passive forces for microRNA-treated

muscle bundles. ANCOVA analysis of linear regression slopes did not show any significant difference between rates of passive force amplitude change with increasing construct elongation, indicating that there is likely no significant difference in ECM content between microRNA treatments. Additionally, the increased forces produced by joint inhibition engineered muscle bundles are likely not due to presence of ECM, but the differentiated muscle itself.

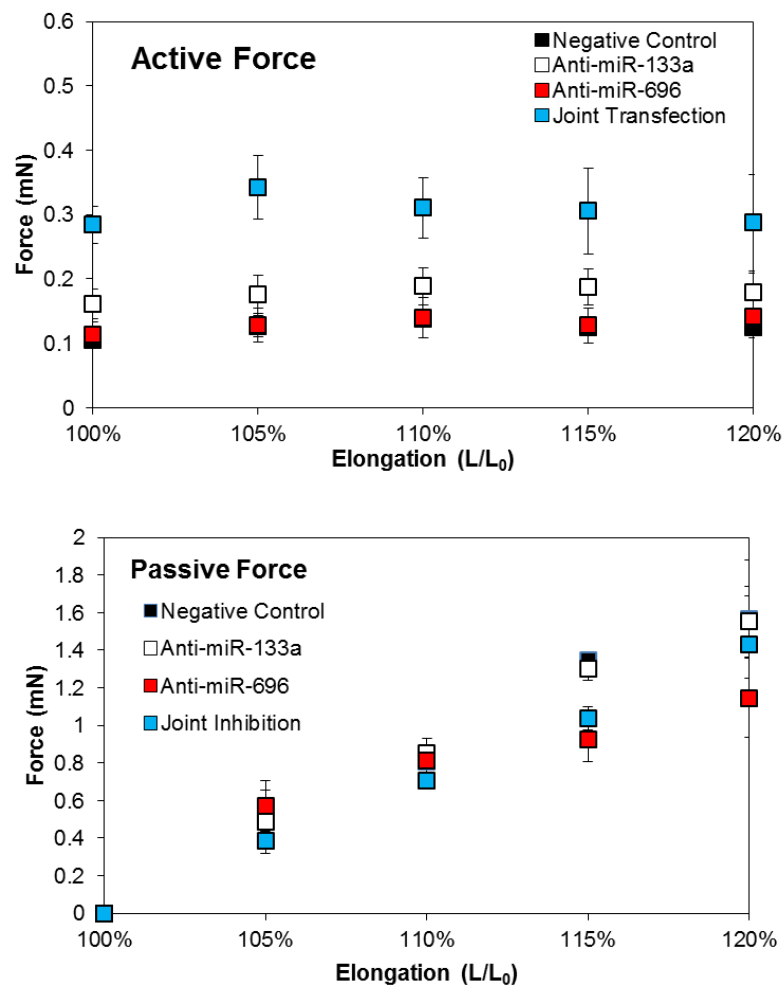


Figure 25: Active and passive forces generated by engineered human skeletal muscle. Both active and passive forces measured exhibited characteristic force-elongation relationship. Active forces were maximal within optimal length elongation. Passive forces linearly increased with increasing force elongation. Error bars denote SEM.

Muscle bundles derived from myoblasts that were transfected with both anti-miR-133a and anti-miR-696 exhibited increases in twitch and tetanic forces compared to other conditions: over 130% compared to negative control ($p < 0.005$ twitch, $p < 0.0001$ tetanus, both $n=4$, Figure 26), over 65% compared to anti-miR-133a ($p < 0.005$ twitch, $p < 0.0001$ tetanus, both $n=4$), and over 120% compared to anti-miR-696 bundles ($p < 0.005$ twitch, $p < 0.0001$ tetanus, both $n=4$). Bundles with anti-miR-133a HSkM showed over 35% increase in tetanic force relative to the negative control ($p < 0.05$, $n=4$). These bundles also gave over 40% higher active tetanic forces compared to anti-miR-696 bundles ($p < 0.05$, $n=4$). Magnitudes of twitch force and tetanus force (20 and 40 Hz) were used to calculate tetanus-to-twitch ratio (TtR). All TtR fell in the range of 2.0-2.5, and there was no significant difference in TtR between all tested bundle conditions.

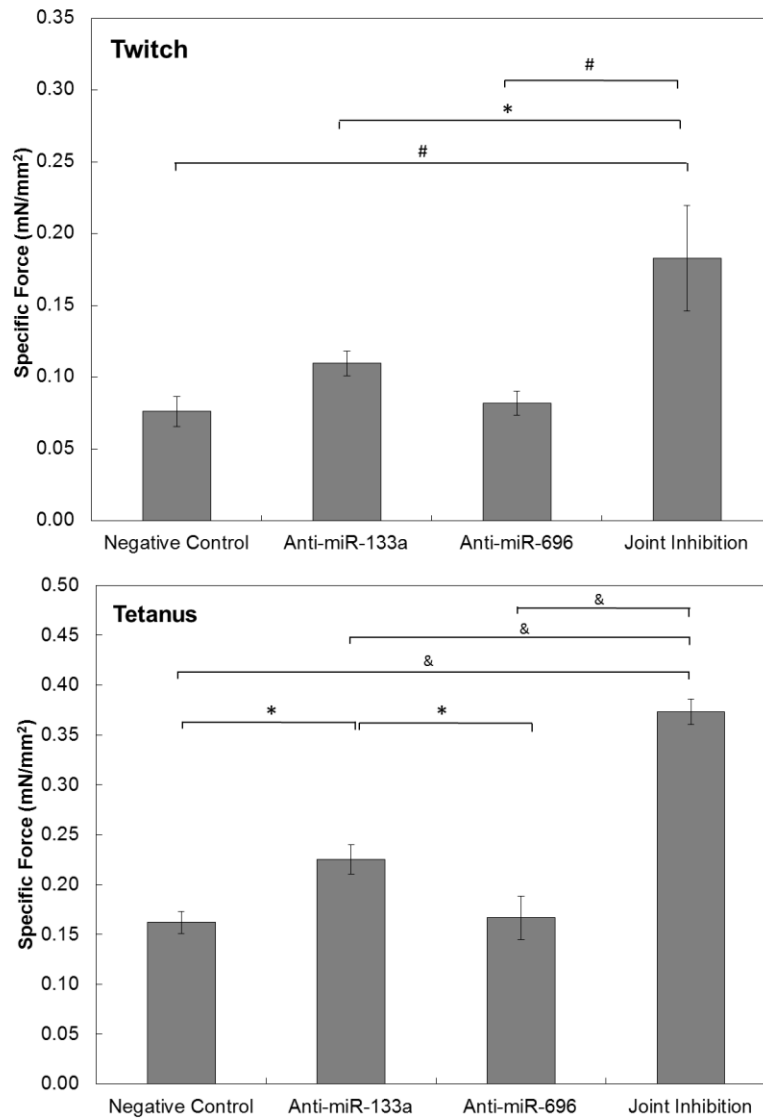


Figure 26. Isometric force testing of muscle bundles. Functional force output was measured after excitation with 100V electrical impulses at various frequencies. Twitch forces were recorded at 1 Hz and tetanic forces between 10-40 Hz frequencies. Anti-miR-133a bundles gave significantly higher tetanic forces compared to negative control (* $p < 0.05$, $n = 4$) and anti-miR-696 (* $p < 0.05$, $n = 4$). Joint inhibition demonstrated significantly higher twitch and tetanic forces compared to all other transfection conditions (* $p < 0.05$, # $p < 0.005$, & $p < 0.0001$, $n = 4$). Error bars denote SEM.

Area fraction of fibers was quantified by ImageJ to estimate proportion of area containing fibers and proportion of area of ECM of images taken at varying depths throughout the bundle. There was no significant difference between area fraction of fibers for conditions tested: negative control contained $58.4 \pm 8.3\%$ of the total area occupied by fibers, anti-miR-133a contained $68.2 \pm 7.4\%$ of the total area occupied by fibers, anti-miR-696 contained $63.9 \pm 7.0\%$ of the total area occupied by fibers, and joint inhibition contained $61.5 \pm 8.2\%$ of the total area occupied by fibers ($n=4$ for all). While force per fiber area is most accurately calculated utilizing measurements from transverse cross-sections of the muscle bundle, the area fraction quantified here may provide an informative estimate. Using the calculated area fraction of fibers and specific force results per bundle presented above, we calculated the force produced by fiber area for each microRNA treatment condition. This analysis was important as it accounts for variables of extracellular matrix area and discrepancies in muscle fiber density between microRNA treatments. Calculating force per cross-sectional area allows for better comparison with published work. Although we did not measure cross-sectional area occupied by fibers, area fractions are equivalent to volume fraction for thin sections of tissues. Therefore, the area fraction in the longitudinal direction is a good approximation to the area fraction of fibers in the cross-section.

From this analysis, we found that while anti-miR-133a bundles produced significantly higher tetanus specific forces than negative control and anti-miR-696

bundles, the myofiber density of anti-miR-133a bundles was higher than other conditions. This led to equal twitch force per fiber cross-sectional area produced by individual fibers between negative control, anti-miR-133a, and anti-miR-696 (Figure 27). Additionally, tetanus force per fiber cross-sectional area amplitudes for negative control, anti-miR-133a, and anti-miR-696 individual fibers were equal as well. Joint inhibition conditions saw significant increases in specific force amplitudes per fiber area over all other conditions. Twitch and tetanus force amplitudes per fiber area saw over 2-times increase in magnitude between joint inhibition and all other conditions (* $p < 0.05$ compared to negative control, # $p < 0.05$ compared to anti-miR-133a, ^ $p < 0.05$ compared to anti-miR-696, $n = 4$ for all). Therefore, the increase in anti-miR-133a bundle tetanus forces may be partially attributed to the increased fiber density within the engineered constructs. These forces per fiber saw a range of 1.4-1.8-times increase in specific force compared to specific force per bundle, due to the area fraction containing myofibers. The low specific force of individual myofibers estimated from studies with small bundles suggests that engineered muscles are failing to reproduce the differentiated state found *in vivo*. Individual myofibers from engineered small bundles of rodent muscle have been reported to exert 0.69 ± 0.13 mN/mm² [160], individual myotubes on cantilevers exerted 0.94 mN/mm² [161], and 3D aligned muscle bundles exerted 0.80 ± 0.15 mN/mm² [162]. Our studies found specific forces from human muscle to fall within this range: 0.61 ± 0.02 mN/mm² at tetanus in the joint inhibition condition.

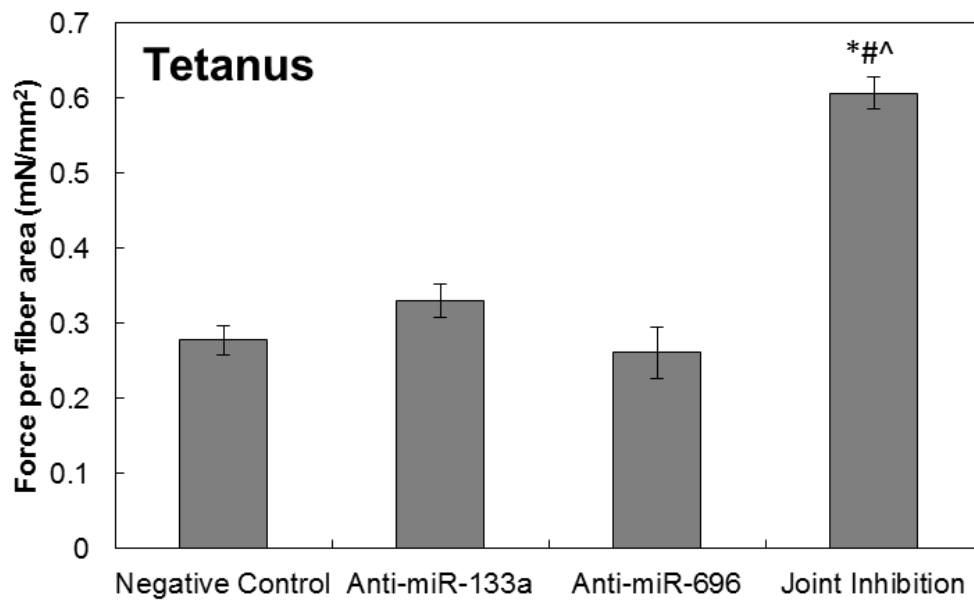
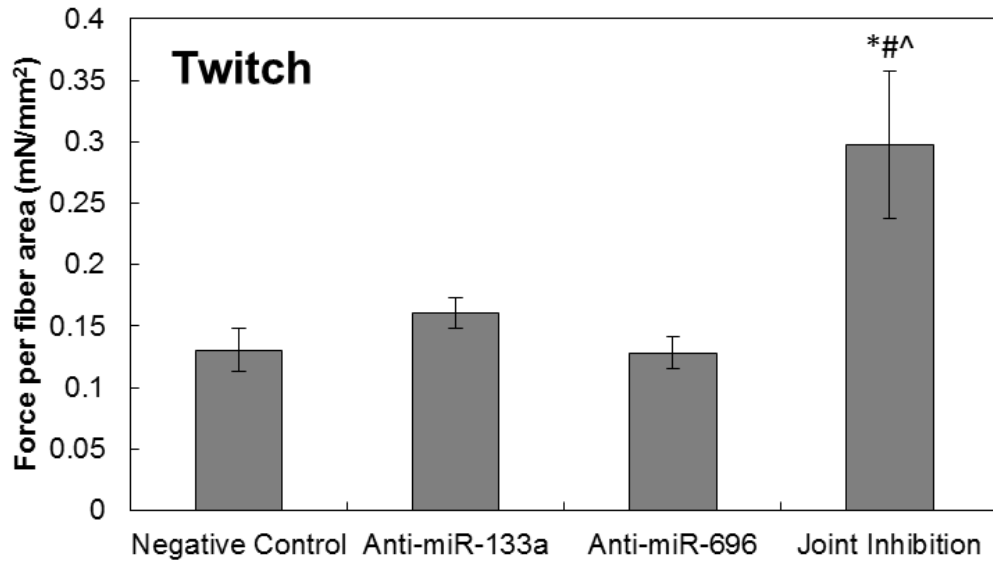


Figure 27: Specific force per muscle fiber area. Twitch and tetanus specific forces normalized to fiber area showed significantly higher forces in joint inhibition conditions compared to all other conditions. The forces reported here are comparable to those reported in literature for engineered muscle [160-162]. * $p < 0.05$ compared to negative control, # $p < 0.05$ compared to anti-miR-133a, ^ $p < 0.05$ compared to anti-miR-696, $n = 4$ for all

We next examined whether microRNA treatments on human muscle bundle contraction affected contraction kinetics by measuring time to peak twitch (TPT), half relaxation time ($\frac{1}{2}$ RT), and time to tetanus (TT). No difference was observed between TPT and TT kinetics: TPT ranged from 160-190 msec for all conditions, and TT ranged from 1100-1125 msec for all conditions. However, $\frac{1}{2}$ RT demonstrated a larger range, from 260-320 msec. In fact, negative control bundles took 10.4% longer to reach half relaxation compared to anti-miR-696 treated constructs ($p < 0.05$), Anti-miR-133a treated bundles took 17.6% longer to reach half relaxation than anti-miR-696 treated bundles ($p < 0.0005$), and anti-miR-696 bundles reached half relaxation 13.9% faster than bundles treated with both anti-miR-133a and anti-miR-696 ($p < 0.01$) (Figure 28).

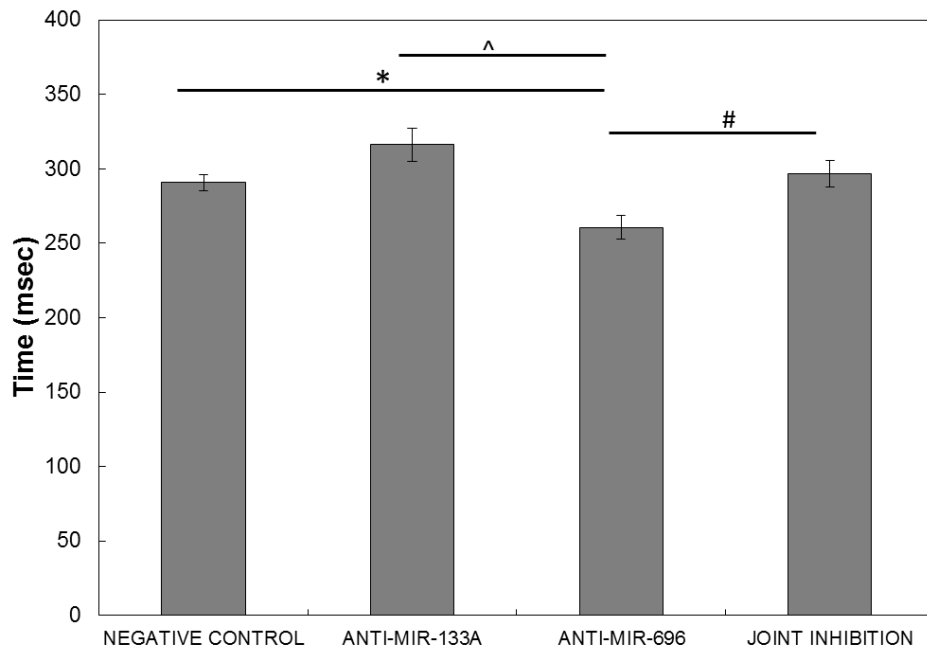


Figure 28. Half Relaxation Time. Measurements of half relaxation time showed significantly decreased time for miR-696 inhibition bundles compared to all other conditions: Negative Control, miR-133a Inhibition, and Joint Inhibition. * $p < 0.05$, # $p < 0.01$, ^ $p < 0.0005$, all $n = 3$.

Studies of microRNA transfection in 2D showed a change in gene expression of PPARGC1A. In 3D, real-time qPCR was also used to assess the presence of slow and fast myosin heavy chain within engineered 3D human skeletal muscle tissues at day 14 post-differentiation. Following 2D results which showed increased PPARGC1A gene expression levels at day 14 for the joint inhibition condition, it was expected that joint transfection in 3D would lead to increased slow myosin heavy chain gene expression. Instead, heightened expression of slow myosin heavy chain was measured for anti-miR-133a (over 2-times compared to negative control, $p < 0.05$, $n=3$) and anti-miR-696 (almost 3-times compared to negative control, $p < 0.005$, $n=3$) bundles only, with slow myosin heavy chain gene levels falling significantly in joint inhibition samples (Figure 29A). Slow myosin heavy chain gene levels fell over 60% between anti-miR-133a bundles and joint inhibition bundles ($p < 0.05$, $n=3$) and over 70% between anti-miR-696 bundles and joint inhibition samples ($p < 0.005$, $n=3$). Fast myosin heavy chain showed over 2-times higher expression in anti-miR-696 conditions compared to negative control ($p < 0.05$, $n=3$, Figure 29B) and over 3-times higher expression in joint inhibition conditions compared to negative control ($p < 0.05$, $n=3$). Ratios of slow:fast myosin heavy chain gene expression fell over 80% between anti-miR-133a bundles and joint inhibition bundles ($p < 0.05$, $n=3$, Figure 29C) and over 75% between anti-miR-696 bundles and joint inhibition bundles ($p < 0.05$, $n=3$).

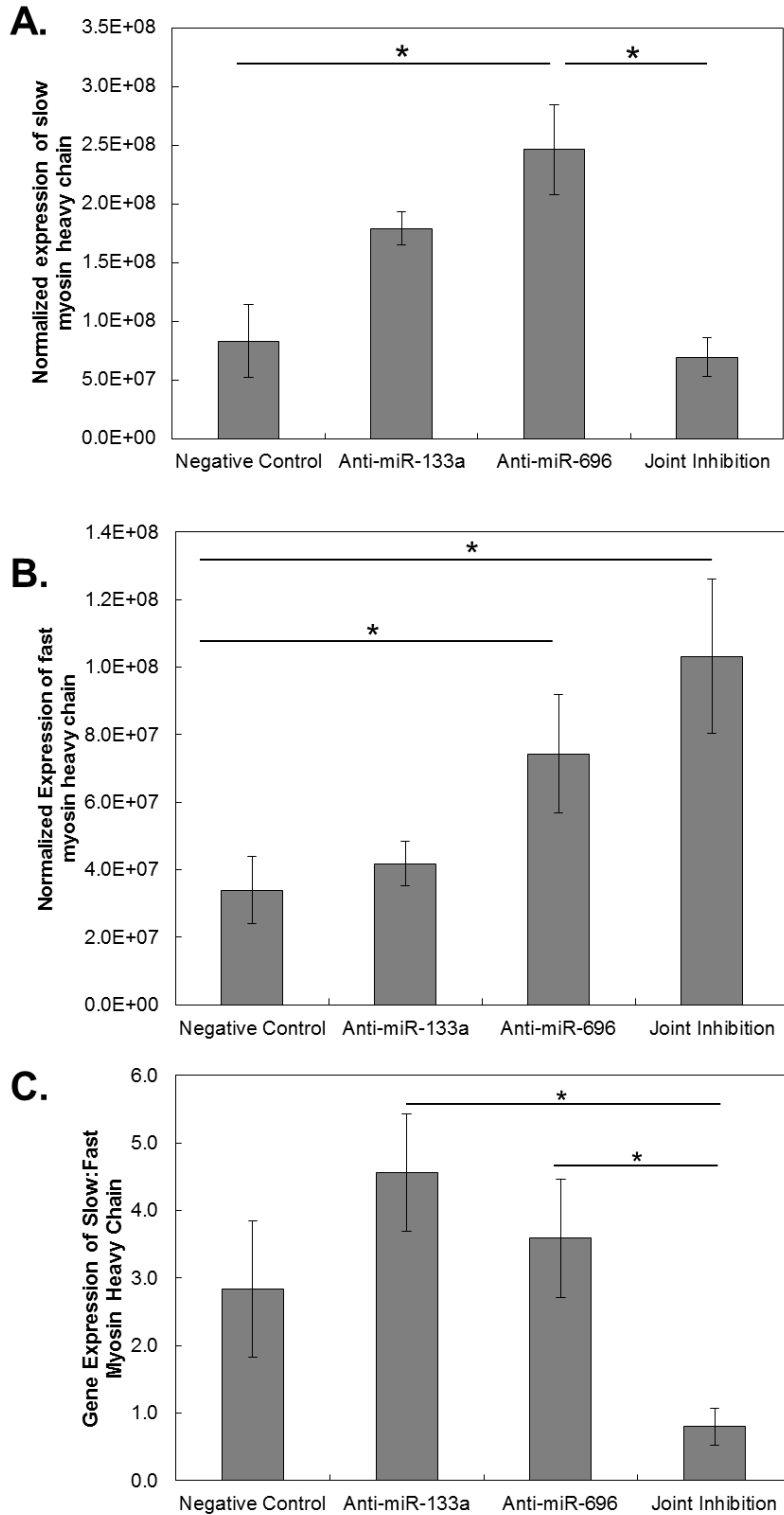


Figure 29: Myosin heavy chain presence. (A-B) Total RNA isolated from engineered human skeletal muscle bundles treated with various miR inhibitors was used for real-time qPCR for slow and fast myosin heavy chain. (A) Slow myosin heavy chain showed significantly higher ratios for anti-miR-696, compared to negative control and joint inhibition conditions (* $p < 0.05$, $n = 3$). Error bars denote SEM. (B) Fast myosin heavy chain showed significantly higher expression in anti-miR-696 and joint inhibition conditions, compared to negative control (* $p < 0.05$, $n = 3$). Error bars denote SEM. (C) Ratios of slow:fast myosin showed significantly higher ratios for anti-miR-133a and anti-miR-696, compared to joint inhibition (* $p < 0.05$, $n = 3$). Error bars denote SEM.

While immunofluorescence for slow and fast myosin heavy chain did not show a difference in percent of fiber stained (92-97% slow and 90-100% fast), assessment of stain intensity did support PCR findings. Slow myosin heavy chain stain intensity showed highest values for anti-miR-133a over negative control and joint inhibition conditions ($p < 0.05$, $n = 3$, Fig. 30A). Anti-miR-696 bundles showed over 60% higher slow myosin staining intensity compared to negative control ($p < 0.05$, $n = 3$). Immunofluorescence for fast myosin heavy chain (Type II myofibers) showed over 65% increase in stain intensity for joint inhibition compared to negative control, over 55% increase in stain intensity compared to anti-miR-133a, and over 40% increase in stain intensity compared to anti-miR-696 ($p < 0.05$ for all, $n = 3$, Figure 30B). Figure 30C show representative immunofluorescence images for slow and fast myosin heavy chain staining. These findings indicate that proportion of Type II fibers may be higher when miR-133a and miR-696 are simultaneously inhibited, compared to negative control and each anti-miR individually.

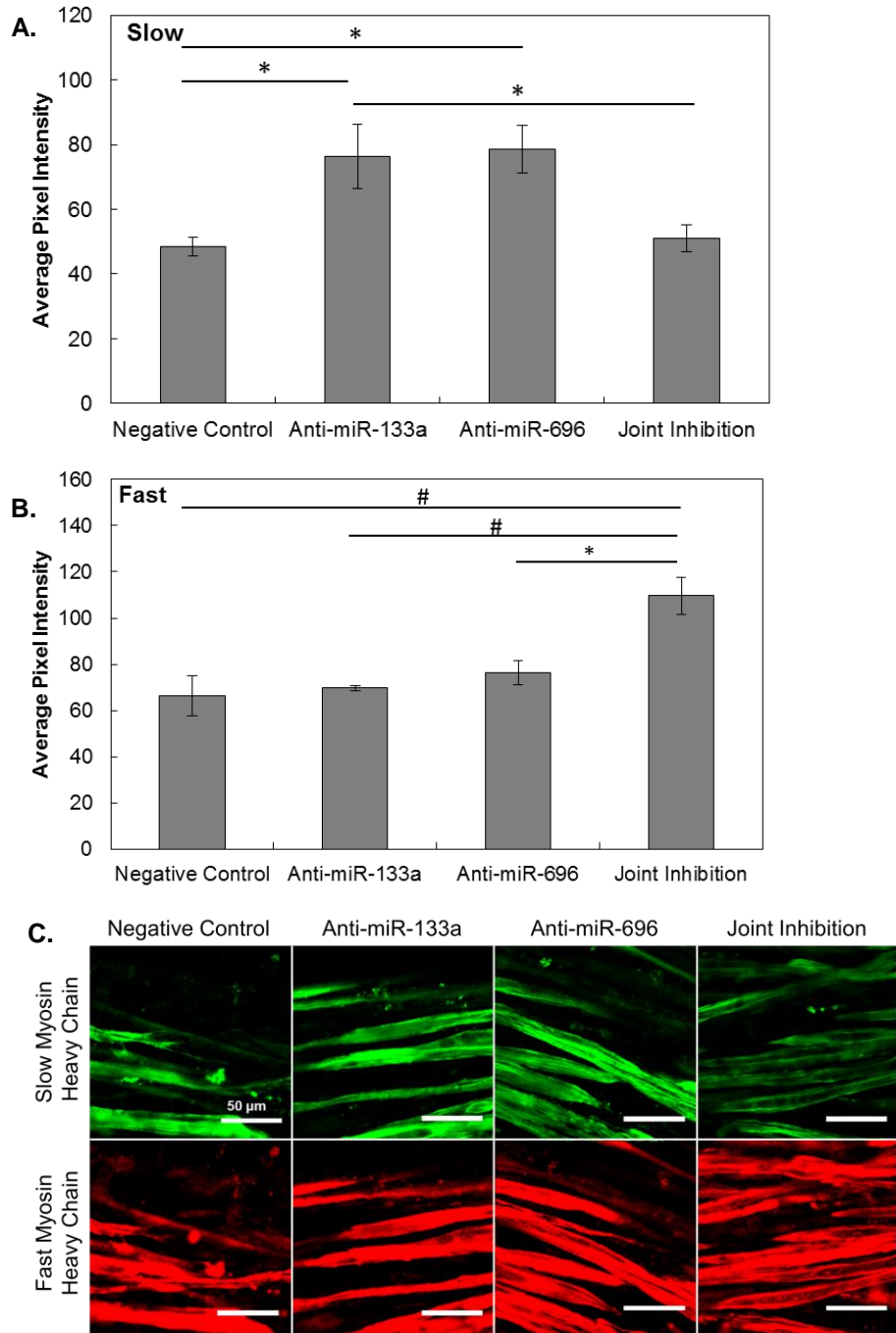


Figure 30: Immunofluorescence for slow and fast fibers. (A-B) Immunofluorescence for slow and fast myosin heavy chain was analyzed for pixel intensity. Images for slow myosin showed increased intensity in anti-miR-133a samples ($*p < 0.05$, $n = 3$). Images for fast myosin showed increase intensity for joint inhibition ($*p < 0.05$, $\#p < 0.005$, $n = 3$). Error bars denote SEM. (C) Engineered human skeletal muscle bundles treated with various miR inhibitors were stained for slow (green) and fast (red) myosin heavy chain. Anti-miR-133a and Anti-miR-696 showed highest proportion of fibers and intensity of stain positive for slow myosin heavy chain antibody. Joint inhibition showed the least slow myosin heavy chain staining and most intense fast myosin heavy chain compared to all other conditions. All other conditions stained similarly for fast myosin. All scalebars are 50 μm . 106

Mef-2C is an important transcription factor involved in the activation of PGC-1 α and the further development of oxidative metabolism as well as the onset of myogenesis. Mef-2C gene expression levels were measured in engineered muscle bundles to assess any correlation of the transcription factor with the distribution of muscle fiber type. Mef-2C levels were over 20-times higher in anti-miR-133a condition compared to joint inhibition ($p < 0.05$, $n = 3$, Figure 31).

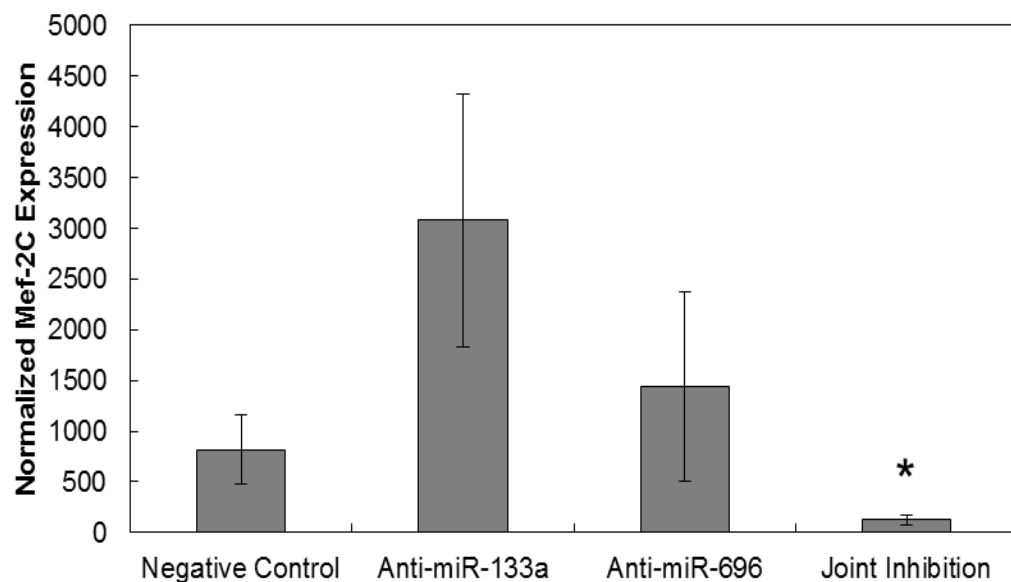


Figure 31: Mef-2C expression of engineered human skeletal muscle. After 2 weeks of culture, Mef-2C gene expression was measured by qPCR. Expression was normalized to GAPDH and reference total mouse embryo RNA. Joint inhibition constructs exhibited significantly lower expression of Mef-2C compared to anti-miR-133a constructs after 2 weeks. (* $p < 0.05$, $n = 3$ for all)

3.4. Discussion

In this study, we successfully induced contraction of engineered three-dimensional muscle bundles by increasing the cell density and promoted differentiation by inhibition of miR-133a and miR-696. While inhibition of miR-133a and miR-696 separately promoted differentiation, when these two microRNAs were

inhibited simultaneously, 2D engineered human skeletal muscle *in vitro* showed over 55% increase in presence of sarcomeric α -actinin protein and over 70% increase in PGC-1 α protein 14 days after onset of differentiation compared to negative control. In 3D engineered human skeletal muscle, joint inhibition of miR-133a and miR-696 led to 153% higher peak specific forces when subjected to electrical stimuli.

We used microRNAs for the modulation of human skeletal muscle myogenesis and metabolism due to their potent effects on myogenesis [129], endogenous presence, and localization to the cytoplasm [1]. The endogenous presence of microRNAs allows for their modulation without the need of introducing viral vectors, and the localization of microRNAs to the cytoplasm allowed for easier access and manipulation of nucleic acids that reside primarily within the cell nucleus [1]. MicroRNAs can be effectively delivered to the cytoplasm using liposomal transfection, which holds great potential as therapy for individuals with muscular dystrophy or sarcopenia. The ability to deliver gene therapy nonvirally and transiently, as opposed to constitutively, is advantageous due to lower cell cytotoxicity [163]. While microRNA transfection is transient in nature, our studies found that the half-lives of single and joint microRNA inhibition are over 4 days, enough time for anti-miRs to exert their effects on myofiber development.

While our cultures are predominantly composed of human skeletal myoblasts, there still exists some infiltration of fibroblasts. In fact, fibroblasts have been shown to help stabilize engineered muscle tissue and produce important ECM

[55]. Thus, it is important to consider the effects of anti-miR transfections on not only skeletal myoblasts, but on fibroblasts as well. Duisters et al. reported that levels of miR-133 were 15-fold higher in rat cardiac myocytes compared to rat fibroblasts [164]; therefore, inhibition of miR-133a would most likely leave the fibroblasts unaffected due to the low endogenous levels of this microRNA. Furthermore, there exists no literature quantifying the levels of miR-696 in fibroblasts – likely owing to the low endogenous levels as well.

These results are the first to show active contractile forces in response to electrical stimulation of static 3D tissue-engineered human skeletal muscle. Our fibrin-based muscle bundles are not subjected to mechanical conditioning or electrical stimulation during the culture period – rather, myogenesis occurs over the course of 2 weeks in a controlled, static environment. Similar to the results of Mudera et al. [147], we did find a drastic difference in specific force output when constructs were seeded at different cell densities. Mudera et al. found that 30×10^6 primary isolated human skeletal myoblasts seeded into a 5 mL compliant collagen gel construct produced the highest passive force contraction: $1372 \pm 313 \mu\text{N}$ compared to $622 \pm 254 \mu\text{N}$ for 20×10^6 cells and $926 \pm 249 \mu\text{N}$ for 40×10^6 cells. Our results showed a significant elevation of active force amplitude with the increase from 10×10^6 to 15×10^6 HSkM/mL; however results presented by Mudera et al. indicate the existence of an optimal range of densities at which force production is greatest. Above this range, the force production may be impaired due to

overcrowding of cells, leading to cell death [165, 166], diffusion limitations of nutrients and oxygen [167, 168], and inability to adequately form muscle fibers.

In 2D culture, joint inhibition of miR-133a and miR-696 significantly increased PPARGC1A gene expression, which encodes metabolism co-activator PGC-1 α [169], whereas inhibition of either miR-133a or miR-696 did not affect PPARGC1A levels. It is important to remember, however, that the mechanism of microRNA involves silencing of specific mRNA seed sequences for protein translation. Since the transcription of these genes are not affected, the levels of mRNAs may likely remain unchanged [170], similar results of unchanged PPARGC1A expression were shown by Aoi et al. for miR-696 overexpression and inhibition [101]. This may be the reason for the unchanged gene expression in individual miR-133a and miR-696 inhibition. MicroRNAs control the translation of thousands of target mRNAs, and each mRNA is targeted by multiple microRNAs [170]. Inhibition of miR-133a and miR-696 both upregulate Mef-2: miR-133a inhibition affects Mef-2-dependent myogenesis and miR-696 inhibition affects Mef-2-mediated PGC-1 α activation and promotion of oxidative metabolism. Simultaneous inhibition of these two microRNAs may overexpress Mef-2 to an extent that negative feedback loops (necessary for maintaining homeostasis) may be used to retain normal cell function. In this case, negative feedback of Mef-2 influenced by miR-133a and miR-696 inhibition may lead to a decrease in Mef-2, slowing myogenesis and development of oxidative metabolism. This, in turn, would negatively affect PGC-

1 α , a potent metabolism co-activator that is under careful control by many different pathways, leading to increased transcription of PPARGC1A to increase PGC-1 α expression.

Measurement of PGC-1 α protein found an increase in presence for all cases, compared to negative control after 14 days of differentiation in 2D culture. Our findings for miR-696 inhibition complement those of Aoi et al., who reported an increase in PGC-1 α protein expression 24 hours after miR-696 transfected with miR-696 inhibitor after 24 hours, compared to negative control [101]. We also saw an increase in PGC-1 α protein for miR-133a inhibition due to the activation of the PGC-1 α promoter by Mef-2. Our PGC-1 α protein findings show that this elevation is retained for a much longer time period than the initial 24 hours and, therefore, may have a major impact on skeletal myofiber development. Additionally, joint inhibition led to significantly higher levels of sarcomeric α -actinin protein compared to negative control levels after 14 days in 2D culture. An increase in sarcomeric α -actinin expression indicates increased levels of organization and muscle maturity within engineered tissues.

Placing cells into a 3D environment containing a native, tissue-like extracellular matrix allows for the testing of more detailed responses and key factors controlling behavior in response to various biological stimuli, including oxygen depletion [171], microRNA inhibition, and drug toxicity testing. The ultrastructure of skeletal muscle cultured in 2D and 3D geometries may differ quite drastically: the

generation of tension in 3D allows for the orientation and alignment of myofibers while 2D cultures usually lack necessary stimuli to elicit this level of organization. Interactions between skeletal myoblasts and their surrounding extracellular matrix proteins are also essential to the development of mature skeletal muscle [172]. Specifically, Thorsteinsdóttir et al. reported the importance of the “extracellular matrix dimension” as a contributing factor to skeletal myogenesis. Therefore, the maturation of engineered skeletal muscle in a 2D conformation may not be at same degree of engineered tissue cultured in a 3D ECM-rich geometry.

Isometric force testing of transfected bundles after 2 weeks of differentiation showed at least 65% higher twitch and tetanic forces by joint inhibition engineered muscle bundles compared to all other tested conditions. This phenomenon may be explained by the muscle fiber type distribution within each microRNA treatment condition. Our results of miR-133a inhibition matched those reported by Liu et al in an *in vivo* mouse model: miR-133a inhibition led to an increase in Type I fibers [173]. Additionally, our results for miR-696 inhibition were expected, as an increase in PGC-1 α has been shown to increase Type I fiber as well [69, 142]. However, we hypothesized that the joint inhibition of miR-133a and miR-696 would lead to increased proportion of Type I fibers within the engineered 3D human tissue, but we found that Type II fibers were actually more prominent by immunofluorescence and qPCR for slow and fast myosin heavy chain. Herein may lay the reason that joint inhibition 3D muscle constructs exhibited far higher twitch and tetanus forces

compared to negative control and inhibition of each microRNA individually: a highly aligned, dense, and striated type II myofiber-rich muscle tissue is capable of higher and faster active contractile forces compared to type I myofiber-rich tissue of the same maturation due to the nature of glycolytic metabolism.

The mechanism for fiber type switch to favor Type II in joint inhibition cases, compared to each anti-miR individually, remains to be elucidated. However, the role of the transcription factor Mef-2 may play an important factor, as mentioned above. The Mef-2 transcriptional activator is stimulated by calcineurin and other calcium-regulated signaling molecules [174]. Mef-2 binding sites have been found to be necessary for fiber type-specific activities of myoglobin and troponin I slow promoters – specifically, Mef-2 binding is required for the function of slow fiber-specific enhancers [174]. Furthermore, inactivation of Mef-2 has been reported to lead to loss of slow fiber formation [97]. Myostatin, a secreted growth factor of skeletal muscle, has also been reported to affect fiber type development. Hennebry et al. reported that lack of myostatin resulted in an increase in fast twitch fiber formation and that this growth factor positively regulates Mef-2C levels in skeletal muscle [175]. They showed that skeletal muscle containing a deficiency in myostatin also contained low levels of Mef-2. Rachagani et al. reported altered expression of miR-1, miR-133, and miR-206 in myostatin knockout mice, implicating that there may be an interaction between miR-133 and myostatin as well [176]. However, the

mechanism of interaction remains to be elucidated between myostatin, microRNAs, and fiber type [177].

Anti-miR-133a and anti-miR-696 individually both lead to enhanced differentiation and development of oxidative metabolism and Type I myofibers, by repression of serum response factor (SRF) and upregulation of Mef-2/myogenin/MyoD transcription factors, respectively (Fig. 32). Similarly, Horie et al. found that miR-133 overexpression in cardiomyocytes led to a downregulation of Mef-2C expression [178]. Haberland et al. have found that Mef-2 activity is closely regulated by HDAC9, a member of the class II histone deacetylase family of enzymes [179]. As Mef-2 expression increases, HDAC9 activity increases as well, serving as a negative feedback loop to control overexpression of Mef-2 in skeletal muscle. HDAC9 associates with the MADS (MCM1, Agamous, Deficiens, serum response factor) domain of Mef-2 and prevents activation of Mef-2 target genes. HDAC9 was found to be directly controlled by Mef-2 both *in vitro* and *in vivo*. [179, 180] Figure 32 shows that the joint inhibition of miR-133a and miR-696 leads to upregulation of Mef-2 to a higher extent than cases of each anti-miR alone, which may trigger the negative feedback of HDAC9. Measurement of Mef-2C levels in engineered human skeletal muscle bundles found that joint inhibition conditions resulted in depressed gene levels at 2 weeks post-differentiation, evidence that downregulation of Mef-2 by HDAC9 may indeed cause the switch in fiber type to predominantly Type II myofibers.

Therefore, it is clear that while microRNAs may have huge potential as therapy for enhancing growth and differentiation of engineered human skeletal muscle, there is still much to be learned about their interactions and targets. The research presented here shows the importance of understanding these interactions in order to effectively and specifically modulate various biological processes.

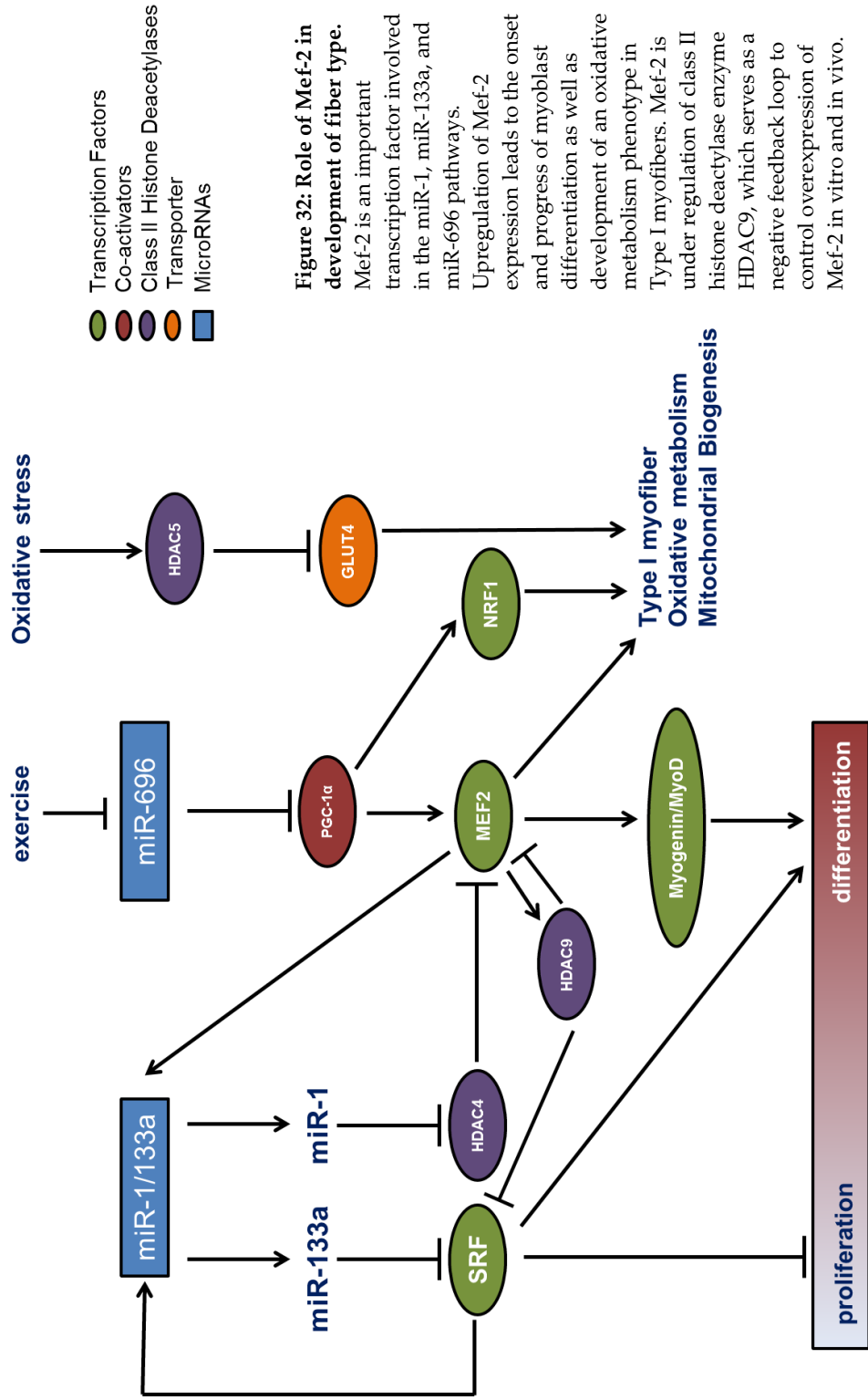


Figure 32: Role of Mef-2 in development of fiber type.

Mef-2 is an important transcription factor involved in the miR-1, miR-133a, and miR-696 pathways. Upregulation of Mef-2 expression leads to the onset and progress of myoblast differentiation as well as development of an oxidative metabolism phenotype in Type I myofibers. Mef-2 is under regulation of class II histone deacetylase enzyme HDAC9, which serves as a negative feedback loop to control overexpression of Mef-2 in vitro and in vivo.

3.5. Chapter Acknowledgements

We extend a very special thank you to the Bursac lab for their collaboration and help with these studies. Specifically, thank you to Mark Juhas, Chris Jackman, and Lauran Madden for help with the muscle bundle protocol and force testing equipment. We would like to thank Dr. Weining Bian for use of her LabVIEW force measurement VI. Also, a big thank you to members of the Truskey Lab and other colleagues who helped with troubleshooting immunofluorescence and Western blots: Tracy Cheung, Lydia Ran, Dr. Mina Wu, Dr. Caroline Rhim, and Brittany Davis. Thank you to the Reichert Lab and Duke Light Microscopy Core Facility (LMCF) for their excellent microscopy facilities (especially help from Mike Nichols and Dr. Yasheng Gao). This work truly represents a collaborative effort.

We would like to thank our funding sources: NIH Grant UH2TR000505 and the NIH Common Fund for the Microphysiological Systems Initiative.

CHAPTER 4. Endothelialization of Human Skeletal Muscle Bundles (Specific Aim 4)

4.1. Introduction

Over 40% of the human body is comprised of skeletal muscle, therefore, it is necessary to study the effects of any drug introduced into the body, regardless of the targeted tissue. Developing a direct co-culture model of the human skeletal muscle-endothelial cell interface is important for studying the effects of other cell types on the differentiation of skeletal muscle in the body. As no tissue exists in a vacuum biologically, it is important to understand the interactions between cell types and model a more native-like environment for subsequent study of human skeletal muscle tissue.

In this chapter, we explored the interactions between human cord blood-derived endothelial cells (ECs) and human skeletal muscle *in vitro*. A co-culture model using these two cell types would provide insight into the effects of endothelial cells on the organization and functionality of skeletal muscle - an important interaction to study as capillaries (lined with ECs) run throughout muscle tissue *in vivo*. Three dimensional co-culture systems have been approached using many different cells types and have utilized a variety of cell seeding techniques, including mixed and lamellar conformations [181]. Ye et al. described a co-culture system of human skeletal myoblasts and human endothelial cells separated by a permeable membrane used to test the transport of drugs across endothelium and to the differentiated skeletal muscle [182]. They found that perfusion with doxorubicin led

to transport across the endothelium and resulted in cytotoxic effects on differentiated human skeletal muscles, indicating suitability of the co-culture model for testing trans-membrane transport [182]. In developing a replicable EC and HSkM 3D co-culture system, we decided to pursue a direct lamellar co-culture to allow for skeletal muscle fusion to myofibers, important cell-cell junctions to form between ECs, and direct contact between the two cell types to facilitate interactions. Physiologically, a lamellar co-culture could model the skeletal muscle-capillary interface at a micro-scale.

An important consideration when developing a successful co-culture system is an appropriate culture medium capable of supporting both cell types. Developing conditions to co-culture ECs and HSkM *in vitro* is particularly difficult, however, due to the nutrients required to develop mature, confluent cell coverage for both cell types. Countless studies have reported successful co-culture of two or more different cell type *in vitro*, including ECs and smooth muscle cells (SMCs) [183], ECs and hepatocytes [184], skeletal muscle and adipocytes [185], and skeletal muscle and motoneurons [44]. Studies of co-culture systems using skeletal muscle and endothelial cells have been reported as well, but none using only primary isolated human cell types. Levenberg et al. developed a 3D co-culture system consisting of mouse myoblasts and human embryonic stem cell-derived endothelial cells or human umbilical vein endothelial cells (HUVECs) seeded into biodegradable porous polymer scaffolds [186]. They found that skeletal muscle differentiation and

endothelial lumens developed better in DMEM containing 10% FBS, 10% calf serum (CS), and HEPES compared to endothelial cell media (EBM-2 with 2% FBS and endothelial growth factor supplements). [186] As mentioned previously, the formation of cell-cell junctions are important for EC cell culture. Studies seeding porcine ECs onto a layer of porcine SMCs have noted the importance of seeding at confluent densities – the resulting co-culture of ECs on SMCs expressed PECAM, a marker of EC-EC cell junctions, by immunofluorescence. [183, 187, 188]

We hypothesized that identification of appropriate media conditions would allow for a 3D human skeletal muscle bundle – EC co-culture capable of producing functional force output similar in magnitude to monoculture tissue-engineered human skeletal muscle constructs.

4.2. Materials and Methods

4.2.1. Endothelial Progenitor Cell Isolation and Culture

Human cord blood-endothelial cells (ECs) were isolated from blood as described previously by Ingram et al. [189]. Umbilical cord blood was obtained from the Carolina Cord Blood Bank for isolation of ECs. The Institutional Review Board of Duke University approved the protocol for the collection and use of human blood used in this study.

Blood was diluted 1:1 with HBSS (Invitrogen), placed into Histopaque 1077 (Sigma), and centrifuged for 30 minutes. Mononuclear cells contained in the buffy coat were collected and washed 3 times with 10% complete EBM-2 EC media (10%

FBS, endothelial basal medium EBM-2, supplemented with EGM-2 (1% antibiotic/antimycotic solution). Cells were then plated onto 35-mm diameter dishes coated with rat tail collagen type I (BD Biosciences) in 10% complete EBM-2 media. Media was exchanged every 24 hours for 1 week to remove nonadherent cells. Colonies of cells were trypsinized, and 200 cells were plated into a collagen-coated T25 flask as passage 1 (P1).

ECs were cultured using 10% complete EBM-2 media to confluency, then split 1:10 using 0.025% trypsin (Lonza) for each passage. Cells were used between P6-P8 for co-culture studies.

4.2.2. Human Skeletal Muscle and Endothelial Progenitor Cell Co-Culture in 2D

HskMs were seeded into 6-well plates at a density of 16,000 cells/cm² in GM. Once HskM reached 80% confluency, media was shifted to DM and kept in DM for 4-5 days before being seeded with ECs. ECs were seeded at 125,000 cells/cm² based on previous 2D co-culture optimization studies (performed by Lydia Ran). Co-culture media was added upon seeding of ECs onto skeletal muscle; media tested included: 1:3 DM:EBM-2 and 3.3% FBS in DMEM based on previous monoculture and indirect co-culture studies performed by Lydia Ran. 3.3% FBS in DMEM was chosen for its reported use for culture of tissue-engineered blood vessels (TEBV) [190]. DM was used as control for 2D co-culture studies.

4.2.3. Human Skeletal Muscle and Endothelial Progenitor Cell Co-Culture in 3D

Human skeletal muscle bundles were constructed and cultured as previously described. For control HSkM-only bundles, DM (2% equine serum in DMEM) was used for the entire 2-week post-differentiation culture period. For co-culture bundles, DM was aspirated after 10-12 days post-differentiation and 45 μ L of an EC cell solution at a density of 1×10^6 cells/mL was pipetted on top of the muscle bundle. The compaction of the bundle away from the PDMS mold allowed room for the EC cell solution. The ECs were allowed to attach to the surface of the muscle bundle for 1 hour at 37C, after which co-culture media was added back on top of the construct. Muscle bundles were co-cultured with ECs for 48 or 96 hours, up to day 14 post-differentiation.

The co-culture media conditions tested included 1:3 DM:EBM-2 with 2% equine serum and 3.3% FBS in DMEM. 1:3 DM:EBM-2 with 2% equine serum was chosen based on 2D co-culture. All muscle bundles were tested for functional force output and immunofluorescence for skeletal muscle morphology and EC coverage.

4.2.4. Isometric Force Testing

Force testing was conducted as previously described in Section 3.2.9. Briefly, at Day 14 post-differentiation, bundles were removed from PDMS molds and pinned into a custom chamber and immersed in 37°C DM. Bundles were pinned to a fixed tissue anchor at one end and a PDMS holder suspended by the force transducer

(custom-made by Dr. Robert Dennis, University of North Carolina, Chapel Hill, NC, USA) at the other end. Positioning of the force transducer was controlled by a motorized linear actuator (Thorlabs). A pair of parallel platinum foil electrodes applied the electrical stimuli to suspended bundles to elicit isometric muscle contractions.

Using the motorized linear actuator, the initial length of the engineered muscle bundle was set to the length of culture (8 mm). Twitch measurements at 1 Hz and 100V were repeated for 5% increments up to 120% of initial construct length. The maximum twitch force was recorded and this percent length used for further isometric force testing at 5, 10, 20, and 40Hz. Force traces were recorded into LabVIEW and exported to Microsoft Excel files.

For analysis, Microsoft Excel files were loaded into a custom MATLAB program and peak forces found for each frequency and length condition. Photos taken at 100% length prior to force testing were assessed in ImageJ for muscle bundle cross-sectional area; specific forces were calculated by dividing force output (mN) by cross-sectional area (mm²).

4.2.5 Immunofluorescence

Co-culture 3D muscle bundles were fixed using ice-cold methanol for 5 minutes. Constructs were then rinsed 3 times with DPBS without Ca and Mg. Next, bundles were blocked in 10% goat serum in DPBS overnight with gentle tilting at room temperature. The next day, the primary antibodies were added and allowed to

bind overnight with gentle tilting at room temperature. Antibodies used included: mouse anti-CD31 (PECAM-1, 1:300 dilution, Life Technologies) and rabbit anti-alpha sarcomeric actin antibody (1:300 dilution, Thermo Scientific). The primary antibody was rinsed 3 times with DPBS for 5 minutes each with gentle tilting at room temperature. Next, the secondary antibodies were added: Alexa Fluor 488 goat anti-mouse (1:250, Invitrogen) and Alexa Fluor 546 goat anti-rabbit (1:250, Invitrogen). Nuclei were stained with Hoescht 33342 (1:1000, Invitrogen). Secondary antibodies were diluted in DPBS and added to the cultures for 45 minutes, protected from light with gently tilting at room temperature. Finally, the secondary antibody solution was rinsed 3 times with DPBS for 5 minutes each with gently tilting at room temperature and images via Zeiss 510 inverted confocal microscope.

4.2.6. Statistical Analysis

Data are presented as mean \pm standard error (SEM) unless otherwise noted. ANOVA and Fisher's PLSD post-hoc tests were performed using STATVIEW 5.0 statistical analysis package. HSkM and ECs isolated from separate individuals were considered distinct n values. A value of $p < 0.05$ was considered significant.

4.3. Results

4.3.1. Endothelial Cell Coverage of Fused Skeletal Muscle in 2D Studies

Initial studies were conducted in a 2D conformation onto 6-well plates to quickly and more efficiently assess proper culture conditions, as these studies

required fewer cells. Immunofluorescence for PECAM and sarcomeric α -actinin showed formation of an EC layer on top of fused muscle. (Figure 33)

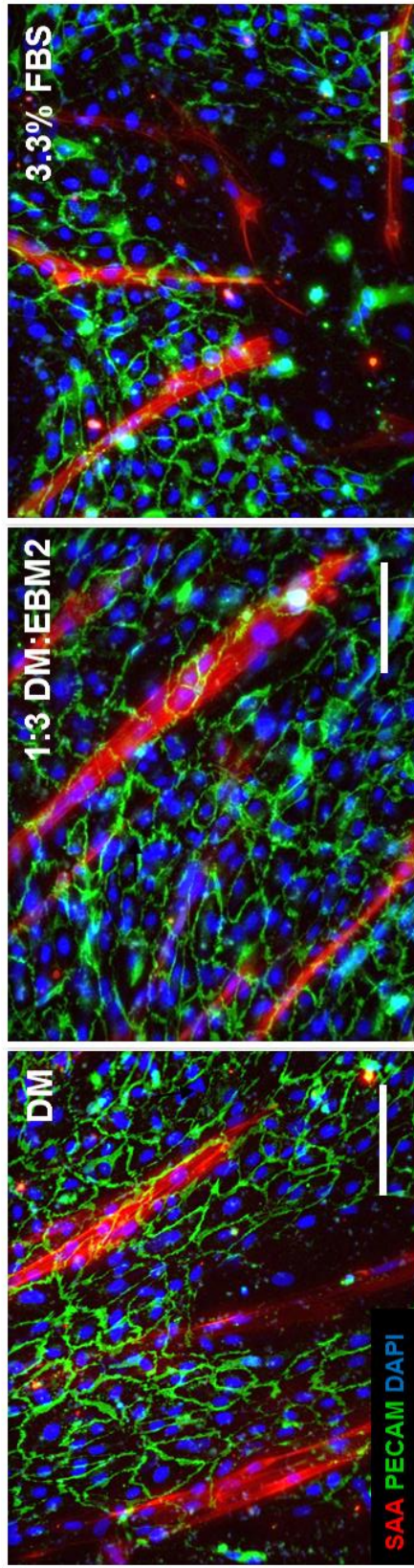


Figure 33: 2D Co-Culture Media Studies. HSKMs in direct co-culture were grown to 80% confluency cultured in differentiation media. ECs were added in EBM-2 for 24h before co-culture media was added. HSKMs were stained for sarcomeric α -actin (red), ECs for platelet endothelial cell adhesion molecule (PECAM, green) and nuclei for Hoechst (blue). PECAM staining was maximal with 1:3 DM:EBM2 media, indicating greater coverage of ECs and more cell-to-cell contact. HSKMs show fusion, indicating maturity. Scale bars are 125 μ m, Images were taken at 20x magnification.

Of the conditions tested, 1:3 DM:EBM-2 appeared to have the best EC coverage on fused skeletal muscle, although these findings were not significant (Figure 34). All conditions tested showed equal fused skeletal muscle coverage.

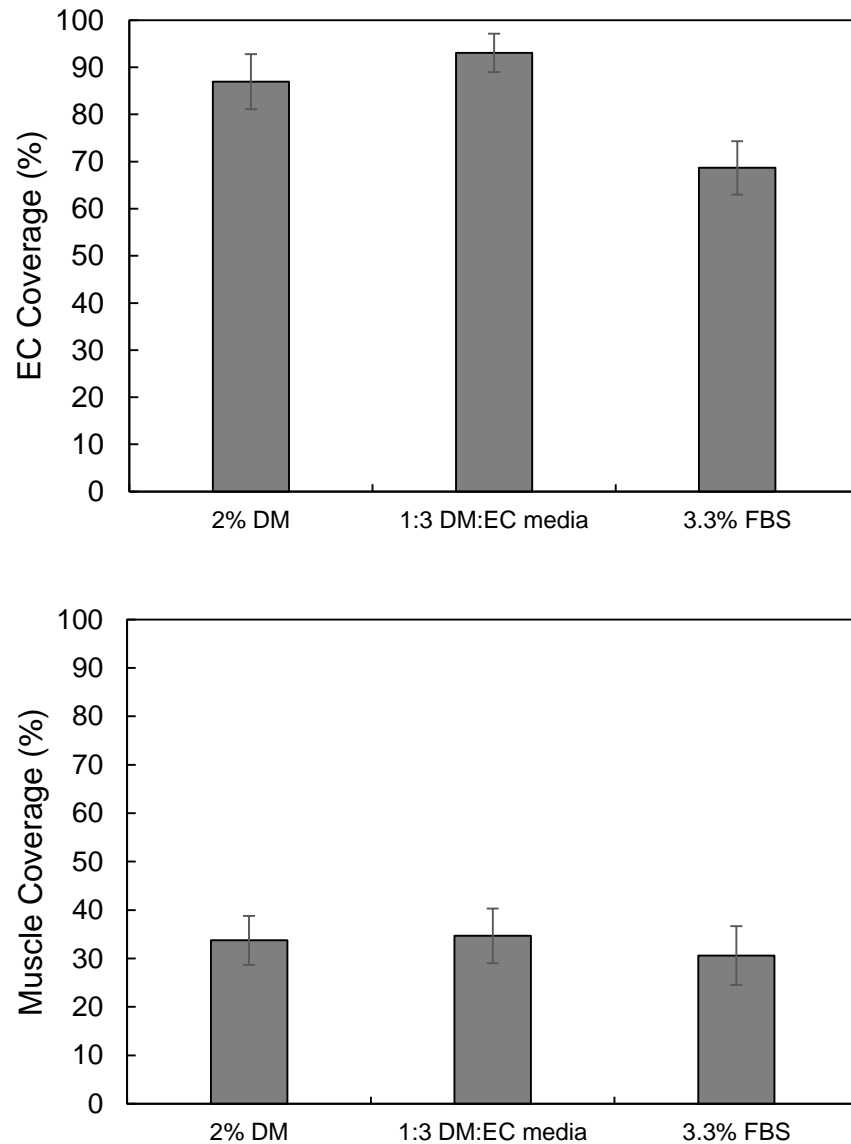


Figure 34: Percent Coverage of EC and HSkM. (A) Quantification of area covered by PECAM-stained ECs showed >60% coverage for all cases. 3.3% FBS in DMEM appeared to have least PECAM-coverage. (B) Quantification of area covered by sarcomeric α -actinin-stained skeletal muscle fibers showed equal coverage by all conditions. All error bars denote SEM ($n=2$).

4.3.2. Identification of Co-culture Media for Retention of HSkM Bundle Functionality

Based on the results in 2D, the culture conditions tested in 3D models were: DM (control), 1:3 DM:EBM-2 (due to high EB coverage and equivalent skeletal muscle coverage to control in DM), and 3.3% FBS in high-glucose DMEM (since this media has been used in literature to successfully culture tissue-engineered blood vessels [190]). High-glucose DMEM contains 25mM glucose, as noted by the manufacturer. Additionally, DMEM is the base media used for skeletal muscle culture; therefore, it may be instrumental in retention of muscle functionality *in vitro*. Two potential co-culture media were first tested on HSkM-only bundles to observe any effects on functional force output as well as protein expression and formation of myofibers. DM was used as control and 1:3 DM:EBM-2 and 3.3% FBS in DMEM were tested for use as co-culture media. After 1 week of differentiation in DM and 1 additional week of culture in one of the three tested media conditions, force testing showed over 70% decrease in twitch force (* $p < 0.05$, $n=3$) and over 60% decrease in tetanic forces (* $p < 0.05$, $n=3$) from muscle bundles cultured in 1:3 DM:EBM-2 media compared to DM and 3.3% FBS in DMEM conditions (Fig. 35). 3.3% FBS in DMEM did not change twitch or tetanic force compared to DM. Bundles in 3.3% FBS in DMEM also exhibited over 3.5-times higher twitch (* $p < 0.05$, $n=3$) and almost 3-times higher tetanus forces ($^{\wedge}p < 0.01$, $n=3$) compared to 1:3 DM:EBM-2 media.

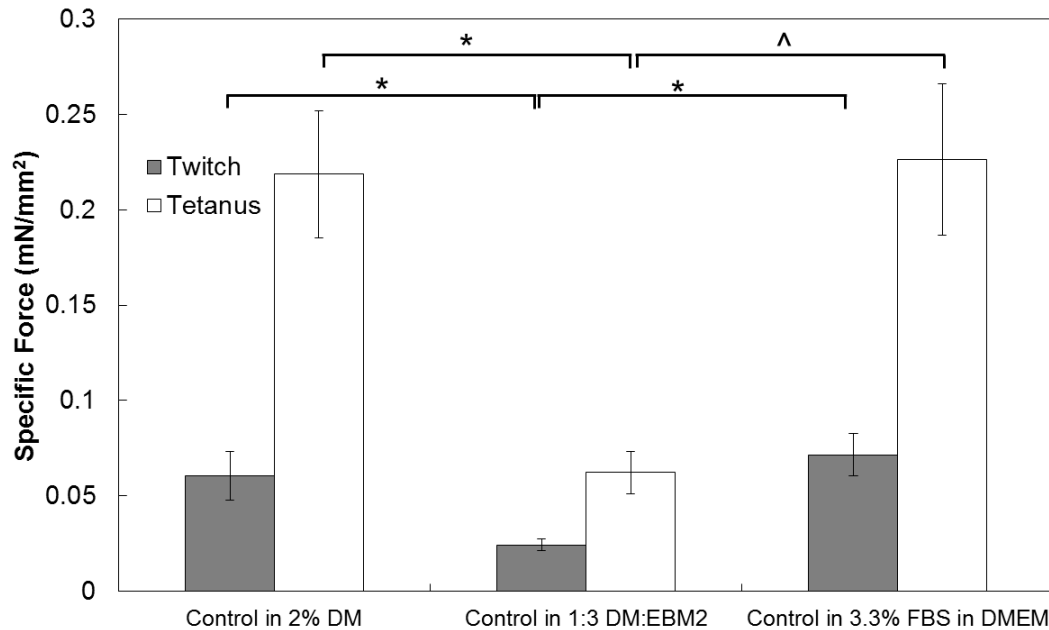


Figure 35: Testing co-culture media in muscle-only engineered constructs. Muscle bundles were tested in potential co-culture media to assess retention of functionality. 2% equine serum in DM was used as control. Bundles cultured for 1 week in 1:3 DM:EBM2 media saw significantly decreased twitch and tetanus forces compared to control forces. However, bundles tested in 3.3% FBS in DMEM exhibited comparable forces to the control condition. (* $p < 0.05$, ^ $p < 0.01$, $n = 3$ for all)

Sarcomeric α -actin immunofluorescence of HSkM-only bundles in DM, 1:3 DM:EBM-2, and 3.3% FBS in DMEM showed elongated myofibers and the clear presence of striations in all conditions (Fig 36). Bundles cultured in DM (Fig. 36A) and 3.3% FBS in DMEM (Fig. 36C) expressed most intense staining of sarcomeric α -actinin compared to 1:3 DM:EBM-2 (exposure time held constant).

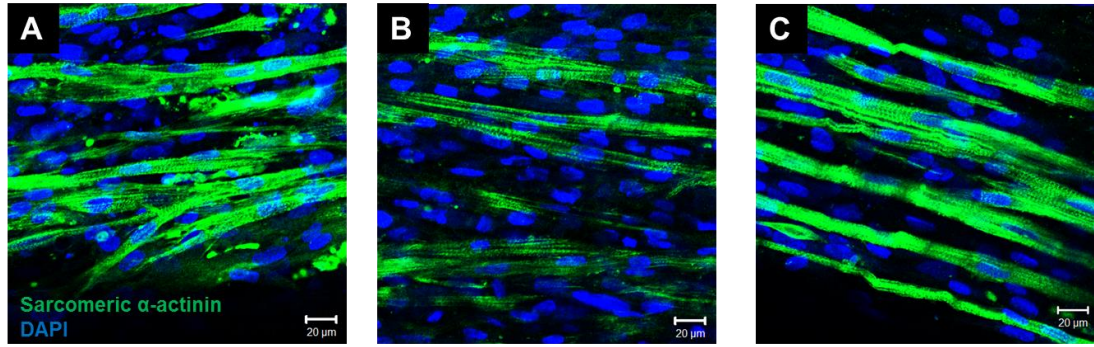


Figure 36: Ultrastructure of muscle-only bundles in tested co-culture media. Engineered human skeletal muscle was cultured in (A) control DM media, (B) 1:3 DM:EBM-2 media, and (3) 3.3% FBS in DMEM. Myofibers were stained for sarcomeric α -actinin (green) and DAPI (blue). Bundles cultured in DM and 3.3% FBS in DMEM exhibited the more intense sarcomeric α -actinin staining compared to those cultured in 1:3 DM:EBM-2 media. All condition exhibited alignment and development of striations.

4.3.3. Co-culture Bundle Functionality is Retained in 3.3% FBS in DMEM

From initial studies with 1:3 DM:EBM-2 and 3.3% FBS in DMEM media, it was clear that the latter was beneficial to the formation of mature, functional myofibers. Therefore, twitch and tetanus forces were measured for control (no ECs) muscle bundles and co-culture muscle bundles in 3.3% FBS in DMEM. (Fig. 37) Results showed an over 4-times increase in twitch force of co-culture bundles with ECs for 48 hours compared to control in DM ($p < 0.01$, $n = 3$) and over 2.5-times compared to control in 3.3% FBS in DMEM ($p < 0.05$, $n = 3$). Tetanus force amplitudes rose significantly over these conditions as well: 48 hour co-culture saw over 3-times tetanus forces compared to control in DM ($p < 0.005$, $n = 3$) and over 2.5-times compared to control in 3.3% FBS in DMEM ($p < 0.01$, $n = 3$). Twitch and tetanus force amplitudes fell in 96 hour co-culture bundles compared to 48 hour bundles; however, this result was not significant.

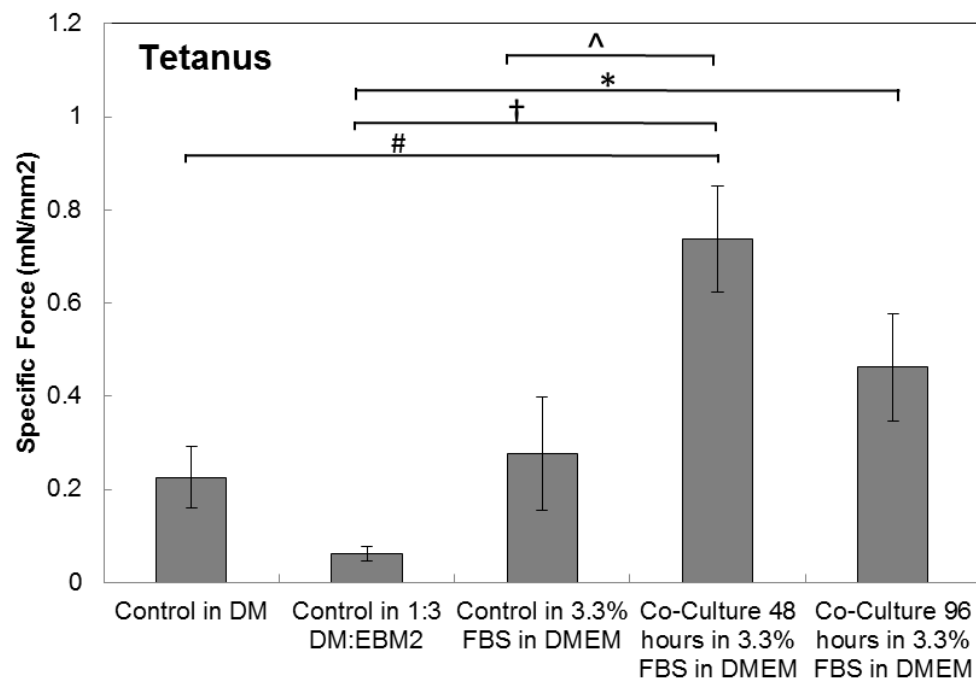
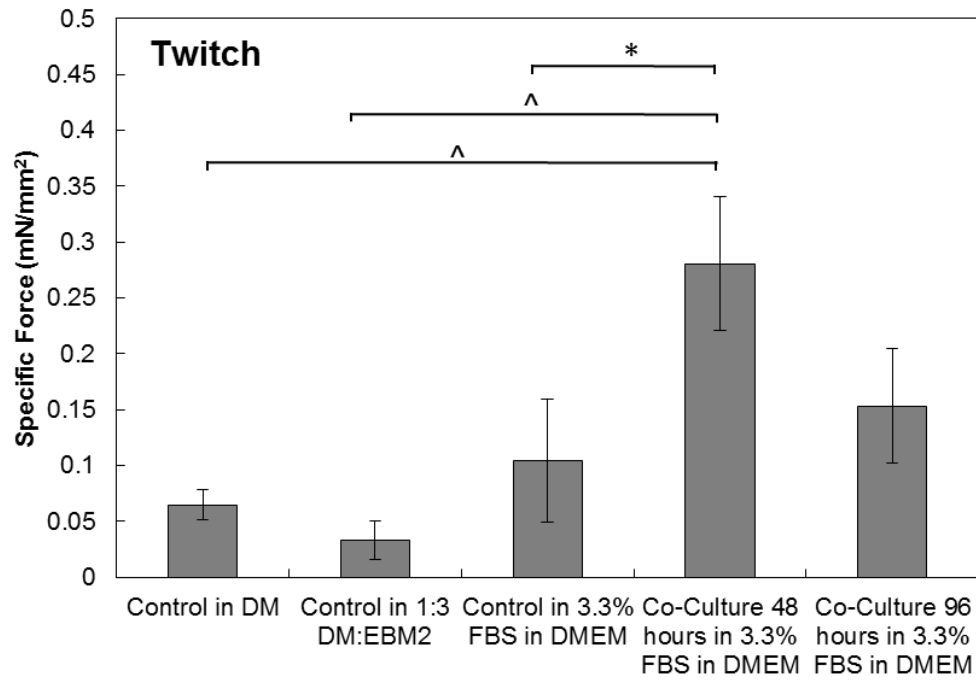


Figure 37: Twitch and tetanus force amplitude for co-culture bundles. The addition of ECs for 48 hours led to an increase in twitch and tetanus specific force amplitudes compared to all

control conditions. Co-culture of cells for 48 hours led to higher forces than longer cultures of 96 hours. (*p<0.05, ^p<0.01, #p<0.005, †p<0.001, n=3 for all)

To see whether a discrepancy in muscle fiber density within the engineered constructs was the cause of increased forces, fibers stained positively for sarcomeric α -actinin were quantified per area in each field of view taken from confocal microscopy. We found that the fiber density within control in DM was 97.4 ± 3.4 fibers/mm², and the densities for 48 and 96 hour co-culture were 71.7 ± 16.4 and 75.1 ± 13.6 fibers/mm², respectively. These findings were not significantly different. Fibers were slightly thicker in co-culture bundles compared to control: 10.9 ± 0.7 μ m for control bundles, 13.2 ± 1.2 μ m for co-culture for 48 hours, and 13.8 ± 0.3 μ m for co-culture for 96 hours. Fiber diameters were thinner than previously reported values of ~ 50 μ m [1] likely due to the difference in geometry: HSkM were previously plated in a 2D conformation, with considerable cell spreading on the surface of the substrate whereas HSkM contained in a 3D fibrin gel do not spread since they are suspended within the construct.

4.3.4. Endothelial Cell Coverage of Muscle Bundle in 3.3% FBS in DMEM

Confocal microscopy for PECAM (an indicator of the formation of important cell-cell junctions essential to EC health and functionality) was used to visualize the spreading and coverage of ECs on the surface of the construct. Co-culture of ECs with HSkM in 3.3% FBS in DMEM for 48 hours yielded $21.8 \pm 10.4\%$ PECAM-stained area, compared to $9.8 \pm 2.6\%$ in 96 hour co-culture bundles (n=2). Co-culture with

ECs for 48 hours led to over 30% more coverage of engineered muscle with ECs compared to co-culture for 96 hours. (Fig. 38)

For both 48 and 96 hour cases, though, there did not appear to be infiltration of ECs into the muscle bundle. Orthogonal views of confocal Z-stacks show PECAM on the bundle surface (green), but not within the interior of the construct (red). This is important for retention of construct functionality, as EC networks throughout the muscle may interrupt fiber formation and decrease the magnitude of bundle contraction (Fig. 39). This could be due to the difficulty of forming cell-cell junctions within the inside of the fused muscle bundle due to space constraints and oxygen and nutrient diffusion limitations.

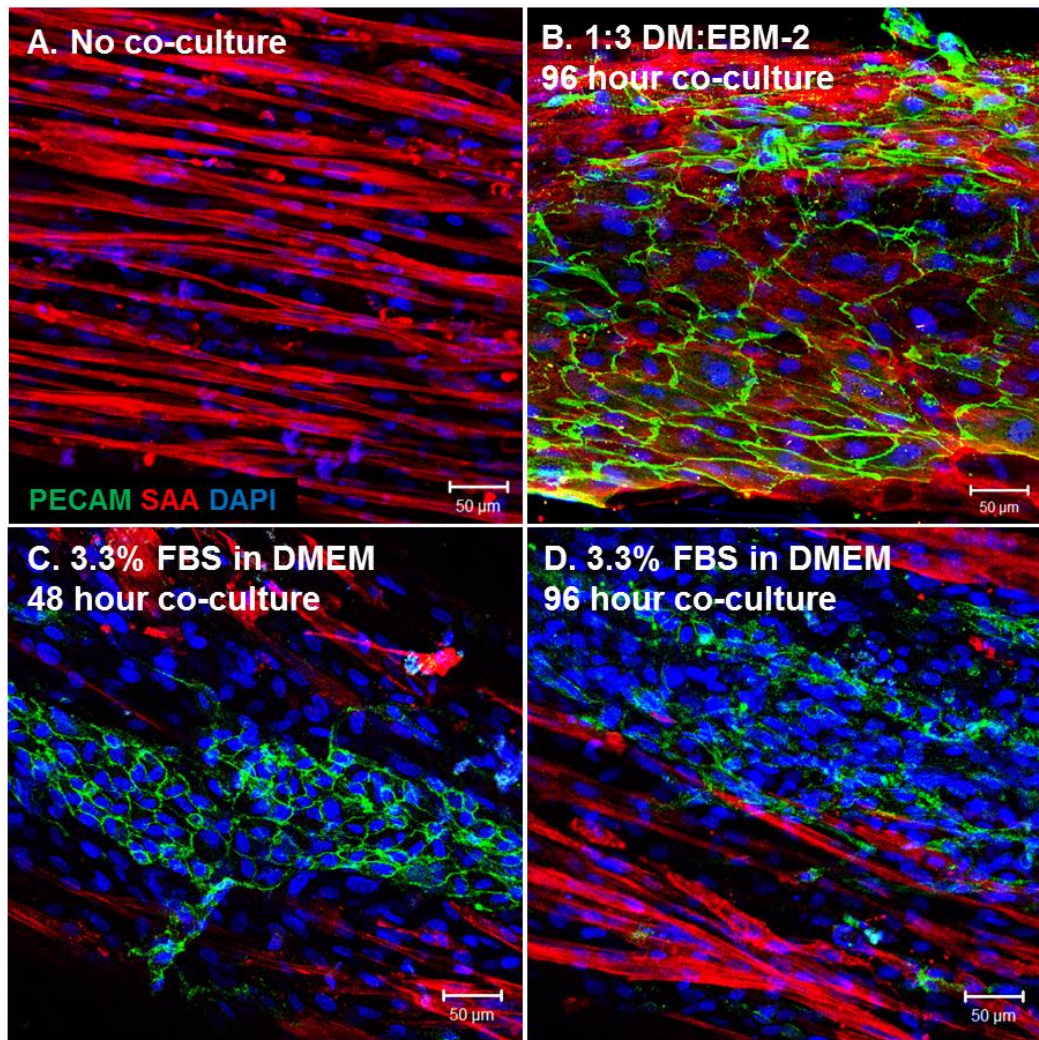


Figure 38: Endothelial cell coverage on engineered muscle bundles. Control and co-culture bundles seeded for 48 and 96 hours with ECs were stained with sarcomeric α -actinin, PECAM, and DAPI. (A) Control bundles showed highly aligned and striated muscle fibers. (B) Co-culture bundles cultured for 96 hours in 1:3 DM:EBM2 media showed high EC coverage and PECAM staining. (C-D) Co-culture bundles showed PECAM staining on the surface of muscle bundles, but not over 50% coverage. There appeared to be more PECAM staining (spread ECs) on the surface of co-culture bundles for 48 hours compared to those for 96 hours.

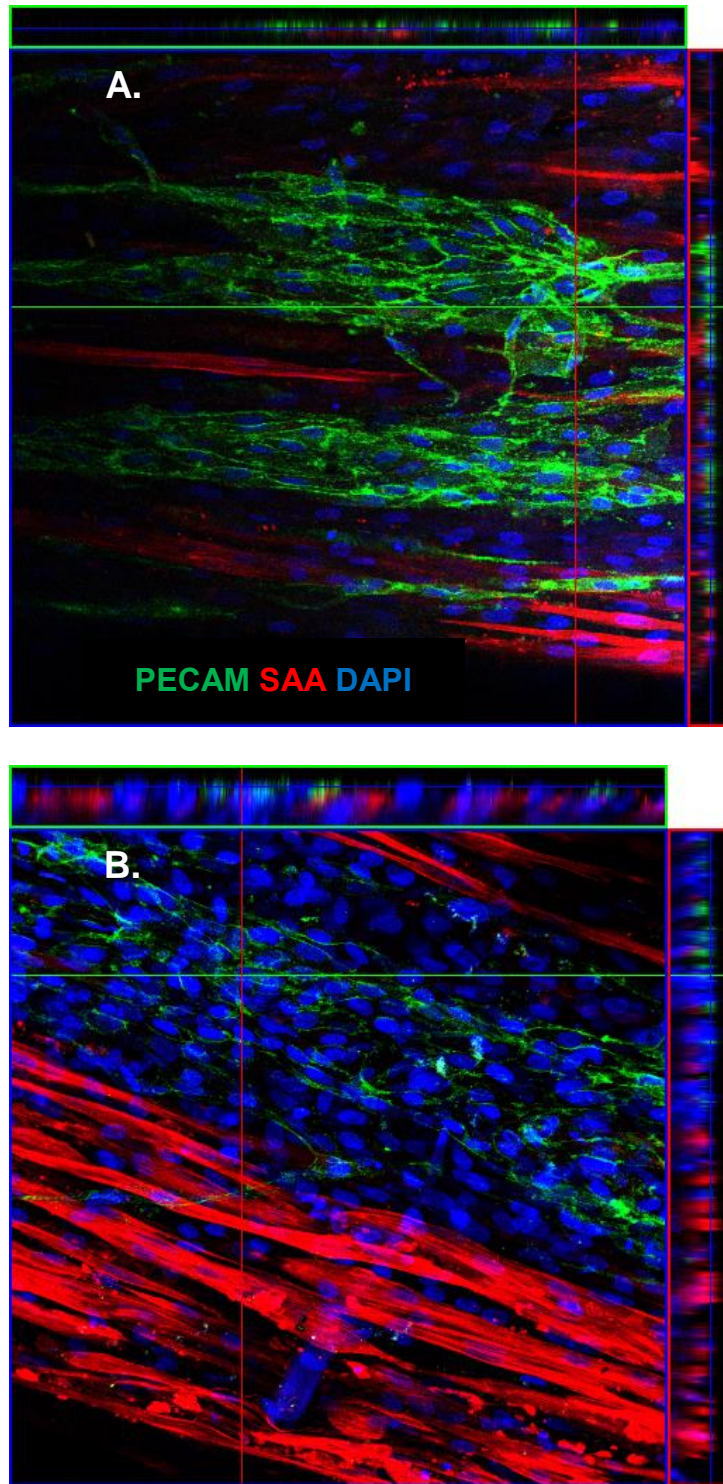


Figure 39: Orthogonal views of co-culture bundles. Z-stacks of co-culture bundles were taken and orthogonal views reconstructed to visualize localization of PECAM and sarcomeric α -actinin staining. Co-culture bundles for (A) 48 hours and (B) 96 hours were visualized. In both cases, PECAM staining was localized to the surface of the bundle, with muscle fibers underneath.

4.4. Discussion

In this study, we identified conditions for the co-culture of functional human skeletal muscle with human cord blood-derived endothelial cells in a 3D engineered model. Two co-culture media conditions were tested, 1:3 DM:EBM-2 and 3.3% FBS in DMEM, and compared to skeletal muscle DM to assess retention of engineered muscle functionality and EC spreading and coverage on muscle. 3.3% FBS in DMEM resulted in retention of active contractile force magnitude in muscle-only engineered constructs, and increased force magnitude at least 2-times after addition of ECs to the muscle for 48 or 96 hours. Co-culture engineered human muscle with ECs exhibited the greatest twitch and tetanus forces and EC coverage when cultured in 3.3% FBS for 48 hours – an over 6.5-fold increase in twitch force and over 3.5-fold increase in tetanic force compared to control muscle bundles in DM. These studies serve as proof of principle for developing a human only skeletal muscle and endothelial cell 3D co-culture model.

Many factors influence the choice of media used for co-culture, including metabolic differences between cells types and growth factors necessary for proper cell growth and maintenance of proper cell and tissue function [191, 192]. Many growth factors have been implicated in the culture of healthy skeletal muscle from myoblasts, including vitronectin, basic fibroblast growth factor (bFGF), cardiotrophin-1 (CT1), glial cell line-derived neurotrophic factor (GDNF), brain-

derived neurotrophic factor (BDNF), and neurotrophin 3 and 4 (NT3, NT4) [193]. Growth factors important for endothelial cell growth include human epidermal growth factor (hEGF), hydrocortisone, vascular endothelial growth factor (VEGF), fibroblast growth factor (FGF), insulin-like growth factor-1 (IGF-1), and heparin [194, 195]. After the identification of proper growth factors, it is then imperative to test culture health and growth in potential co-culture media as certain morphologies or functions may be desired. In this study, the identification of a proper co-culture media for human skeletal muscle and human CB-ECs necessitated recapitulating a lamellar morphology between cell types and the retention of skeletal muscle functionality, as demonstrated by active contractile forces. Additionally, the hCB-ECs layered on top of human skeletal muscle must be spread and express the important junctional marker PECAM.

Van der Schaft et al. described a co-culture system of vascularized 3D muscle constructs composed of murine embryonic heart-derived endothelial cells and C2C12 murine myoblasts. [196] They achieved aligned, vascularized murine skeletal muscle constructs cultured in muscle differentiation media: high-glucose DMEM supplemented with L-glutamine, 20 mM HEPES buffer, 0.4% Ultrosor G (a serum replacement), 0.1 mM nonessential amino acids, penicillin, and streptomycin. Vascularized muscle constructs were assessed for myofiber and endothelial cell directionality, construct stiffness, and role of VEGF in vascular orientation within engineered muscle. [196] However, there was no verification of retention of muscle

construct contractile force, a key factor for engineering of muscle tissue. In this study, we found that identifying proper culture media is extremely important to retaining or enhancing the functionality of tissue-engineered skeletal muscle.

It was unexpected that the addition of ECs in a lamellar fashion to fused human skeletal muscle *in vitro* would increase the twitch and tetanus force amplitudes significantly. We hypothesized that introduction of ECs into the culture could lead to infiltration of ECs into the interior of the bundle and interrupt myofiber formation and hinder active force generation – this phenomenon has been observed in mixed skeletal muscle-EC co-cultures. However, this was not observed, as isometric forces increased significantly for 48 hour co-culture and PECAM staining was localized to the surface of the tissue engineered bundle for both co-culture conditions. Tissue engineered skeletal muscle has been shown to differentiate more quickly in the presence of nitric oxide [4, 197-200]. Additionally, endothelial cell production of nitric oxide increases dramatically when cells are exposed to high glucose conditions [201]. Since the basal media for co-culture was high glucose-DMEM (with 3.3% FBS), it is plausible that the glucose contained within the media led to increased nitric oxide production from ECs, resulting in accelerated muscle maturity. Additionally, metabolic byproducts of active muscle have been shown to dilate surrounding blood vessels, resulting in increased endothelial nitric oxide production [202]. Retention of ECs on the surface of the muscle may be important to the levels of nitric oxide produced, as the isometric forces dropped after 96 hours of

co-culture, which had over 30% less retention of ECs as compared to 48 hour co-culture.

The co-culture results presented here provide proof of principle that a functional 3D model of the human skeletal muscle-capillary interface can be developed *in vitro*. Further studies are needed to understand the increase in functional force output with the addition of ECs to culture. This may be due to endothelial cells in co-culture with HSkM producing higher amounts of nitric oxide, leading to an increase in differentiation. Zhang et al. showed that addition of nitric oxide donor L-arginine onto stretched C2C12 myoblasts resulted in an increase in accumulation of focal contact proteins talin and vinculin, leading to an increase in apparent elastic modulus of muscle cells and increased muscle differentiation [4]. Studies to measure the nitric oxide production of muscle-only bundles and co-culture bundles would help elucidate whether there is a difference in nitric oxide levels between conditions. Additionally, nitric oxide donor and inhibitor studies could be performed to test the functionality of engineered skeletal muscle (without added ECs) in response to nitric oxide levels. Following the studies of Zhang et al., L-arginine could be used as the nitric oxide donor and *N*^ω-nitro-L-arginine methyl ester (L-NAME) could be used as the inhibitor [4].

Such models that replicate key elements of *in vivo* physiology are necessary for development of human drugs [203, 204]. Due to the large percentage of human body mass given to skeletal muscle, this tissue is both a potential target for drug

delivery and a site of drug toxicity [135]. Being able to model the transport and delivery of drugs across human endothelium to functional engineered human skeletal muscle will be extremely useful in helping streamline the therapeutic development process.

4.5. Acknowledgements

We would like to acknowledge Tracy Cheung, Alexandra Jantzen, and Cristina Fernandez for their hard work in isolating endothelial progenitor cells for the Truskey Lab. Thank you very much for your EPC expertise! I would like to extend a very special and heartfelt thank you to Lydia Ran - my amazing and diligent undergraduate student who paved the way for this co-culture work by tirelessly completing 2D feasibility and optimization studies as well as helping extensively with the 3D work. These studies would not be possible without you!

This work was made possible by our funding sources: NIH Grant UH2TR000505 and the NIH Common Fund for the Microphysiological Systems Initiative.

CHAPTER 5. Dissertation Summary & Future Work

5.1. Dissertation Summary

Overall, the results within this dissertation provide the novel results that (1) engineered human skeletal muscle can generate active contraction when cultured in static conditions at 10×10^6 cells/mL or more, (2) inhibition of miR-133a and miR-696 simultaneously significantly accelerate human myogenesis *in vitro* and increase development of Type II fast myofibers, and (3) direct lamellar co-culture of ECs on engineered muscle bundles are feasible and can be maintained in culture for at least 4 days. These results suggest that there may be a connection between the pathways for miR-133a and miR-696, as inhibition of miR-696 typically increases metabolism co-activator PGC-1 α expression and leads to preferential development of Type I slow myofibers. These results also demonstrate the importance of microRNAs in the process of human muscle myogenesis and the potential they hold for musculoskeletal therapies.

The global hypothesis that motivated this research was that joint inhibition of miR-133a and miR-696 would accelerate and direct human skeletal muscle myogenesis *in vitro*. The proposed research tested the following hypotheses: (1) HSkM require different culture conditions than those optimal for C2C12 culture, (2) joint inhibition of miR-133a and miR-696 would result in 2D human skeletal muscle cultures with accelerated differentiation and increased Type I muscle fibers compared to control and individual inhibition of each microRNA, (3) joint inhibition

would result in functional 3D human skeletal muscle capable of active contractions significantly higher than control and individual inhibition by each microRNA, and (4) HSkM and EC lamellar co-culture can exert active contraction when maintained in the proper co-culture media.

Chapter 2 showed that culture conditions optimized for C2C12 murine myoblast culture are not optimal for efficient HSkM culture due to low microRNA levels and few striated fibers. To promote human skeletal muscle differentiation it was necessary to coat substrates with 100 µg/mL growth factor reduced Matrigel and reduce the serum content from 8% to 2%. This change in culture conditions elevated levels of myogenic microRNAs and Mef-2C and increased the presence of striations increased after 14 days of differentiation compared to C2C12 culture conditions. Further evidence that serum content in differentiation medium is highly influential of HSkM gene expression was found in the opposing responses of microRNA levels to cyclic stretch at ±10% and 0.5 Hz for 1 hour alternating with 5 hours of rest for 2 weeks. However, when microRNA expression was compared between HSkM culture conditions and human explant tissue, there still existed a large gap between *in vivo* and *in vitro* tissue. Native tissue is dynamic as it is exposed to many biological stimuli that aid in the differentiation process. Cultured tissue, in contrast, tends to exist in a static state as the stimuli are minimal and unchanging. As well, the 3D microenvironment provides the necessary interactions with ECM and cells to achieve a much more differentiated state than that which is achieved *in vitro*.

However, there exist other methods of promoting differentiation of cultured HSkM *in vitro*. We focused on microRNA inhibition to accelerate differentiation *in vitro* due to their endogenous presence and demonstrated potent effects on skeletal muscle myogenesis. As we had observed with C2C12 cells, inhibition of miR-133a in HSkM accelerated HSkM differentiation in 2-week cultures, as shown by increased sarcomeric α -actinin protein expression and accelerated striation development by immunofluorescence. Thus, the results in Chapter 2 confirm the hypothesis that HSkM require culture conditions different from C2C12 for efficient differentiation *in vitro*. Inhibition of miR-133a served as proof of principle for the studies presented in Chapter 3.

Results from **Chapter 3** showed that joint inhibition of miR-133a and miR-696 in HSkM accelerated and directed myogenesis. In 2D, joint inhibition led to significantly increased PPARGC1A gene expression and the corresponding increased expression of PGC-1 α compared to negative control, while individual inhibition of microRNAs did not. Joint inhibition also led to increased expression of sarcomeric α -actinin. These 2D studies served as proof of principle for studies of joint inhibition in a 3D functional human skeletal muscle model. This work is the first to show that when seeded at 15×10^6 HSkM/mL into a 45 μ L fibrin hydrogel and allowed to differentiate for two weeks, engineered muscle exhibited spontaneous contractions as well as active contraction in response to electrical stimuli. Muscle seeded with HSkM transfected with miR-133a and miR-696 inhibitors exerted twitch

and tetanus forces higher than all other conditions studied. Anti-miR-133a engineered muscle gave tetanus forces higher than negative control and anti-miR-696 bundles. Thus, the increase in force magnitude seen for joint inhibition samples may be due to the distribution of muscle fiber type. PCR and immunofluorescence for slow myosin heavy chain showed low gene expression and low staining intensity, respectively, in joint inhibition constructs. However, immunofluorescence for fast myosin heavy chain showed an increase in presence for fast myosin heavy chain protein in joint inhibition conditions compared to all other conditions. Therefore, there may be a higher proportion of fast:slow myofibers in joint inhibition bundles, leading the force production to favor the higher magnitude forces characteristic of Type II myofibers. The results in Chapter 3 confirmed the hypothesis that joint inhibition of miR-133a and miR-696 inhibitors would accelerate differentiation in 2D and 3D conformation; however, joint inhibition led to increased Type II fiber presence in 3D rather than Type I – possibly as a result of Mef-2 negative feedback loops.

Results from **Chapter 4** identified a 3.3% FBS in DMEM as common media to co-culture HSkM and ECs and retain active contraction of engineered skeletal muscle interface. Use of 3.3% FBS in DMEM has also been reported for co-culture of SMCs and ECs [183] as well as tissue-engineered blood vessels seeded with human aortic ECs or primary coronary artery disease ECs [188]. Isometric force testing of muscle-only constructs in control DM, 1:3 DM:EMB-2, and 3.3% FBS in DMEM

found that 1:3 DM:EBM-2 led to significant depression of forces and 3.3% FBS in DMEM saw retention of forces compared to control. 3.3% FBS in DMEM was then tested in co-culture bundles containing ECs seeded onto fused 3D skeletal muscle constructs for 2-4 days. Isometric force testing found co-culture for 48 hours led to over 2.5-times increase in twitch and tetanus force amplitudes compared to all control cases (DM, 1:3 DM:EBM-2, 3.3% FBS in DMEM). Force amplitudes of bundles co-cultured with ECs for 96 hours appeared elevated compared to controls as well; however, these findings were not significant. EC retention on the surface of the engineered muscle bundle was over 30% higher at 48 hours compared to 96 hours of co-culture. Therefore, there appears to be a strong correlation between presence of ECs and increasing twitch and tetanus force amplitudes, however, further work is needed to obtain higher EC coverage. This may be achieved by using low glucose DMEM rather than high glucose DMEM, since the latter has been implicated to activate EC inflammation [205]. Overall, the results from Chapter 4 confirm the hypothesis that HSkM and ECs can be co-cultured in appropriate media to retain functionality of the engineered skeletal muscle. In fact, we found a significant increase in force production for short co-culture times (48 hours).

5.2. Strengths & Weaknesses of Work

As with any research project, there exist strengths and weaknesses to the study, both in approach and application. Here, we discuss both with respect to the studies performed in each specific aim of this dissertation.

The culture conditions identified in **Chapter 2** provide significant elevation to microRNAs and presence of striations without the introduction of drastic changes to the culture procedure, which is beneficial overall. The conditions studied were by no means exhaustive and further enhancement of differentiation could be obtained by addition of other microRNAs or further modification of culture conditions. For example, optimization of growth factors added to the media or modulation of microRNAs can regulate fiber type (such as miR-696).

Perhaps the most important finding of Chapter 3, though, is the ability to tissue engineer human skeletal muscle *in vitro* capable of active contractile forces. This has not been previously demonstrated in the literature, so developing a human model of contractile skeletal muscle is a large step forward for the field of musculoskeletal tissue engineering. We demonstrated that seeding density plays an important factor in the generation and magnitude of forces produced; however, full optimization of HSkM seeding density into the fibrin hydrogels was not conducted. It is possible that even higher seeding densities could produce significantly higher forces as well.

Other important aspects of the work shown in Chapter 3 are consistency of anti-miR studies using human myoblasts with previously published work, including PGC-1 α protein presence after miR-696 inhibition in C2C12 cells by Aoi et al. [101] and muscle bundle forces after miR-133a inhibition in C2C12 cells by Rhim et al. [49], and the extension of these results further by introducing longer culture times of anti-

miR-696-transfected HSkM before PGC-1 α protein measurement as well as the addition of anti-miR-696 conditions to anti-miR-133a conditions for force measurement. Therefore, our studies built upon the published literature and found important information, including long-lasting effects of anti-miR-696 on PGC-1 α protein presence and the effect of both microRNAs on human muscle force production.

In Chapter 3, isometric force testing of joint inhibition muscle bundles found significantly elevated specific forces and increased fast myofiber phenotype, compared to all other conditions. This result was surprising due to previous findings that miR-696 inhibition leads to increased slow myofiber formation in C2C12 cells. The results suggest that inhibition of miR-133a and miR-696 simultaneously must have some shared regulation within their pathways affecting fiber type development. Since this was a tissue engineering study and not a detailed mechanistic study the Mef-2C gene expression data provide limited insight into the mechanism. Since samples were only taken at one timepoint, it is not known whether Mef-2C expression decreases (due to negative feedback) after an initial overexpression, or whether expression is depressed from the onset of differentiation. Measuring class II histone deacetylases (HDAC4, HDAC5, HDAC9) that negatively affect Mef-2C [206] would also help provide insight into the mechanism behind Mef-2C expression and the resulting fiber type development. Mef-2C expression and

class II histone deacetylase information would all be instrumental in understanding the role of miR-133a and miR-696 inhibition on slow and fast fiber development.

Chapter 4 identified culture media capable of maintaining human skeletal muscle active function with the co-culture of human endothelial cells on the surface. Thus far, there have been no reports of skeletal muscle and endothelial cell co-culture capable of active contraction. Additionally, there has not been development of a human-only co-culture system as well. Therefore, our protocol is quite novel. Strengths of this study include the ability to obtain PECAM-expressing endothelial cells on the surface of the fused human muscle and the generation of high specific forces. The identification of a common culture media is quite important to the ultimate identification of a common media capable of sustaining multiple cell types. While the results presented in Chapter 4 are exciting, further work is needed identify suitable co-culture media, optimal seeding conditions for a confluent layer of endothelial cells, and the reason for higher specific force amplitudes. Similar to the results in Chapter 2, our testing of possible co-culture media was not exhaustive, and thus, the media identified is not necessarily optimal. In fact, the media used may not be favorable since it contained high glucose (25 mM), which has been shown to activate the inflammatory response of endothelial cells, disrupt cell-cell connections, and enhance passive force contraction [207]. Additionally, while we did see PECAM-staining, indicating endothelial cell junction formation, the layer of endothelial cells was not confluent on the surface of the fused human skeletal muscle. Further

evaluation of seeding conditions (duration, density, etc.) is necessary to find ways to increase cell retention and spreading. Finally, the reason behind the increase in specific force output is known, as we did not study the mechanism. However, this is important to understanding the interactions between skeletal muscle and endothelial cells and the effects on muscle functionality.

5.3. Implications for Tissue Engineering

Overall, the results presented in this dissertation showed that that modulation of microRNAs can robustly affect engineered skeletal muscle differentiation and functional force output. Others have reported this as well [49, 92, 113], but this is the first demonstration with muscle with the addition of multiple microRNAs. Results presented in Chapter 3 demonstrate that engineering of functional human skeletal muscle bundles cultured in static conditions is possible. The ability to engineer functional human skeletal muscle *in vitro* after static conditions is novel and has important functional implications to the study of skeletal muscle myogenesis and the treatment of musculoskeletal disease. Tissue-engineered human skeletal muscle has great potential to be used as implantable tissue to replace injured native tissue or as models to study diseases and treatments. Our results demonstrate the ability to accelerate differentiation and direct fiber type *in vitro*, and these techniques are great tools that can be used to grow mature human skeletal muscle for implantation purposes. Our demonstration of regulating fiber type in a static culture provides room for additional stimuli to provide environmental cues to

further encourage development of specific fiber phenotypes. Additionally, this method of primary myoblast isolation from human explant tissue lends itself well to establishing a method of engineering autologous muscle constructs that could be transplanted back into the individual to replace lost or injured tissues, especially in elderly patients whose regenerative potential is lessened by age. Those with diseased tissue, however, cannot provide healthy skeletal myoblasts for isolation, and instead must rely on therapies to help treat their musculature. In this scenario, our model could be used to model various disease states and test drugs and therapies prior to use in human subjects [208]. Furthermore, our work with delivering microRNA therapies to muscle have shown their effects and great potential to be used as therapies targeting various pathways, including differentiation, fiber type, and metabolism. Our findings that multiple microRNA transfection does not diminish the transfection efficiency allows for great flexibility when designing microRNA treatments to target several desired pathways. As more microRNAs are discovered that affect myogenesis, the more possibilities there are for genetically designing engineered muscle, including miR-208b and miR-499 for increased type I myosin heavy chain protein expression [209], miR-181 for enhanced muscle differentiation [210], and miR-24 for regulating myogenesis by TGF- β , myogenin, and Mef-2 [211].

The findings presented in Chapter 4 show the feasibility of human skeletal muscle with human cord blood-derived endothelial cells. The identification of co-

culture media that can support both human skeletal muscle and human endothelial cells is the first step towards the engineering of vascularized human skeletal muscle *in vitro*. With the identification of EC seeding time and density to increase EC coverage, this method could be utilized to model the important skeletal muscle-endothelial cell interface. Such a model is important to the study of drug delivery to skeletal muscle and the accumulation and toxicity of drugs within the muscle. As stated previously, skeletal muscle comprises over 40% of the human body, so the effects of all drugs must be considered – even if the skeletal muscle is not the targeted tissue [212]. Drugs must pass through the skeletal muscle, and inevitably, there will be accumulation within the muscle tissue. This could possibly lead to tissue toxicity and other unpredicted effects. A model of the skeletal muscle-endothelial cell interface will allow for the study of drug diffusion across the endothelial cell layer into the skeletal muscle and the effects of drug accumulation on muscle organization and functionality. This model could prove very useful for preclinical testing of drugs.

APPENDICES

APPENDIX A. Antibodies

Antibody	Manufacturer	Species	Catalog No.
Sarcomeric α -actinin	Sigma	Mouse	A7811
Desmin	Sigma	Mouse	D1033
Collagen IV	AbCam	Rabbit	ab6586
PECAM/CD31	Life Technologies	Mouse	370700
Sarcomeric α -actin	Thermo Scientific	Rabbit	PA5-21396
Slow Myosin Heavy Chain	AbCam	Mouse	ab11083
Fast Myosin Heavy Chain	AbCam	Rabbit	ab91506
PGC-1 α	Calbiochem	Mouse	ST1203
β -actin	Santa Cruz Biotechnology	Mouse	sc-47778

APPENDIX B. Primer Sequences for Quantitative Real Time RT-PCR

Gene of Interest	Forward	Reverse
MHC I	GCCGAGTCCCAGGTCAACAAG	TGAGCAGATCAAGATGTGGCAAAG
MHC IIA	TTGCTGAGTCCCAGGTGAACA	TTTGTGCCTGTCTTCAGTCATTCC
MHC IIX	CTGAGGGTGAAGAGCAGGGAGGT	TTTTCACATTTTGTGCATTTCCTTGG
GAPDH	TCAACAGCAACTCCCCTCTTCCA	ACCCTGTTGCTGTAGCCGTATTCA
PPARGC 1A	TGTGCAACTCTCTGGAAGT	TGAGGACTTGCTGAGTGGTG
MEF-2C	ACTTCCTGGAGAAGCAGAAAGGCA	AACACGTTTCCTTCTTCAGCACGC

APPENDIX C. MATLAB Code for Force Measurements

```
%% HBAM FORCE TESTING DATA ANALYSIS %%
%% Written by C.S.Cheng, August 2012 %%
%% George A. Truskey Lab %%

clear all
p=input('Enter the percent length: ');
length=p*ones(1,5);
hz=[1,5,10,20,40];
for k=1:5

    % Import force data from excel
    [filename, pathname, filterindex]=uigetfile('*.xls');
    filelocation=strcat(pathname,filename); %concatenate strings
    [num, txt, raw]=xlsread(filelocation,'a15:a2014');

    % Calculate Offset and Adjust data
    offset(k)=mean(num(25:30));
    data(k,1:2000)=num-offset(k);

    % Find Peak Force Output (mN)
    if hz(k)<4
        Peak(k)=max(data(k,100:2000));
    elseif 4<hz(k)<9
        Peak(k)=max(data(k,950:2000));
    else
        Peak(k)=max(data(k,1500:2000));
    end
end

% Plot Force Output data (adjusted for offset)
t=(1:2000); % msec
figure(1)
for m=1:5
    subplot(2,3,m)
    plot(t,data(m,1:2000))
    title(sprintf('%g. %d%%Length, %dHz, Peak Force =
%gmN',m,length(m),hz(m),Peak(m)))
    xlabel('msec')
    ylabel('mN')
end
subplot(2,3,6)
plot(hz,Peak,'o--')
title('Peak Forces')
ylabel('mN')
xlabel('Frequency (Hz)')
axis([0 max(hz) 0 max(Peak)+0.5])
```

APPENDIX D. HSkM Culture Media Recipes

Growth Media (GM):

Component	Vendor	Product Number
DMEM, low glucose	Gibco	11885
8% fetal bovine serum (FBS)	Hyclone	SH30071.03
SkGM Singlequots (insulin removed)	Lonza	CC-4139

Differentiation (Shift) Media (DM/SM):

Component	Vendor	Product Number
DMEM, high glucose	Gibco	11995
2% Equine (Horse) Serum (HS)	Hyclone	SH30074.03
0.1% Gentamicin (1X)	Gibco	15750-060

Aliquots (all sterile, stored at -20°C, except Gentamicin, which is stored at room temperature)

45-50ml FBS; 550µl Gentamicin; 10.2ml HS

For GM:

To a 500ml bottle of LG-DMEM, add 45-50ml FBS, and all components of SkGM Singlequots except insulin in sterile fashion. If sterility is compromised, sterile filter with 0.2µm bottle top filter.

For SM:

To a 500ml bottle of HG-DMEM, add 10.2ml HS and 550µl Gentamicin in sterile fashion (either by carefully pouring or by pipetting in). If sterility is compromised, sterile filter with 0.2µm bottle top filter.

Protocol:

1. Before thaw, warm up growth media.
2. Thaw the cryovial containing the cell solution quickly at 37C with agitation
3. Transfer the contents of the vial to a 15ml conical containing 9ml of warm growth media
4. Pellet the cells for 5min at 1000rpm
5. Aspirate the media and add fresh media to resuspend the cells
6. Transfer cell solution evenly between uncoated tissue culture flasks. Label flasks with date, patient ID, passage number, and initials.

7. Cells should start growing and reach 30% confluency in 3 days. Feed the plates every other day until they reach about 80-85% confluency. Note that they grow much slower than other cell lines
8. To plate cells for experiments, first coat substrate with 100ug/mL growth factor reduced Matrigel (BD # 356231) diluted in HG-DMEM for 2 hours, then rinse 2X with cold HG-DMEM. Add warmed GM and seed HSkM. Note: to trypsinize, rinse 1-2 times with sterile DPBS-/- before adding 0.05% trypsin/EDTA (Gibco 25300-054)

APPENDIX E. Matrigel Coating Protocol

Updated by CC on Jan2010

Materials:

Phenol-free growth-factor-reduced (GFR) Matrigel (BD Biosciences)
HG-DMEM (11995, Gibco)
6-well plates
DPBS +/- (14040, Gibco)
Growth Media

Protocol:

1. Place phenol-free Matrigel on ice and place in sterile hood
2. Thaw Matrigel on ice (thaw out *entire* aliquot and mix by tipping tube!) Keep on ice to prevent solidification!
3. Using concentration given on chemical sheet, dilute stock Matrigel to 100 μ g/ml using cold HG-DMEM; make enough for 2ml per well.
4. Incubate for 2 hours at 37°C
5. After incubation, rinse 2X with cold DMEM
6. Plate cells onto Matrigel-coated well

APPENDIX F. HSkM Isolation Protocol

Updated on 9.5.2012 by C.Cheng

Contributions from Dorothy Slentz, Yasser El-Abd

Dr. Kraus and Dr. Truskey, Duke University

Stage 1: Isolation

Day before isolation

1. Make sure that the forceps, scalpel, glass petri dish to be used are packaged sterile or autoclaved.
2. Check for stock of trypsin cocktail, HBS (HBSS), growth media, and both collagen and non-coated T25 flasks.

Day of Isolation (Day Zero)

1. Obtain the muscle biopsy in a conical or vial of ice-cold DMEM.
2. Place muscle under laminar flow hood. Collect required sterile supplies: glass petri dish, scalpel, pair of forceps.
3. Aspirate excess media, leaving only 2-5ml of liquid to keep muscle moist.
4. Using forceps, carefully move tissue onto glass petri dish. Clean it from any fat, connective tissue, blood clots, etc.
5. Add 0.5ml HBS (Ca and Mg free) and begin mincing muscle tissue using scalpel and forceps. Dissect away fat, connective tissue, and blood clots missed in first cleaning.
6. Once the tissue has been cut into fine pieces (less than 1-2mm in width), add about 4.5ml HBS to petri dish.
7. Using 5ml pipette, transfer minced muscle tissue into 50ml conical and bring total volume up to 20ml (do this through 5ml aliquots, rinsing petri dish with each wash). *Note: keep muscle in tip of pipette to avoid muscle getting stuck to side of pipette.
8. Centrifuge muscle at 550xg for 10min
9. Aspirate supernatant and resuspend in 20ml HBS. Recentrifuge at 550xg for 10min. This will rid cells of any Ca/Mg that was present in the growth media (necessary for trypsin to work).
10. Aspirate supernatant, resuspend pellet in 5ml warmed trypsin cocktail (see recipe, attached). Place tube to incubate in 37C shaker water bath for 30min. Swirl tube periodically by hand during incubation. Note: do not refreeze any leftover trypsin cocktail, as effects on the solution of multiple thaws are not known.
11. Once the 30min incubation is done, add 15ml warmed growth media (see recipe, attached). Centrifuge tissue at 550xg for 10min.

12. Aspirate trypsin and resuspend tissue in 3.2ml growth media. Note: you want volume to be low
13. Preplate cells onto uncoated T25 flask for 3 hours at 37C. This will allow time for cells other than undifferentiated skeletal myoblasts to adhere to T25 flask.
14. After preplate is complete, carefully transfer media and unattached cells (including tissue) to collagen-coated T25 flask. Make sure to gently flush down the muscle stuck on the sides of the preplated T25.
15. Place flask in 37C incubator.

Day 3

1. Add 3ml warmed growth medium to T25 flask. Make sure that the flask is lying down and add the growth media slowly, to disturb the myoblasts as little as possible.

Day 8

2. Change media in T25 flask. Keep the total volume at 6ml. Try to take up as much of the old liquid as possible without drawing up any tissue in the process.
3. Continue to change the media every 5 days, as the human cells tend to grow fairly slow. Culture should reach about 60-75% confluency around 4-5weeks.

Stage 2: Expansion

At this point, you should have a single collagen-coated T25 flask in which the original muscle sample was grown. The confluency of the cells should be approximately 60-75%, yielding roughly 10^6 cells total.

1. Aspirate the old media and wash twice with 1X PBS (add about 2ml)
2. Add 2ml of 0.05% trypsin (this is not the trypsin cocktail used in the isolation!). Keep track of passage number. Rock the plate back and forth to immerse the cells in the trypsin. View underneath the microscope periodically to see that the cells have detached.
3. When the cells have detached, add 7ml of growth media to the T25 flask. This will stop the trypsinizing process. Transfer the solution to a new 15ml conical tube.
4. Mix the cell suspension and take out a small aliquot to count the cells. Determine the concentration and the total number of cells.
5. Pellet the cells for 5min at 1000rpm in the centrifuge
6. While the cells are in the centrifuge, prepare 3 100mm collagen-coated petri dishes with 8ml warmed growth media added to each plate.
7. After the centrifuge, aspirate the media solution in the tube and add 6ml of the growth media to resuspend the cells. Split the cell solution evenly among the 3 petri dishes.
8. Mix gently by moving the plates side to side. The cells should start sitting down within 1-2 hours.

9. Check the cells every day; change media every other day. Cells should reach about 90% confluency within 1 week.

Stage 3: Storage

At this point, you should have 3 petri dishes that have reached 90% confluency

1. Aspirate the old media. Wash 2X with 7-8ml of 1X sterile PBS.
2. Add 2ml of trypsin to each plate. Warm up and tap to loosen the cells.
3. Add 8ml of growth media to stop the trypsinizing process. Wash down the petri dish with the growth media to make sure all of the cells are collected. Transfer the entire solution to a 50ml conical.
4. Count the cells using the hemacytometer. Should have at least 6E6 cells total.
5. Centrifuge the 50ml conical containing the cell solution at 100rpm for 5min.
6. Aspirate the trypsin/media solution. Make freezing solution: 10% DMSO in growth media. Resuspend cells so that there are 0.5E6 cells/ml
7. Aliquot 1ml of cell solution to cryovial. Label with patient ID, date, passage number, and initials. Place in Frosty and keep in -20C for 24 hours. Then transfer to -80 freezer.

Stage 4: Thawing/expanding cells

At this point, the cells should be stored in the -80C freezer. Their concentration should be 0.5E6 cells/vial.

9. Before thaw, warm up growth media.
10. Thaw the cryovial containing the cell solution quickly at 37C with agitation
11. Transfer the contents of the vial to a 15ml conical containing 9ml of warm growth media
12. Pellet the cells for 5min at 100rpm
13. Aspirate the media and add fresh media to resuspend the cells
14. Transfer cell solution evenly between uncoated tissue culture flasks. Label flasks with date, patient ID, passage number, and initials.
15. Cells should start growing and reach 30% confluency in 3 days. Feed the plates every other day until they reach about 80-85% confluency. Note that they grow much slower than other cell lines

Trypsin Cocktail Recipe

<u>Final Concentration</u>	<u>For 50ml</u>
0.25% trypsin	5ml 10X trypsin (2.5) (Invitrogen 15090-046)
0.1% collagenase	0.05g collagenase (Invitrogen 17104-109)
0.1% BSA	5ml 1% BSA (Sigma A-7888)
0.05% EDTA	1.25ml 2% EDTA (Sigma E-6511)
	Sterile water to 50ml

Weight out collagenase into 50ml conical
In the tissue culture hood add EDTA, BSA, trypsin

Add water in the hood
Filter (0.2 μ m) sterilize and aliquot 5ml/15ml tube
Store at -20C

Materials

Company	Product	Cat Number	Application
Invitrogen (Gibco)	Hanks' Balanced Salt Solution (HBSS)(1X)(liquid 100ml)	14170-120	Isolation
	Trypsin/EDTA (0.05%) 1X liquid 100ml	25300-054	Splitting after isolation
	Trypsin 2.5% (10X) 100ml	15090-046	Trypsin cocktail
	Type IV collagenase (1g)	17104-019	Trypsin cocktail
	DMEM low glucose	11885	Growth media
	DMEM high glucose	11995	Differentiation media
Hyclone	Fetal Bovine Serum 500ml	SH30071.03HI	Growth media
	Horse Serum heat inactivated	SH30074.04HI	Differentiation media
Sigma	EDTA	E-6511	Trypsin cocktail
	BSA	A-7888	Trypsin cocktail
	DMSO	D-2650	Freezing media
Lonza	SkGM Singlequots	CC-4139	Growth media
VWR	Biocoat collagen I coated dishes (by BD)	62405-425 (100mm dish) 62405-025 (T25)	Isolation
	No. 10 scalpel blades (pk 10)	BD371110	isolation

APPENDIX G. HSkM Muscle Bundle Protocol

C.Cheng, 5/2013

Materials:

Sterile forceps	ice+bucket	12-well culture plate
45µl PDMS molds	2% pluronics solution	minutien pins
Velcro (cut into small pieces)	70% ethanol	100ml media bottle
Sonicator	0.05% trypsin/EDTA	sterile PBS-/-
10ml syringe+needle	Syringe filter	Growth media
Fibrinogen (Sigma F8630)	Thrombin (T9649, 50U/ml)	Matrigel (BD, 356231)

Methods:

Sterilization of PDMS molds

1. Rinse molds with DI water (soak for 15 minutes)
2. Using sterilize forceps, transfer all molds to 100ml glass media bottle containing 70% ethanol. Make sure all molds are submerged in the ethanol. Sonicate for 60 minutes.
3. Place molds in 12 well plate to dry (about 1 hour). Unused molds can be kept in the ethanol until needed.
4. In the meantime, place pins and Velcro in 70% ethanol to soak for 1 hour.
5. Once molds are dry, UV for at least 30 minutes. Place pins and Velcro in a petri dish and UV along with molds.
6. After UV, place 2% pluronics solution in each mold and place in incubator (anywhere from 20-60min). **Do not** place pins and Velcro in pluronics! Pins and Velcro should remain in petri dish in hood to continue drying.
7. Aspirate pluronics solution and check that no liquid remains. Pin Velcro into molds and set aside.

Seeding HBAM (Human Bioartificial Muscle)

1. Gather the following materials: ice, sterile forceps/tweezers, thrombin, Matrigel, growth media (GM). Place thrombin, Matrigel, and GM on ice.
2. Make fibrinogen fresh each time: weigh out 15mg and dissolve in 1ml sterile PBS-/. Use syringe filter to sterilize. Label and place on ice with other reagents.
3. Warm 0.05% trypsin/EDTA and GM. Rinse hSKM with sterilize PBS-/- and add trypsin/EDTA. Make sure cells are detached after 3 min, if not wait another 2 minutes. Stop action of trypsin with warm GM. Transfer cell solution to 50ml conical and count cells using hemacytometer. Calculate

volume to centrifuge in order to seed 15E6 cells/mL. Spin cells at 1000rpm for 5 min.

4. After spin, aspirate all supernatant, leaving only cell pellet. Resuspend in cold GM. Add Matrigel and fibrinogen. Finally, add thrombin and quickly pipet 45µl into each mold. (Note: thrombin starts the fibrin gel formation, so work quickly!) Make sure the mixture is pipetted around and into the Velcro for anchoring!
5. Place 12-well plate into incubator to gel for 1 hour. During this time, make GM supplemented with 1.5mg/ml aminocaproic acid (ACA) – syringe filter for sterility.
6. After 1 hour, gently add GM+ACA on top of molds and gels, making sure to keep molds from floating to top.
7. After 48 hours, change media to 2%SM+ACA (again, 1.5mg/ml ACA but now dissolved into 2% shift media)
8. Culture for 2 weeks, exchanging 2%SM+ACA every other day. Then, treat with drugs and/or measure forces.

	2 HBAMs (1 mold)	4 HBAMs (2 molds)	6 HBAMs (3 molds)
Matrigel	20 µl	38 µl	56 µl
15mg/ml Fibrinogen	26.7 µl	50.7 µl	74.7 µl
50U/ml Thrombin	3.9 µl	7.5 µl	11 µl
Cell solution (in GM)	49.4 µl	93.9 µl	138.3 µl
Total (45ul/HBAM)	100 µl	190 µl	280 µl

APPENDIX H. Immunostaining Protocol

1. Aspirate media from all wells and rinse once with DPBS-/- (does not need to be sterile). Aspirate all DPBS.
2. Add ice-cold methanol (3mL/well) to wells to fix cells. Let sit at RT for 2-3 minutes. You may see white residue in the well (this is ok). Aspirate methanol and rinse twice with DPBS-/-.
3. Store cultures in DPBS-/- in fridge until ready to stain.
4. Aspirate DPBS-/- from wells and block for at least 1 hour with 10% goat serum on rocker at RT (up to overnight is fine).
5. Aspirate goat serum and add primary antibody solution (diluted in 10% goat serum, see Table below). Incubate for at least 4 hours (up to overnight) on rocker at RT.
6. Aspirate primary antibody solution and rinse 3X with DPBS-/- (5 min/wash, on rocker).
7. Make secondary antibody solution (Alexa Fluor, 1:250 dilution in DPBS-/-) and incubate for 45 minutes, protected from light (foil) on rocker at RT.
8. Wash 3X with DPBS-/- (5min/wash on rocker). Add 3 mL DPBS-/- to each well and image.

Antibody	Species	Dilution	Vendor/Cat#
Sarcomeric alpha-actinin (SAA)	Mouse	1:800	Sigma, A7811
Collagen IV	Rabbit	1:500	AbCam, ab6586
Laminin	Rabbit	1:500	AbCam, ab11575
Fast myosin heavy chain	Rabbit	1:500	AbCam, ab91506
Slow myosin heavy chain	Mouse	1:500	AbCam, ab11083

APPENDIX I. HSkM miR Transfection Protocol

Updated by C.Cheng 12/2009, taken from CRIII Lab Notebook p. 8C

Updated by C.Cheng 3/2014

Materials

T75 flasks

GM

Opti-MEMI Reduced Serum Media 1X (Life Technologies 31985-070)

siPORT NeoFX Transfection Agent (Life Technologies AM4511)

Negative Control #1 (NC#1; Life Tech AM17010)

Anti-miR

Anti-miR-133a: Life Technologies AM17000 ID AM10413

Anti-miR-696: Life Technologies AM17000 ID AM11434)

Methods

1. Bring up HSkMs into T75 flasks. Grow to 75-80% confluence.
2. Warm up Growth Media (GM)
3. Prepare transfection solutions: NTC, NC, A133a, A696, Joint (A133a+A696)

NTC: non-transfected control	4.9ml Opti-MEM
NC: negative control (transfected with scrambled miR sequence)	98.28 μ l siPORT + 2.36ml Opti-MEM 196.56 μ l NC#1 + 2.26ml Opti-MEM
A133a: transfected sample	98.28 μ l siPORT + 2.36ml Opti-MEM 196.56 μ l anti-miR-133a + 2.26ml Opti-MEM
A696: transfected sample	98.28 μ l siPORT + 2.36ml Opti-MEM 196.56 μ l anti-miR-696 + 2.26ml Opti-MEM
Joint: transfected sample	98.28 μ l siPORT + 2.36ml Opti-MEM 196.56 μ l anti-miR-133a + 196.56 μ l anti-miR-696 + 2.26ml Opti-MEM

4. Place each transfection solution into a different T75 flask and spread evenly on the bottom of the flask. Let sit for at least 10 minute to equilibrate to RT.
5. Passage cells at 75-80% confluence. Resuspend cells in warm GM and place 1E6 cells/flask into flasks with tranfection solutions. Make sure to clearly label each flask to avoid confusion!
6. Add warm GM to each T75 (for a total of 19.7ml of GM and 4.9ml transfection solution in each T75)
7. Place in incubator and allow transfection to sit for 18 hours (do not exceed!)
8. After 18 hours, trypsinize and count cells for studies.

APPENDIX J. miR Isolation Protocol

Updated on 11.21.2011 by C.Cheng

Life Technologies mirVANA microRNA Isolation Kit (Cat# AM1560)

Setup/Prep

1. RNasZap benchtop, pipettors, and tip of Pasteur pipette
2. Get bucket of ice from autoclave room
3. Gather two 1.5-2.0 RNase/DNase-free tubes per sample/condition and two tubes from mirVANA miR isolation kit box (one filter per 2 tubes)
4. Label tubes with conditions, hSKM ID#, SD#, and date
5. Get box of miR isolation solutions from fridge, place Lysis Buffer and miR homogenate additive on ice. Let Wash Solutions #1 and #2/3 equilibrate to RT. Aliquot 110 μ l/condition of Elution Solution and place on heating block (on HIGH with dial turned to KO – should be around 95°C).
6. Gather plate(s) from incubator and place on ice.

Cell Lysis Procedure

1. Aspirate media, rinse 1X with 1000 μ l DPBS and aspirate. Add 500 μ l DPBS to each well and use cell scraper to collect sample. Be sure to use new scraper and pipette tip for each condition!
2. Centrifuge samples at 10k rpm for 5 minutes. While spinning, discard plates and scraper wrappers. After pelleting cells, aspirate DPBS
3. Resuspend each cell pellet in 300 μ l Cell Lysis Buffer; vortex each tube for 1 min (the lysis buffer tends to drip, so make sure tubes are open and ready!)
4. Add 30 μ l miR homogenate additive to each tube. Vortex for 15sec. Incubate on ice for 10min.
5. Return Cell Lysis Buffer, miR homogenate additive, and Elution Solution to the fridge. Keep Wash Solutions out to reach RT.

Organic Extraction: all steps to be done in fume hood!

1. Before the 10-min incubation is complete, gather pipettors (P200 and P1000) and tubes and take to fume hood.
2. Double-glove with *nitrile* gloves and wear lab coat!
3. Get metal canister from top shelf of large fridge. *Be very careful carrying/handling this chemical! It is toxic!* Take to fume hood and carefully remove bottle from canister and open lid.
4. Make sure all tubes are open and pipette 300 μ l from the *bottom phase* of the chemical into each tube. You may use the same pipette tip if you do not touch any tubes! (Try to be quick and very careful! The chemical tends to drip)
5. Close bottle and all tubes **carefully**, place bottle back into canister and promptly return to fridge.

6. Vortex each tube 1 min in the fume hood. Minimize exposure by closing doors as much as possible.
7. Use centrifuge in fume hood to spin for 5min at 10k rpm.
8. After spin, carefully remove each tube and pipette out *upper phase* and transfer into new tube (about 300-320 μ l). Discard lower phase into waste bottle and used tubes into biohazard in fume hood.
9. Add 430ul 100% Ethanol to each tube, pipette to mix and transfer 700 μ l to filter. Spin for 15sec at 10k rpm
10. Pipette waste into waste bottle, add 700 μ l Wash Solution #1 to each filter. Spin for 15sec at 10k rpm
11. Discard waste into waste bottle, add 500 μ l Wash Solution #2/3. Spin for 15sec at 10k rpm.
12. Repeat Step #11 above
13. Dry spin for 1min at 10k rpm. During spin, get warmed Elution Solution, turn off heat block.
14. Transfer each filter to correspondingly labeled clean tube, pipette 100 μ l warm Elution Solution and spin for 15sec at 10k rpm.
15. Discard filters and store in -80C until RT-PCR.

APPENDIX K. TAQMAN qRT-PCR for miR Expression

C.Cheng, created 7.19.2010; Updated 11.01.2010

Materials Needed

- miR samples isolated previously (frozen in -80°C freezer)
- RNase/DNase-free water
- 20, 200, 1000 µl barrier tips
- Appropriate primers for RT and Real Time PCR reactions
- Endogenous control
- Reference RNA (isolated or bought)
- TaqMan MicroRNA Reverse Transcription Kit (ABI: 4366596, 4366597)
- TaqMan Universal PCR Master Mix, No AmpErase UNG (ABI: 4324018)
- DNase/RNase-free tubes (0.2ml, 2.0ml) with caps
- 96-well optical plate for PCR

miR Purity

1. After miR isolation, aliquot samples and take to NanoDrop ND-1000 (outside CIEMAS 2208B) to measure purity and concentration
2. Log in, open program
3. Choose RNA Assay and Blank once
4. Place 1ul of sample carefully on NanoDrop and click Measure
5. Record 260/280 and RNA concentration
6. Calculate amount of nuclease-free water to add to dilute to 1-10ng of total RNA per 15 µl reaction

Reverse Transcription (RT) Reaction

1. Calculate number of reactions to perform.
2. Prepare RT Master Mix (MM) by scaling volumes to desired number of RT reactions. Account for 10% pipetting loss; mix by pipetting up and down.

Color Tube	Reagent/Component	Volume for 1 reaction	Volume for N reactions
Yellow	10X RT Buffer	1.5 µl	(1.5ul)(N)(1.1)
Blue	dNTP mix	0.15 µl	(0.15ul)(N)(1.1)
White	RNase Inhibitor	0.19 µl	(0.19ul)(N)(1.1)
Purple	Multiscribe RT enzyme	1.00 µl	(1.00ul)(N)(1.1)
--	Nuclease-free water	4.16 µl	(4.16ul)(N)(1.1)
TOTAL for 1 RT reaction		7.0 µl	(7.0ul)(N)(1.1)

3. Add 5ul of total RNA (for final concentration of 1-10ng/reaction) to RT MM. Mix gently by pipetting up and down.
4. Thaw primers on ice and centrifuge briefly. Label tubes.
5. Place 12 µl of RNA + MM mix into each labeled tube.
6. Add 3 µl of RT primer to appropriate tubes for a final volume of 15 µl. Mix by pipetting. Seal with caps.
7. Centrifuge, place plate on ice for at least 5 minutes. Load thermal cycler.
8. Set thermal cycler at reaction volume of 15 µl and start run listed below:

STEP	TIME	TEMP
Hold	30 min	16°C
Hold	30 min	42°C
Hold	5 min	85°C
Hold	∞	4°C

qPCR Amplification

1. Use clean 1.5ml microcentrifuge tubes for each sample (Nuclease-free!)
2. To each tube add the following volumes for *triplicates*:

Component	Single Reaction	Triplicate Reaction
TaqMan RNA Assay (20X) – primer	1.00 µl	3.60 µl
Product from RT reaction	1.33 µl	4.80 µl
TaqMan Universal PCR Master Mix II (2X)	10.00 µl	36.00 µl
Nucelase-free water	7.67 µl	27.61 µl
TOTAL Volume	20.00 µl	72.01 µl

3. Cap tube and invert to mix. Centrifuge.
4. Transfer 20 µl of qPCR reaction mix to 3 corresponding wells on a 96-well optical plate. Place optical plate on ice pack to keep cold.
5. Seal plate with cover and centrifuge.
6. Load into instrument. Be sure to use “Erase” to denote empty wells. Setting on thermal cycler should be set to Standard Run Mode and Sample Volume of 20 µl. Thermal cycling conditions are below:

STEP		TIME	TEMP
Enzyme Activation	Hold	10 min	95°C
PCR (40 cycles)	Denature	15 sec	95°C
	Anneal	60 sec	60°C

Setting up RT-PCR Plate with Reference and Housekeeping Gene

Investigating treatments A, B, and C

Looking at genes 1, 2, 3

Common **housekeeping genes**: 18s, GAPDH, beta-2-microglobulin.

- Housekeeping genes are primers that you use to test that the Ct values for all treatments of interest are the same (or very similar)

References are samples that *must* be constant through *every* RT-PCR plate!

- Can be anything, but must contain some quantity of the genes of interest.
- Can either collect RNA and aliquot into many many tubes, or order an RNA sample from a company. Since miR's are low in quantity, will order Mouse 11-day Embryo Total RNA (Cat. No. 636608) from Clontech

Sample plate setup:

	A	A	A	B	B	B	C	C	C	REF	REF	REF
1	A1.1	A1.2	A1.3	B1.1	B1.2	B1.3	C1.1	C1.2	C1.3	REF1.1	REF1.2	REF1.3
2	A2.1	A2.2	A2.3	B2.1	B2.2	B2.3	C2.1	C2.2	C2.3	REF2.1	REF2.2	REF2.3
3	A3.1	A3.2	A3.3	B3.1	B3.2	B3.3	C3.1	C3.2	C3.3	REF3.1	REF3.2	REF3.3
HS	AH.1	AH.2	AH.3	BH.1	BH.2	BH.3	CH.1	CH.2	CH.3	REFH.1	REFH.2	REFH.3

Note: HS = housekeeping gene; run samples in triplicate

Once the plate is run and the raw data retrieved, average each triplicate set and use the **Housekeeping gene** to calculate ΔCt . Let A1 = average of A1.1 and A1.2 and A1.3, and so on.

$$\Delta Ct_{A1} = A1 - AH$$

$$\Delta Ct_{A2} = A2 - AH$$

:

:

$$\Delta Ct_{B2} = B2 - BH$$

:

:

$$\Delta Ct_{C3} = C3 - CH$$

After finding ΔCt , use the **Reference** to find the $\Delta\Delta Ct$:

$$\Delta\Delta Ct_{A1} = \Delta Ct_{A1} - REF_1$$

$$\Delta\Delta Ct_{A2} = \Delta Ct_{A2} - REF_2$$

:

:

$$\Delta\Delta Ct_{C3} = \Delta Ct_{C3} - REF_3$$

Finally, calculate $2^{-\Delta\Delta C_t}$ to find fold-difference of each sample from the Reference.

APPENDIX L. SYBR Green qRT-PCR Protocol

3June2012

Measuring RNA Concentration using Nanodrop (NOTE: Avoid rethaw cycles as RNA degrades quickly. Keep RNA samples in labtop cooler/on ice.)

1. Place RNA samples (and REF sample) in cooler and grab nuclease-free water, P2 pipette, and 10 μ l filter tips.
2. Log into computer (username: microarray, password: nanodrop) and select *ND-1000 V3.7.1 >> Nucleic Acids*.
3. Wipe down stage with Kimwipe. Add 1 μ l of nuclease-free water onto the stage and click "ok" in the initialization window that pops up.
4. Change *DNA-50 (green)* to *RNA-40 (pink)* using the pull-down menu in the upper-right corner.
5. Click "Blank" in the upper-left corner.
6. Wipe down stage with Kimwipe. Add 1 μ l of sample onto the stage and click "Measure" in the upper-left corner.
7. Record the RNA concentration (ng/ μ l), $A_{260/280}$, and $A_{260/230}$ of the sample. The $A_{260/280}$ purity level should be ~ 2 ; the $A_{260/230}$ purity level should be ~ 2.5 .
8. Repeat steps 6-7 for each RNA sample.
9. After measuring the last sample, wipe clean the stage.
10. Exit out of the program and log off

Making cDNA (NOTE: Complete RT on the same day that the RNA concentration measurements are made to avoid freezing and rethawing RNA samples.)

1. Calculate the appropriate volume (μ l) of RNA sample needed for a desired x ng of RNA. This is done by dividing x ng by *RNA concentration in μ g/ μ l*.
2. Calculate the volume (μ l) of nuclease-free water such that the total amount of nuclease-free water + RNA sample is 18 μ l.
3. Wipe down bench, pipettes, and gloves with RNase Zap. Grab the 96-well freezer boxes in the -20°C freezer pull-out shelf and wipe down the lid with RNase Zap.
4. Add 5x iScript Reaction Mix (blue tube) and iScript Reverse Transcriptase (yellow tube) to ice bucket.
5. Take a 0.2ml colored reaction tube for each sample and place in the 96-well freezer box.
6. Add the calculated amount of nuclease-free water to the reaction tubes.
7. Add the calculated amount of RNA to the reaction tubes.
8. Add 5 μ l of the 5x iScript Reaction Mix (blue tube) to each reaction tube.
9. Add 1.25 μ l of the iScript Reverse Transcriptase (yellow tube) to each tube (NOTE: This is the polymerase that initiates the reaction, so add this component last.).

10. Mix by gently pipetting up and down (NOTE: Do not vortex.).

If thermocycler is available for use, continue through steps 11-17; if not, skip to step 18.

11. Turn the thermocycler on by switching the button on the power supply box first followed by switching on the unit. Place the tubes inside.
12. Select *Registered User* >> *Duke*.
13. Select *F1 (Protocol Library)* >> *cDNA*
14. Select *Run Protocol* and set the sample volume to $25\mu\text{l}$
15. Select *F5 (Begin Run)*
16. Sample will take about 45 minutes to run. Once the RT process is complete, you may choose to complete the PCR step or wait to complete the PCR a different day (PCR takes 2.5hr to complete) and store the cDNA in the -20°C freezer in a sample box.)
17. If you choose to complete the PCR on a different day, turn the thermocycler off.

If thermocycler is being used, you may use the MWG-Biotech thermocycler at the RNA station.

18. Turn the thermocycler on (behind the machine above the plug) (NOTE: Be careful when moving the thermocycler to avoid unplugging the machine.).
19. Select 2. *Select Protocol* >> *25-42.cyc*.
20. Continue selecting *Run/Enter* until the thermocycler begins.
21. Sample will take about 45 minutes to run. Once the RT process is complete, you may choose to complete the PCR step or wait to complete the PCR a different day (PCR takes 2.5hr to complete) and store the cDNA in the -20°C freezer in a sample box.)
22. If you choose to complete the PCR on a different day, turn the thermocycler off.

PCR (NOTE: Keep everything on ice or in freezer boxes during this process as this step is heat-sensitive; also, turn off the lights as this step is light-sensitive.)

1. Wipe down bench, pipettes, and gloves with RNase Zap. Grab cDNA samples and dilute with $20\mu\text{l}$ of RNA-ase/DNA-ase free water; mix gently by pipetting up and down (NOTE: Be sure to mark that the samples have been diluting to avoid confusion with undiluted cDNA samples.).
2. Take two freezer boxes from the -20°C freezer. Wipe down the lids with RNase Zap and place a 96-well PCR plate in the freezer box. (NOTE: Make sure that you do not touch the bottom of the 96-well PCR plate. Hold the plate by its sides to avoid initiating the reaction when samples have been aliquoted into the wells.)
3. Let y be the number of genes of interest (2 in the case of gene of interest, PPARGC1A, and housekeeping gene, GAPDH). For x cDNA samples, obtain $x*y$ 0.2ml clear reaction tubes and place in the second freezer box.

4. Place iQ SYBR Green Supermix (orange tube) and primers (both 5' and 3' primers) in ice bucket.
5. Let y be the number of genes of interest (2 in the case of gene of interest, PPARGC1A, and housekeeping gene, GAPDH). Label a 2.0ml colored microtube with the name of the gene for each gene of interest.
6. Let z be the number of conditions (2 if conducting a study comparing static vs. stretch conditions; 2 if Plastic static vs. Bioflex static). Then, combine the following reagents in each 2.0ml tube:
 - 6.6*[(3.5*x*z)+3] μ l nuclease-free water
 - 1.2*[(3.5*x*z)+3] μ l 3' primer for gene of interest
 - 1.2*[(3.5*x*z)+3] μ l 5' primer for gene of interest
 - 10*[(3.5*x*z)+3] μ l iQ SYBER Green Supermix
7. Mix solutions by pipetting up and down.
8. Repeat steps 6-7 for each y 2.0ml tube labeled with the gene of interest.
9. Add 66.5 μ l of the solution prepared in step 6 to each of the 0.2ml microtubes from step 3.
10. Add 3.5 μ l of the cDNA sample from the RT step to each 0.2ml clear reaction tube.
11. Mix the solution by pipetting up or down.
12. Add 20 μ l of the mixed solution to each of 3 wells of the 96-well plate (NOTE: Add the mixed solution to the side of the well and let it drip down to the bottom. Make sure to avoid making air bubbles.). Repeat for the other microcentrifuge tubes in an order according to the determined plate set-up.
13. Cover the 96-well PCR plate with optical tape and secure the cover.
14. Centrifuge the PCR plate at 1400rpm for 2-3 minutes (NOTE: When transferring the PCR plate to the centrifuge, hold by the sides and avoid touching the bottom of the plate.).
15. Place the 96-well PCR plate in the thermocycler.
16. Open the *MyiQ* program and select the protocol *2StepAmp+Melt4ebd.tmo*.
17. Select the tab *View Plate Setup* and select *Edit This Plate Setup*.
18. Label each triplicate set with a unite number and erase all blank wells.
19. Save the plate setup and click *Run with Selected Protocol*. Enter in 20 μ l and double check that SYBR-40 has been selected in the lower right window. Select *Begin Run*.
20. The thermocycler will run for about 2.5 hours; double check ~10 minutes into the process that the program has not exited out due to an error.

APPENDIX M. Western Blot Protocol

Tracy Cheung

April 2011

Modified from CR and SW Protocols

Materials

- Lysis Buffer: CellLytic-M (Sigma C2978)+Protease inhibitor cocktail (Sigma P8340)
- Mini Ready Gel
- Laemmli's Sample Buffer (Biorad #161-0737)
- Beta-Mercaptoethanol (Biorad 161-0710)
- TBST: Dilute 10x Tris-Buffered Saline (Biorad #170-6435) to 1X with DI water and add 0.1 % Tween 20 (Biorad 170-6531) (i.e. 50mL TBS, 450mL DI water, 0.5mL Tween 20)
- Transfer Buffer: 100 mL 10x Tris Glycine Buffer (Biorad #161-0771), 700mL distilled water, 200mL methanol (if using PVDF membrane, otherwise 900mL distilled water)
- Running Buffer: 100mL 10x Tris/Glycine/SDS Buffer (Biorad #161-0772), 900mL distilled water
- PVDF membrane
- Fiber pads
- Filter paper
- Kaleidoscope Ladder (Biorad 161-0375)
- SuperSignal West Pico Stable Peroxide Solution
- SuperSignal West Pico Luminal/Enhancer Solution
- RESTORE Stripping Solution (21059)
- Pierce BCA Assay Kit (Pierce 23227)
- Film
- Non-Fat Dry Milk Powder
- Primary and Secondary Antibodies
- Methanol
- PBS -/-
- Eppendorf tubes
- Micropipettes
- Pipettes
- 96-well plate for BSA
- 50mL and 15mL conical tubes

DAY 1

Buffer Preparation

1. Mix ingredients together for Transfer and Running Buffers and put into labeled 1L jars. These can be stored in the fridge overnight.
2. Mix ingredients together for TBST. Tween 20 is very viscous. Store in fridge overnight.

DAY 2

Protein Harvest (Can be done as cells are ready and stored in -20C)

1. Prepare Lysis Buffer (KEEP ON ICE)
 - Cell-lytic M (Add 0.5mL protease/phosphatase inhibitor cocktail to every 5mL Cell-lytic M used)
2. Carefully aspirate media from cells. The whole process should be done on ice.
3. Wash once with cold DPBS -/-
4. Add DPBS to each flask or well (~400 μ l /well).
5. Scrape cells with cell scraper. Keep plate tilted at all times in order to keep all the cellular debris in the PBS. Pipette out all liquid and cells. Add suspension to 2.0mL eppendorf tube.
6. Spin down tubes with microcentrifuge at speed 3 for 5 minutes.
7. Remove supernatant and resuspend cells in ~70 μ l of lysis buffer.
8. Shake for 30 minutes at 4C with lab quake.
9. Spin down tubes at max speed for 15 minutes at 4C (place microcentrifuge in fridge).
10. Remove supernatant (this is the protein soluble fraction) and place each into sterile vials. Store in -20C.

BSA Protein Concentration Determination Protocol

1. Prepare BSA Standards as described in the manual that comes with the BSA kit, EXCEPT dilute in lysis buffer rather than PBS. (Note: The standards can be prepared ahead of the time and aliquoted and stored at -20C.)
2. Prepare BCA indicator solution (# samples + # of samples) * (number of replicates) * (volume of indicator solution per sample) = total volume of indicator solution needed. Make the solution with 50 parts Reagent A with 1 part Reagent B (example: 2500 μ l Reagent A, 50uL Reagent B).
3. Add 100 μ l of BCA solution to each well of a 96-well plate.
4. Add 2 μ l of each BSA standard to the wells (do in duplicate in rows A and B of plate).
5. Add 2 μ l of each unknown sample to wells (do in duplicate, rows C and D).
6. Shake for 30s on plate shaker.
7. Incubate at 37C for 35 minutes.
8. Read using plate reader in Yuan lab (ABS 590) or Bursac Lab (Mina_BSA).

Prepare Proteins

1. Use Excel spreadsheet and BSA results to calculate volume of lysate needed to get desired amount of protein (usually, 10 μ g-30 μ g).
2. In 1.5mL eppendorf tubes, add amount of DI water calculated on spreadsheet, then add protein lysate (amount specified on spreadsheet).
3. Make Loading Buffer in a separate 1.5mL tube; solution should be 19 parts Laemmli's Sample Buffer, 1 part BME (calculation on spreadsheet). This should be added 1:1 with the rest of your protein solution (protein+water made in step 2), see spreadsheet for calculation. ADD AND STORE BME in fume hood.
4. Put samples on heat block set at 100C for 5 minutes. Squirt DI H₂O on set to help seal space between tube and set. Make sure tubes are sealed and use forceps to poke holes in top of tube so that the pressure does not build up. DO NOT BOIL STANDARD.

Run Gel

1. During 5 minutes-Add gel to box
 - a. Cut bottom film from ready gel (leave no black from cut line).
 - b. Add gel to box with comb facing inward (push all the way down and lock). The shorter plate faces the inside.
 - c. Carefully remove comb.
 - d. Add running buffer and then add to box (fill to top in inner and near top to outer).
2. Add protein samples and ladder (15 μ l for ladder, usually 30 μ l for protein samples depending on gel lane size).
3. Run the gel at 150 volts, max current and power for ~30-45 min (until visible bands reach bottom of gel, near wire).

Transfer

1. While the gel is running, soak the PVDF membrane in 100% methanol.
2. Soak PVDF membrane, 2 fiber pads, 2 pieces of thin transfer/filter paper in transfer buffer right before the gel is done.
3. Take the gel out of the cassette and gently break it open in transfer buffer. Pour out Running Buffer, but DO NOT wash gel box (need a small amount of SDS in transfer buffer).
4. Cut off top and bottom parts of gel with green blade.
5. Open up the cassette (black and clear parts) and lay the black part down.
6. Put items in following order on the black part: fiber pad, filter paper, gel, PVDF membrane, filter paper, fiber pad. Roll out air bubbles with pipette after you add membrane, paper, and pad.
7. Cut one corner of the membrane so that you remember which side of the membrane is in contact with the gel.
8. Close and clamp cassette.

9. Place the holder into the trans-blot, BLACK FACING BLACK.
10. Put box in bin (like the small autoclave bin) on stir plate with magnetic stirrer set at a 9, add transblot, and BioIce (in freezer).
11. Fill box to the top with transfer buffer.
12. Add ice to the bin to surround the box. This is to keep the transfer cold.
13. Set transfer for 200V, 500mA, 40W current for 3 hours for proteins above 175kDa, 2.5 hours for proteins 100-175kDa, 1.5 hours for 45-100kDa, and 1 hour for less than 45kDa (RT) and stir at Fast setting.

Probe with Antibodies

14. While transferring, make 5% milk (1g non-fat milk with 20ml TBST) in 50mL conical tube and 1% milk (1g non-fat milk with 100mL TBST) in flask. Add stir bar to flask and stir to mix.
15. Take apart trans-blot and remove the membrane and put into a tray with 5% milk, rock at RT for 1 hour (this can be extended if there is a lot of background).
16. Rinse membrane quickly with 1% milk in TBST.
17. Place the membrane in 1% milk and add the primary antibody (usually about 5mL milk needed) at the proper dilution.
18. Incubate overnight in the cold room using gentle tilting.

DAY 3

19. Rinse once quickly, then 3X for 10 minutes each in TBST using gentle tilting.
20. Add secondary antibody to the membrane in 1% nonfat dry milk (usually about 1:5000 dilution).
21. Incubate for 45 minutes at RT using gentle tilting.
22. Rinse 3X, 10 minutes each in TBST using gentle tilting.

Expose Membrane to Film

1. In foil-wrapped 15mL conical tube, mix together 2.5mL of SuperSignal West Pico Stable Peroxide Solution and 2.5mL of SuperSignal West Pico Luminal/Enhancer Solution (1:1 ratio) (ECL Solution).
2. Lay the membrane on Plastic Wrap and put ECL solution on the membrane (~5mL/membrane).
3. Turn off the lights and let the solution sit on the membrane for 5 minutes.
4. Transfer membrane with forceps over to new Plastic Wrap which is laid on top of a book or the film box.
5. Add a new piece of Plastic Wrap over the top of the membrane and seal. Roll out any air bubbles with pipette.
6. Cut Plastic Wrap around membrane.
7. Place and tape membrane into the cassette.
8. Take cassette, film, scissors, pen, and timer to the dark room (2nd floor C wing of LSRC).
9. Remove film and cut corner to match the cut corner on the membrane. Place film on membrane, and close cassette. The film can be cut in half if only one membrane is being used.
10. Set timer for exposure time (3 minutes is a good place to start).
11. Remove film from cassette at end of exposure time, flip over, and add to developing machine.
12. Repeat film exposure with other pieces of film and adjust exposure time as necessary.

13. Analyze films using densitometry (see protocol below).

Strip Membrane (Only necessary if reprobing)

1. Submerge membrane in RESTORE Stripping Solution (Pierce) and incubate at RT for 15 minutes with occasional agitation.
2. Wash with TBST 3X for 5 minutes each. Repeat steps 1 and 2 of this section.
3. Re-block in 5% milk for 1 hour at RT, then can probe for a different primary antibody.

Data Analysis – Densitometry Protocol (Using ImageJ Software)

1. Scan films with scanner.
2. Open ImageJ Software. Go to File>Open and open the scanned image of your membrane.
3. Select the rectangle tool and draw a box around your first lane. Make sure that you do not overlap any other lanes.
4. Once first lane is selected, go to Analyze>Gels>Select First Lane, or type ctrl+1.
5. Drag box onto the next lane and go to Analyze>Gels>Select Next Lane, or type ctrl+2. The box for each lane must be the same size. Make sure that each box encloses only the desired lane and does not overlap with other bands ... this will create error in your data.
6. Repeat this until all lanes on your gel have been selected.
7. Go to Analyze>Gels>Plot Lanes, or type ctrl+3.
8. Select the line drawing tool and draw a horizontal line even with the baseline (no signal) part of the graph for each line. Make sure that the curve corresponding to your band is completely closed in by this line (draw vertical lines if necessary to create a closed shape. NOTE: Your procedure for this part isn't as important as making sure you are consistent with what you do for all bands.
9. Select the wand tool (to the left of the text tool). Click inside each closed curve. Another box will appear, containing the area of the enclosed area (arbitrary units).
10. If you are using a loading control or standard (such as B-actin), divide the numbers you get by the corresponding number for that control for the same lane.
11. Plot your results using excel.

APPENDIX N. Copyright Releases

No permissions are required for reuse of material from American Journal of Physiology – Cell Physiology for thesis/dissertation (Chapter 2).

REFERENCES

1. Cheng, C.S., Y. El-Abd, K. Bui, Y.E. Hyun, R.H. Hughes, W.E. Kraus, and G.A. Truskey, *Conditions that promote primary human skeletal myoblast culture and muscle differentiation in vitro*. *Am J Physiol Cell Physiol*, 2013. **306**: p. C385-C395.
2. Ostrovidov, S., V. Hosseini, S. Ahadian, T. Fujie, S.P. Parthiban, M. Ramalingam, H. Bae, H. Kaji, and A. Khademhosseini, *Skeletal Muscle Tissue Engineering: Methods to Form Skeletal Myotubes and Their Applications*. *Tissue Eng Part B Rev*, 2014.
3. Harms, C.A., *Effect of skeletal muscle demand on cardiovascular function*. *Med Sci Sports Exerc*, 2000. **32**(1): p. 94-9.
4. Zhang, J.S., W.E. Kraus, and G.A. Truskey, *Stretch-induced nitric oxide modulates mechanical properties of skeletal muscle cells*. *Am J Physiol Cell Physiol*, 2004. **287**(2): p. C292-9.
5. Le Grand, F. and M.A. Rudnicki, *Skeletal muscle satellite cells and adult myogenesis*. *Curr Opin Cell Biol*, 2007. **19**(6): p. 628-33.
6. Cosgrove, B.D., A. Sacco, P.M. Gilbert, and H.M. Blau, *A home away from home: challenges and opportunities in engineering in vitro muscle satellite cell niches*. *Differentiation*, 2009. **78**(2-3): p. 185-94.
7. Tidball, J.G. and S.A. Villalta, *Regulatory interactions between muscle and the immune system during muscle regeneration*. *Am J Physiol Regul Integr Comp Physiol*, 2010. **298**(5): p. R1173-87.
8. Thornell, L.E., *Sarcopenic obesity: satellite cells in the aging muscle*. *Curr Opin Clin Nutr Metab Care*, 2011. **14**(1): p. 22-7.
9. McFarlane, C., A. Hennebry, M. Thomas, E. Plummer, N. Ling, M. Sharma, and R. Kambadur, *Myostatin signals through Pax7 to regulate satellite cell self-renewal*. *Exp Cell Res*, 2008. **314**(2): p. 317-29.

10. Chang, N.C. and M.A. Rudnicki, *Satellite cells: the architects of skeletal muscle*. *Curr Top Dev Biol*, 2014. **107**: p. 161-81.
11. von Maltzahn, J., A.E. Jones, R.J. Parks, and M.A. Rudnicki, *Pax7 is critical for the normal function of satellite cells in adult skeletal muscle*. *Proceedings of the National Academy of Sciences of the United States of America*, 2013. **110**(41): p. 16474-16479.
12. Jabart, E. and I.M. Conboy, *Biomaterial applications in the adult skeletal muscle satellite cell niche: Deliberate control of muscle stem cells and muscle regeneration in the aged niche*. *Stud Mechanobiol Tissue Eng Biomater*, 2010.
13. Yin, H., F. Price, and M.A. Rudnicki, *Satellite Cells and the Muscle Stem Cell Niche*. *Physiological Reviews*, 2013. **93**(1): p. 23-67.
14. Aas, V., S. Bakke, Y. Feng, E. Kase, J. Jensen, S. Bajpeyi, G.H. Thoresen, and A. Rustan, *Are cultured human myotubes far from home?* *Cell and Tissue Research*, 2013: p. 1-12.
15. Xu, C., M. Tabebordbar, S. Salvatore Iovino, C. Ciarlo, J. Liu, A. Castiglioni, E. Price, M. Min Liu, E.R. Barton, C.R. Kahn, A.J. Wagers, and L.I. Zon, *A Zebrafish Embryo Culture System Defines Factors that Promote Vertebrate Myogenesis across Species*. *Cell*, 2013. **155**: p. 909-921.
16. Fishman, J.M., A. Tyraskis, P. Maghsoudlou, L. Urbani, G. Totonelli, M.A. Birchall, and P. De Coppi, *Skeletal Muscle Tissue Engineering: Which Cell to Use?* *Tissue Engineering Part B: Reviews*, 2013. **Epub ahead of print**.
17. Zammit, P.S., T.A. Partridge, and Z. Yablonka-Reuveni, *The skeletal muscle satellite cell: the stem cell that came in from the cold*. *J Histochem Cytochem*, 2006. **54**(11): p. 1177-91.
18. Scott, W., J. Stevens, and S.A. Binder-Macleod, *Human skeletal muscle fiber type classifications*. *Phys Ther*, 2001. **81**(11): p. 1810-6.

19. Rassier, D.E., B.R. MacIntosh, and W. Herzog, *Length dependence of active force production in skeletal muscle*. J Appl Physiol (1985), 1999. **86**(5): p. 1445-57.
20. Goodman, B.E., *Channels active in the excitability of nerves and skeletal muscles across the neuromuscular junction: basic function and pathophysiology*. Adv Physiol Educ, 2008. **32**(2): p. 127-35.
21. Plonsey, R. and R. Barr, eds. *Bioelectricity: A Quantitative Approach*. Second ed. 2000, Kluwer Academic/Plenum Publishers: New York.
22. Galpin, A.J., U. Raue, B. Jemiolo, T.A. Trappe, M.P. Harber, K. Minchev, and S. Trappe, *Human skeletal muscle fiber type specific protein content*. Anal Biochem, 2012. **425**(2): p. 175-82.
23. Wells, L., K.A. Edwards, and S.I. Bernstein, *Myosin heavy chain isoforms regulate muscle function but not myofibril assembly*. EMBO J, 1996. **15**(17): p. 4454-9.
24. Greising, S.M., H.M. Gransee, C.B. Mantilla, and G.C. Sieck, *Systems biology of skeletal muscle: fiber type as an organizing principle*. Wiley Interdiscip Rev Syst Biol Med, 2012. **4**(5): p. 457-73.
25. Barany, M., *ATPase activity of myosin correlated with speed of muscle shortening*. J Gen Physiol, 1967. **50**(6): p. Suppl:197-218.
26. Schiaffino, S., *Fibre types in skeletal muscle: a personal account*. Acta Physiol (Oxf), 2010. **199**(4): p. 451-63.
27. Hopkins, P.M., *Skeletal Muscle Physiology*. Continuing Education in Anaesthesia. 2006.
28. LeBrasseur, N.K., K. Walsh, and Z. Arany, *Metabolic benefits of resistance training and fast glycolytic skeletal muscle*. Am J Physiol Endocrinol Metab, 2011. **300**(1): p. 2.
29. Schiaffino, S. and C. Reggiani, *Fiber types in mammalian skeletal muscles*. Physiol Rev, 2011. **91**(4): p. 1447-531.

30. van Wessel, T., A. de Haan, W.J. van der Laarse, and R.T. Jaspers, *The muscle fiber type-fiber size paradox: hypertrophy or oxidative metabolism?* Eur J Appl Physiol, 2010. **110**(4): p. 665-94.
31. Francis, K., *Anaerobic threshold*. Computers in Biology and Medicine, 1989. **19**(1): p. 1-6.
32. Hall, J., *Textbook of Medical Physiology*. Twelfth ed. 2011, Philadelphia: Saunders Elsevier. 1091.
33. Buller, A.J., J.C. Eccles, and R.M. Eccles, *Interactions between motoneurons and muscles in respect of the characteristic speeds of their responses*. J Physiol, 1960. **150**: p. 417-39.
34. Salmons, S. and G. Vrbova, *The influence of activity on some contractile characteristics of mammalian fast and slow muscles*. J Physiol, 1969. **201**(3): p. 535-49.
35. Pette, D. and G. Vrbova, *Adaptation of mammalian skeletal muscle fibers to chronic electrical stimulation*. Rev Physiol Biochem Pharmacol, 1992. **120**: p. 115-202.
36. He, Z.H., R. Bottinelli, M.A. Pellegrino, M.A. Ferenczi, and C. Reggiani, *ATP consumption and efficiency of human single muscle fibers with different myosin isoform composition*. Biophys J, 2000. **79**(2): p. 945-61.
37. Ingjer, F., *Effects of endurance training on muscle fibre ATP-ase activity, capillary supply and mitochondrial content in man*. J Physiol, 1979. **294**: p. 419-32.
38. Andersen, J.L., T. Mohr, F. Biering-Sorensen, H. Galbo, and M. Kjaer, *Myosin heavy chain isoform transformation in single fibres from m. vastus lateralis in spinal cord injured individuals: effects of long-term functional electrical stimulation (FES)*. Pflugers Arch, 1996. **431**(4): p. 513-8.

39. Harridge, S.D., *Plasticity of human skeletal muscle: gene expression to in vivo function*. *Exp Physiol*, 2007. **92**(5): p. 783-97.
40. Goldspink, G., A. Scutt, J. Martindale, T. Jaenicke, L. Turay, and G.F. Gerlach, *Stretch and force generation induce rapid hypertrophy and myosin isoform gene switching in adult skeletal muscle*. *Biochem Soc Trans*, 1991. **19**(2): p. 368-73.
41. McArdle, W., F. Katch, and K. VL, *Exercise Physiology: Nutrition, Energy, and Human Performance*. 7th ed, ed. L.W. Wilkins. 2009.
42. Payne, C.M., L.Z. Stern, R.G. Curless, and L.K. Hannapel, *Ultrastructural fiber typing in normal and diseased human muscle*. *J Neurol Sci*, 1975. **25**(1): p. 99-108.
43. Payne, C.M., L.Z. Stern, R.G. Curless, and L.K. Hannapel, *Ultrastructural Fiber Typing in Normal and Diseased Human Muscle*. *Journal of the Neurological Sciences*, 1975. **25**(1): p. 99-108.
44. Guo, X., M. Gonzalez, M. Stancescu, H.H. Vandeburgh, and J.J. Hickman, *Neuromuscular junction formation between human stem cell-derived motoneurons and human skeletal muscle in a defined system*. *Biomaterials*, 2011. **32**(36): p. 9602-11.
45. van der Schaft, D.W., A.C. van Spreeuwel, K.J. Boonen, M.L. Langelaan, C.V. Bouten, and F.P. Baaijens, *Engineering skeletal muscle tissues from murine myoblast progenitor cells and application of electrical stimulation*. *J Vis Exp*, 2013(73): p. e4267.
46. Dennis, R.G. and P.E. Kosnik, 2nd, *Excitability and isometric contractile properties of mammalian skeletal muscle constructs engineered in vitro*. In *Vitro Cell Dev Biol Anim*, 2000. **36**: p. 327-335.
47. Hinds, S., W. Bian, R.G. Dennis, and N. Bursac, *The role of extracellular matrix composition in structure and function of bioengineered skeletal muscle*. *Biomaterials*, 2011. **32**(14): p. 3575-83.

48. Rhim, C., D.A. Lowell, M.C. Reedy, D.H. Slentz, S.J. Zhang, W.E. Kraus, and G.A. Truskey, *Morphology and ultrastructure of differentiating three-dimensional mammalian skeletal muscle in a collagen gel*. *Muscle Nerve*, 2007. **36**(1): p. 71-80.
49. Rhim, C., C.S. Cheng, W.E. Kraus, and G.A. Truskey, *Effect of microRNA modulation on bioartificial muscle function*. *Tissue Eng Part A*, 2010. **16**(12): p. 3589-97.
50. Powell, C.A., B.L. Smiley, J. Mills, and H.H. Vandeburgh, *Mechanical stimulation improves tissue-engineered human skeletal muscle*. *Am J Physiol Cell Physiol*, 2002. **283**(5): p. C1557-65.
51. Moon du, G., G. Christ, J.D. Stitzel, A. Atala, and J.J. Yoo, *Cyclic mechanical preconditioning improves engineered muscle contraction*. *Tissue Eng Part A*, 2008. **14**(4): p. 473-82.
52. Dennis, R.G. and P.E. Kosnik, 2nd, *Excitability and isometric contractile properties of mammalian skeletal muscle constructs engineered in vitro*. *In Vitro Cell Dev Biol Anim*, 2000. **36**(5): p. 327-35.
53. Aubin, H., J.W. Nichol, C.B. Hutson, H. Bae, A.L. Sieminski, D.M. Cropek, P. Akhyari, and A. Khademhosseini, *Directed 3D cell alignment and elongation in microengineered hydrogels*. *Biomaterials*, 2010. **31**(27): p. 6941-6951.
54. Mertens, J.P., K.B. Sugg, J.D. Lee, and L.M. Larkin, *Engineering muscle constructs for the creation of functional engineered musculoskeletal tissue*. *Regen Med*, 2014. **9**(1): p. 89-100.
55. Li, M., C.E. Dickinson, E.B. Finkelstein, C.M. Neville, and C.A. Sundback, *The role of fibroblasts in self-assembled skeletal muscle*. *Tissue Eng Part A*, 2011. **17**(21-22): p. 2641-50.
56. Engler, A.J., M.A. Griffin, S. Sen, C.G. Bönnemann, H.L. Sweeney, and D.E. Discher, *Myotubes differentiate optimally on substrates with tissue-like stiffness: pathological implications for soft or stiff microenvironments*. *The Journal of Cell Biology*, 2004. **166**(6): p. 877-887.

57. Discher, D.E., P. Janmey, and Y.-I. Wang, *Tissue Cells Feel and Respond to the Stiffness of Their Substrate*. *Science*, 2005. **310**(5751): p. 1139-1143.
58. Sirivisoot, S., R. Pareta, and B.S. Harrison, *Protocol and cell responses in three-dimensional conductive collagen gel scaffolds with conductive polymer nanofibres for tissue regeneration*. *Interface Focus*, 2014. **4**(1): p. 20130050.
59. Janmey, P.A., J.P. Winer, and J.W. Weisel, *Fibrin gels and their clinical and bioengineering applications*. *J R Soc Interface*, 2009. **6**: p. 1-10.
60. Baker, E.L., R.G. Dennis, and L.M. Larkin, *Glucose Transporter Content And Glucose Uptake In Skeletal Muscle Constructs Engineered In Vitro*. *In Vitro Cell Dev Biol Anim*, 2003. **39**: p. 434-439.
61. Huang, Y.-C., R.G. Dennis, L. Larkin, and K. Baar, *Rapid formation of functional muscle in vitro using fibrin gels*. *Journal of Applied Physiology*, 2005. **98**(2): p. 706-713.
62. Saltiel, A.R. and C.R. Kahn, *Insulin signalling and the regulation of glucose and lipid metabolism*. *Nature*, 2001. **414**(6865): p. 799-806.
63. Barnard, R.J. and J.F. Youngren, *Regulation of glucose transport in skeletal muscle*. *The FASEB Journal*, 1992. **6**(14): p. 3238-44.
64. Liang, H. and W.F. Ward, *PGC-1alpha: a key regulator of energy metabolism*. *Adv Physiol Educ*, 2006. **30**(4): p. 145-51.
65. Wang, Y.X., C.L. Zhang, R.T. Yu, H.K. Cho, M.C. Nelson, C.R. Bayuga-Ocampo, J. Ham, H. Kang, and R.M. Evans, *Regulation of muscle fiber type and running endurance by PPARdelta*. *PLoS Biol*, 2004. **2**(10): p. e294.
66. Finck, B.N., C. Bernal-Mizrachi, D.H. Han, T. Coleman, N. Sambandam, L.L. LaRiviere, J.O. Holloszy, C.F. Semenkovich, and D.P. Kelly, *A potential link between muscle peroxisome proliferator-activated receptor-alpha signaling and obesity-related diabetes*. *Cell Metab*, 2005. **1**(2): p. 133-44.

67. Amat, R., A. Planavila, S.L. Chen, R. Iglesias, M. Giralt, and F. Villarroya, *SIRT1 controls the transcription of the peroxisome proliferator-activated receptor-gamma Co-activator-1alpha (PGC-1alpha) gene in skeletal muscle through the PGC-1alpha autoregulatory loop and interaction with MyoD*. J Biol Chem, 2009. **284**(33): p. 21872-80.
68. Canto, C. and J. Auwerx, *PGC-1alpha, SIRT1 and AMPK, an energy sensing network that controls energy expenditure*. Curr Opin Lipidol, 2009. **20**(2): p. 98-105.
69. Lin, J., H. Wu, P.T. Tarr, C.Y. Zhang, Z. Wu, O. Boss, L.F. Michael, P. Puigserver, E. Isotani, E.N. Olson, B.B. Lowell, R. Bassel-Duby, and B.M. Spiegelman, *Transcriptional co-activator PGC-1 alpha drives the formation of slow-twitch muscle fibres*. Nature, 2002. **418**(6899): p. 797-801.
70. Rasbach, K.A., R.K. Gupta, J.L. Ruas, J. Wu, E. Naseri, J.L. Estall, and B.M. Spiegelman, *PGC-1alpha regulates a HIF2alpha-dependent switch in skeletal muscle fiber types*. Proc Natl Acad Sci U S A, 2010. **107**(50): p. 21866-71.
71. Martin, N.R., S.L. Passey, D.J. Player, A. Khodabukus, R.A. Ferguson, A.P. Sharples, V. Mudera, K. Baar, and M.P. Lewis, *Factors affecting the structure and maturation of human tissue engineered skeletal muscle*. Biomaterials, 2013. **34**(23): p. 5759-65.
72. Lewis, D. and S. Chamberlain, *Differences between contractions in vitro of slow and fast rat skeletal muscle persist after random reinnervation*. Journal of Physiology, 1993(465): p. 731-745.
73. Pirozzi, K.L., C.J. Long, C.W. McAleer, A.S.T. Smith, and J.J. Hickman, *Correlation of embryonic skeletal muscle myotube physical characteristics with contractile force generation on an atomic force microscope-based bio-microelectromechanical systems device*. Applied Physics Letters, 2013. **103**(8): p. -.
74. Sakar, M.S., D. Neal, T. Boudou, M.A. Borochin, Y. Li, R. Weiss, R.D. Kamm, C.S. Chen, and H.H. Asada, *Formation and optogenetic control of*

engineered 3D skeletal muscle bioactuators. Lab on a Chip, 2012. **12**(23): p. 4976-4985.

75. Sun, Y., R. Duffy, A. Lee, and A.W. Feinberg, *Optimizing the structure and contractility of engineered skeletal muscle thin films*. Acta Biomaterialia 2013. **9**: p. 7885–7894.
76. Bian, W., M. Juhas, T.W. Pfeiler, and N. Bursac, *Local Tissue Geometry Determines Contractile Force Generation of Engineered Muscle Networks*. Tissue Eng Part A, 2012. **18**: p. 957-967.
77. Larkin, L.M., W.M. Kuzon, and J.B. Halter, *Effects of age and nerve-repair grafts on reinnervation and fiber type distribution of rat medial gastrocnemius muscles*. Mech Ageing Dev, 2003. **124**(5): p. 653-61.
78. Larkin, L.M., J.H. Van der Meulen, R.G. Dennis, and K. J.B., *Functional evaluation of nerve-skeletal muscle constructs engineered in vitro*. In Vitro Cell Dev Biol Anim. , 2006. **42**: p. 75-82.
79. Bian, W. and N. Bursac, *Soluble miniagrin enhances contractile function of engineered skeletal muscle*. FASEB J, 2012. **26**(2): p. 955-65.
80. Donnelly, K., A. Khodabukus, A. Philp, L. Deldicque, R.G. Dennis, and K. Baar, *A novel bioreactor for stimulating skeletal muscle in vitro*. Tissue Eng Part C Methods, 2010. **16**(4): p. 711-8.
81. Mudera, V., A.S. Smith, M.A. Brady, and M.P. Lewis, *The effect of cell density on the maturation and contractile ability of muscle derived cells in a 3D tissue-engineered skeletal muscle model and determination of the cellular and mechanical stimuli required for the synthesis of a postural phenotype*. J Cell Physiol, 2010. **225**: p. 646-653.
82. Kumar, A., R. Murphy, P. Robinson, L. Wei, and A.M. Boriak, *Cyclic mechanical strain inhibits skeletal myogenesis through activation of focal adhesion kinase, Rac-1 GTPase, and NF-kappaB transcription factor*. FASEB J, 2004. **18**: p. 1524-1535.

83. Zhang, S.J., G.A. Truskey, and W.E. Kraus, *Effect of cyclic stretch on beta1D-integrin expression and activation of FAK and RhoA*. *Am J Physiol Cell Physiol*, 2007. **292**(6): p. C2057-69.
84. Nikolić, N., S.S. Bakke, E.T. Kase, I. Rudberg, I. Flo Halle, A.C. Rustan, G.H. Thoresen, and V. Aas, *Electrical pulse stimulation of cultured human skeletal muscle cells as an in vitro model of exercise*. *PLoS One*, 2012. **7**: p. e33203.
85. Nedachi, T., H. Fujita, and M. Kanzaki, *Contractile C2C12 myotube model for studying exercise-inducible responses in skeletal muscle*. *Am J Physiol*, 2008. **295**: p. E1191–E1204.
86. Langelaan, M.P.L., K.J.M. Boonen, K.Y. Rosaria-Chak, D.W.J. van der Schaft, M.J. Mark J. Post, and F.P.T. Baaijens, *Advanced maturation by electrical stimulation: Differences in response between C2C12 and primary muscle progenitor cells*. *J Tissue Eng Regen Med* 2011. **5**: p. 529-539.
87. Richter, E.A. and M. Hargreaves, *Exercise, GLUT4, and skeletal muscle glucose uptake*. *Physiol Rev*, 2013. **93**(3): p. 993-1017.
88. Chen, J.F., Y. Tao, J. Li, Z. Deng, Z. Yan, X. Xiao, and D.Z. Wang, *microRNA-1 and microRNA-206 regulate skeletal muscle satellite cell proliferation and differentiation by repressing Pax7*. *J Cell Biol*, 2010. **190**(5): p. 867-79.
89. Townley-Tilson, W.H., T.E. Callis, and D. Wang, *MicroRNAs 1, 133, and 206: critical factors of skeletal and cardiac muscle development, function, and disease*. *Int J Biochem Cell Biol*, 2010. **42**(8): p. 1252-5.
90. Guller, I. and A.P. Russell, *MicroRNAs in skeletal muscle: their role and regulation in development, disease and function*. *J Physiol*, 2010. **588**(Pt 21): p. 4075-87.
91. Morley, J.E., H.M. Perry, 3rd, and D.K. Miller, *Editorial: Something about frailty*. *J Gerontol A Biol Sci Med Sci*, 2002. **57**(11): p. M698-704.

92. Cheng, C.S., Y. El-Abd, K. Bui, Y.E. Hyun, R.H. Hughes, W.E. Kraus, and G.A. Truskey, *Conditions that promote primary human skeletal myoblast culture and muscle differentiation in vitro*. *Am J Physiol Cell Physiol*, 2014. **306**(4): p. C385-95.
93. Schmelter, M., B. Ateghang, S. Helmig, M. Wartenberg, and H. Sauer, *Embryonic stem cells utilize reactive oxygen species as transducers of mechanical strain-induced cardiovascular differentiation*. *FASEB J*, 2006. **20**(8): p. 1182-4.
94. Potthoff, M.J., M.A. Arnold, J. McAnally, J.A. Richardson, R. Bassel-Duby, and E.N. Olson, *Regulation of skeletal muscle sarcomere integrity and postnatal muscle function by Mef2c*. *Mol Cell Biol*, 2007. **27**(23): p. 8143-51.
95. Molkenin, J.D. and E.N. Olson, *Combinatorial control of muscle development by basic helix-loop-helix and MADS-box transcription factors*. *Proc Natl Acad Sci U S A*, 1996. **93**(18): p. 9366-73.
96. Ornatsky, O.I., J.J. Andreucci, and J.C. McDermott, *A dominant-negative form of transcription factor MEF2 inhibits myogenesis*. *J Biol Chem*, 1997. **272**(52): p. 33271-8.
97. Potthoff, M.J., H. Wu, M.A. Arnold, J.M. Shelton, J. Backs, J. McAnally, J.A. Richardson, R. Bassel-Duby, and E.N. Olson, *Histone deacetylase degradation and MEF2 activation promote the formation of slow-twitch myofibers*. *J Clin Invest*, 2007. **117**(9): p. 2459-67.
98. Wu, H., S.B. Kanatous, F.A. Thurmond, T. Gallardo, E. Isotani, R. Bassel-Duby, and R.S. Williams, *Regulation of mitochondrial biogenesis in skeletal muscle by CaMK*. *Science*, 2002. **296**(5566): p. 349-52.
99. Crist, C.G. and M. Buckingham, *Megarole for microRNA in muscle disease*. *Cell Metab*, 2010. **12**(5): p. 425-6.
100. Zampetaki, A. and M. Mayr, *MicroRNAs in vascular and metabolic disease*. *Circ Res*, 2012. **110**(3): p. 508-22.

101. Aoi, W., Y. Naito, K. Mizushima, Y. Takanami, Y. Kawai, H. Ichikawa, and T. Yoshikawa, *The microRNA miR-696 regulates PGC-1{alpha} in mouse skeletal muscle in response to physical activity*. *Am J Physiol Endocrinol Metab*, 2010. **298**(4): p. E799-806.
102. Finck, B.N. and D.P. Kelly, *PGC-1 coactivators: inducible regulators of energy metabolism in health and disease*. *J Clin Invest*, 2006. **116**(3): p. 615-22.
103. Palikaras, K. and N. Tavernarakis, *Mitochondrial homeostasis: The interplay between mitophagy and mitochondrial biogenesis*. *Exp Gerontol*, 2014.
104. Philp, A., M.Y. Belew, A. Evans, D. Pham, I. Sivia, A. Chen, S. Schenk, and K. Baar, *The PGC-1alpha-related coactivator promotes mitochondrial and myogenic adaptations in C2C12 myotubes*. *Am J Physiol Regul Integr Comp Physiol*, 2011. **301**(4): p. R864-72.
105. Zorzano, A., M.I. Hernandez-Alvarez, M. Palacin, and G. Mingrone, *Alterations in the mitochondrial regulatory pathways constituted by the nuclear co-factors PGC-1alpha or PGC-1beta and mitofusin 2 in skeletal muscle in type 2 diabetes*. *Biochim Biophys Acta*, 2010. **1797**(6-7): p. 1028-33.
106. Gibbons, M.C., M.A. Foley, and K.O. Cardinal, *Thinking inside the box: keeping tissue-engineered constructs in vitro for use as preclinical models*. *Tissue Eng Part B Rev*, 2013. **19**(1): p. 14-30.
107. Rangarajan, A. and R.A. Weinberg, *Opinion: Comparative biology of mouse versus human cells: modelling human cancer in mice*. *Nat Rev Cancer*, 2003. **3**(12): p. 952-9.
108. Kho, A.T., P.B. Kang, I.S. Kohane, and L.M. Kunkel, *Transcriptome-scale similarities between mouse and human skeletal muscles with normal and myopathic phenotypes*. *BMC Musculoskelet Disord*, 2006. **7**: p. 23.
109. Boldrin, L., F. Muntoni, and J.E. Morgan, *Are human and mouse satellite cells really the same?* *J Histochem Cytochem*, 2010. **58**(11): p. 941-55.

110. Harrison, B.C., D.L. Allen, and L.A. Leinwand, *Iib or not Iib? Regulation of myosin heavy chain gene expression in mice and men*. *Skelet Muscle*, 2011. **1**(1): p. 5.
111. Stern-Straeter, J., G.A. Bonaterra, S.S. Kassner, S. Zugel, K. Hormann, R. Kinscherf, and U.R. Goessler, *Characterization of human myoblast differentiation for tissue-engineering purposes by quantitative gene expression analysis*. *J Tissue Eng Regen Med*, 2011. **5**(8): p. e197-206.
112. Koning, M., P.M. Werker, M.J. van Luyn, G. Krenning, and M.C. Harmsen, *A global downregulation of microRNAs occurs in human quiescent satellite cells during myogenesis*. *Differentiation*, 2012. **84**(4): p. 314-21.
113. Koning, M., P.M. Werker, D.W. van der Schaft, R.A. Bank, and M.C. Harmsen, *MicroRNA-1 and microRNA-206 improve differentiation potential of human satellite cells: a novel approach for tissue engineering of skeletal muscle*. *Tissue Eng Part A*, 2012. **18**(9-10): p. 889-98.
114. Chen, Y., D.W. Melton, J.A. Gelfond, L.M. McManus, and P.K. Shireman, *MiR-351 transiently increases during muscle regeneration and promotes progenitor cell proliferation and survival upon differentiation*. *Physiol Genomics*, 2012. **44**(21): p. 1042-51.
115. Baj, A., A.A. Bettaccini, R. Casalone, A. Sala, P. Cherubino, and A.Q. Toniolo, *Culture of skeletal myoblasts from human donors aged over 40 years: dynamics of cell growth and expression of differentiation markers*. *J Transl Med*, 2005. **3**(1): p. 21.
116. Ye, L., H. Haider, W.B. Esa, P.K. Law, W. Zhang, L. Su, Y. Zhang, and E.K. Sim, *Nonviral vector-based gene transfection of primary human skeletal myoblasts*. *Exp Biol Med (Maywood)*, 2007. **232**(11): p. 1477-87.
117. Salic, A. and T.J. Mitchison, *A chemical method for fast and sensitive detection of DNA synthesis in vivo*. *Proc Natl Acad Sci U S A*, 2008. **105**(7): p. 2415-20.

118. Zhang, J., S. Kan, B. Huang, Z. Hao, T.W. Mak, and Q. Zhong, *Mule determines the apoptotic response to HDAC inhibitors by targeted ubiquitination and destruction of HDAC2*. *Genes Dev*, 2011. **25**(24): p. 2610-8.
119. Chang, L., M. Nosedà, M. Higginson, M. Ly, A. Patenaude, M. Fuller, A.H. Kyle, A.I. Minchinton, M.C. Puri, D.J. Dumont, and A. Karsan, *Differentiation of vascular smooth muscle cells from local precursors during embryonic and adult arteriogenesis requires Notch signaling*. *Proc Natl Acad Sci U S A*, 2012. **109**(18): p. 6993-8.
120. Burattini, S., P. Ferri, M. Battistelli, R. Curci, F. Luchetti, and E. Falcieri, *C2C12 murine myoblasts as a model of skeletal muscle development: morpho-functional characterization*. *Eur J Histochem*, 2004. **48**(3): p. 223-33.
121. Yablonka-Reuveni, Z., R. Seger, and A.J. Rivera, *Fibroblast growth factor promotes recruitment of skeletal muscle satellite cells in young and old rats*. *J Histochem Cytochem*, 1999. **47**(1): p. 23-42.
122. Grefte, S., S. Vullingsh, A.M. Kuijpers-Jagtman, R. Torensma, and J.W. Von den Hoff, *Matrigel, but not collagen I, maintains the differentiation capacity of muscle derived cells in vitro*. *Biomed Mater*, 2012. **7**(5): p. 055004.
123. Potthoff, M.J. and E.N. Olson, *MEF2: a central regulator of diverse developmental programs*. *Development*, 2007. **134**(23): p. 4131-40.
124. Goto, S., K. Miyazaki, T. Funabiki, and H. Yasumitsu, *Serum-free culture conditions for analysis of secretory proteinases during myogenic differentiation of mouse C2C12 myoblasts*. *Anal Biochem*, 1999. **272**(2): p. 135-42.
125. Lawson, M.A. and P.P. Purslow, *Differentiation of myoblasts in serum-free media: effects of modified media are cell line-specific*. *Cells Tissues Organs*, 2000. **167**(2-3): p. 130-7.

126. Stern-Straeter, J., G. Bran, F. Riedel, A. Sauter, K. Hormann, and U.R. Goessler, *Characterization of human myoblast cultures for tissue engineering*. Int J Mol Med, 2008. **21**(1): p. 49-56.
127. Boonen, K.J., K.Y. Rosaria-Chak, F.P. Baaijens, D.W. van der Schaft, and M.J. Post, *Essential environmental cues from the satellite cell niche: optimizing proliferation and differentiation*. Am J Physiol Cell Physiol, 2009. **296**(6): p. C1338-45.
128. Carson, J.A. and F.W. Booth, *Effect of serum and mechanical stretch on skeletal alpha-actin gene regulation in cultured primary muscle cells*. Am J Physiol, 1998. **275**(6 Pt 1): p. C1438-48.
129. Williams, A.H., N. Liu, E. van Rooij, and E.N. Olson, *MicroRNA control of muscle development and disease*. Curr Opin Cell Biol, 2009. **21**(3): p. 461-9.
130. Chen, X., K. Wang, J. Chen, J. Guo, Y. Yin, X. Cai, X. Guo, G. Wang, R. Yang, L. Zhu, Y. Zhang, J. Wang, Y. Xiang, C. Weng, K. Zen, J. Zhang, and C.Y. Zhang, *In vitro evidence suggests that miR-133a-mediated regulation of uncoupling protein 2 (UCP2) is an indispensable step in myogenic differentiation*. J Biol Chem, 2009. **284**(8): p. 5362-9.
131. Eisenberg, I., A. Eran, I. Nishino, M. Moggio, C. Lamperti, A.A. Amato, H.G. Lidov, P.B. Kang, K.N. North, S. Mitrani-Rosenbaum, K.M. Flanigan, L.A. Neely, D. Whitney, A.H. Beggs, I.S. Kohane, and L.M. Kunkel, *Distinctive patterns of microRNA expression in primary muscular disorders*. Proc Natl Acad Sci U S A, 2007. **104**(43): p. 17016-21.
132. Tatsuguchi, M., H.Y. Seok, T.E. Callis, J.M. Thomson, J.F. Chen, M. Newman, M. Rojas, S.M. Hammond, and D.Z. Wang, *Expression of microRNAs is dynamically regulated during cardiomyocyte hypertrophy*. J Mol Cell Cardiol, 2007. **42**(6): p. 1137-41.
133. Thum, T., P. Galuppo, C. Wolf, J. Fiedler, S. Kneitz, L.W. van Laake, P.A. Doevendans, C.L. Mummery, J. Borlak, A. Haverich, C. Gross, S. Engelhardt, G. Ertl, and J. Bauersachs, *MicroRNAs in the human heart: a*

- clue to fetal gene reprogramming in heart failure. Circulation, 2007. 116(3): p. 258-67.*
134. Yan, D., E. Dong Xda, X. Chen, L. Wang, C. Lu, J. Wang, J. Qu, and L. Tu, *MicroRNA-1/206 targets c-Met and inhibits rhabdomyosarcoma development. J Biol Chem, 2009. 284(43): p. 29596-604.*
 135. Truskey, G.A., H.E. Achneck, N. Bursac, H. Chan, C.S. Cheng, C. Fernandez, S. Hong, Y. Jung, T. Koves, W.E. Kraus, K. Leong, L. Madden, W.M. Reichert, and X. Zhao, *Design considerations for an integrated microphysiological muscle tissue for drug and tissue toxicity testing. Stem Cell Res Ther, 2013. 4 Suppl 1: p. S10.*
 136. Lambernd, S., A. Taube, A. Schober, B. Platzbecker, S.W. Gorgens, R. Schlich, K. Jeruschke, J. Weiss, K. Eckardt, and J. Eckel, *Contractile activity of human skeletal muscle cells prevents insulin resistance by inhibiting pro-inflammatory signalling pathways. Diabetologia, 2012. 55(4): p. 1128-39.*
 137. Huang, Y.C., R.G. Dennis, L. Larkin, and K. Baar, *Rapid formation of functional muscle in vitro using fibrin gels. J Appl Physiol (1985), 2005. 98(2): p. 706-13.*
 138. Bian, W. and N. Bursac, *Tissue engineering of functional skeletal muscle: challenges and recent advances. IEEE Eng Med Biol Mag, 2008. 27(5): p. 109-13.*
 139. Geiger, P.C., M.J. Cody, R.L. Macken, M.E. Bayrd, Y.H. Fang, and G.C. Sieck, *Mechanisms underlying increased force generation by rat diaphragm muscle fibers during development. J Appl Physiol (1985), 2001. 90(1): p. 380-8.*
 140. Chen, J.F., E.M. Mandel, J.M. Thomson, Q. Wu, T.E. Callis, S.M. Hammond, F.L. Conlon, and D.Z. Wang, *The role of microRNA-1 and microRNA-133 in skeletal muscle proliferation and differentiation. Nat Genet, 2006. 38(2): p. 228-33.*

141. Koning, M., P.M. Werker, D.W. van der Schaft, R.A. Bank, and M.C. Harmsen, *MicroRNA-1 and MicroRNA-206 Improve Differentiation Potential of Human Satellite Cells: A Novel Approach for Tissue Engineering of Skeletal Muscle*. *Tissue Eng Part A*, 2011.
142. Eivers, S.S., B.A. McGivney, J. Gu, D.E. MacHugh, L.M. Katz, and E.W. Hill, *PGC-1alpha encoded by the PPARGC1A gene regulates oxidative energy metabolism in equine skeletal muscle during exercise*. *Anim Genet*, 2012. **43**(2): p. 153-62.
143. van der Ven, P.F., G. Schaart, P.H. Jap, R.C. Sengers, A.M. Stadhouders, and F.C. Ramaekers, *Differentiation of human skeletal muscle cells in culture: maturation as indicated by titin and desmin striation*. *Cell Tissue Res*, 1992. **270**(1): p. 189-98.
144. Bonavaud, S., O. Agbulut, R. Nizard, G. D'Honneur, V. Mouly, and G. Butler-Browne, *A discrepancy resolved: human satellite cells are not preprogrammed to fast and slow lineages*. *Neuromuscul Disord*, 2001. **11**(8): p. 747-52.
145. Mouly, V., F. Edom, J.P. Barbet, and G.S. Butler-Browne, *Plasticity of human satellite cells*. *Neuromuscul Disord*, 1993. **3**(5-6): p. 371-7.
146. Edom, F., V. Mouly, J.P. Barbet, M.Y. Fiszman, and G.S. Butler-Browne, *Clones of human satellite cells can express in vitro both fast and slow myosin heavy chains*. *Dev Biol*, 1994. **164**(1): p. 219-29.
147. Mudera, V., A.S. Smith, M.A. Brady, and M.P. Lewis, *The effect of cell density on the maturation and contractile ability of muscle derived cells in a 3D tissue-engineered skeletal muscle model and determination of the cellular and mechanical stimuli required for the synthesis of a postural phenotype*. *J Cell Physiol*, 2010. **225**(3): p. 646-53.
148. Snyman, C., K.P. Goetsch, K.H. Myburgh, and C.U. Niesler, *Simple silicone chamber system for in vitro three-dimensional skeletal muscle tissue formation*. *Front Physiol*, 2013. **4**: p. 349.

149. Takahashi, M., T. Kubo, A. Mizoguchi, C.G. Carlson, K. Endo, and K. Ohnishi, *Spontaneous muscle action potentials fail to develop without fetal-type acetylcholine receptors*. EMBO Rep, 2002. **3**(7): p. 674-81.
150. Ko, I.K., B.K. Lee, S.J. Lee, K.E. Andersson, A. Atala, and J.J. Yoo, *The effect of in vitro formation of acetylcholine receptor (AChR) clusters in engineered muscle fibers on subsequent innervation of constructs in vivo*. Biomaterials, 2013. **34**(13): p. 3246-55.
151. Geng, L., H.L. Zhang, and H.B. Peng, *The formation of acetylcholine receptor clusters visualized with quantum dots*. BMC Neuroscience, 2009. **10**.
152. Rowe, S.L. and J.P. Stegemann, *Interpenetrating collagen-fibrin composite matrices with varying protein contents and ratios*. Biomacromolecules, 2006. **7**(11): p. 2942-8.
153. Shi, Y., L. Rittman, and I. Vesely, *Novel geometries for tissue-engineered tendonous collagen constructs*. Tissue Eng, 2006. **12**(9): p. 2601-9.
154. Chiron, S., C. Tomczak, A. Duperray, J. Laine, G. Bonne, A. Eder, A. Hansen, T. Eschenhagen, C. Verdier, and C. Coirault, *Complex interactions between human myoblasts and the surrounding 3D fibrin-based matrix*. PLoS One, 2012. **7**(4): p. e36173.
155. Kragstrup, T.W., M. Kjaer, and A.L. Mackey, *Structural, biochemical, cellular, and functional changes in skeletal muscle extracellular matrix with aging*. Scand J Med Sci Sports, 2011. **21**(6): p. 749-57.
156. Gosselin, L.E., C. Adams, T.A. Cotter, R.J. McCormick, and D.P. Thomas, *Effect of exercise training on passive stiffness in locomotor skeletal muscle: role of extracellular matrix*. J Appl Physiol (1985), 1998. **85**(3): p. 1011-6.
157. Siegman, M.J., S. Davidheiser, S.U. Mooers, and T.M. Butler, *Structural limits on force production and shortening of smooth muscle*. J Muscle Res Cell Motil, 2013. **34**(1): p. 43-60.

158. Larkin, L.M., S. Calve, T.Y. Kostrominova, and E.M. Arruda, *Structure and functional evaluation of tendon-skeletal muscle constructs engineered in vitro*. *Tissue Eng*, 2006. **12**(11): p. 3149-58.
159. Buchanan, T.S., D.G. Lloyd, K. Manal, and T.F. Besier, *Neuromusculoskeletal modeling: estimation of muscle forces and joint moments and movements from measurements of neural command*. *J Appl Biomech*, 2004. **20**(4): p. 367-95.
160. Sakar, M.S., D. Neal, T. Boudou, M.A. Borochin, Y. Li, R. Weiss, R.D. Kamm, C.S. Chen, and H.H. Asada, *Formation and optogenetic control of engineered 3D skeletal muscle bioactuators*. *Lab Chip*, 2012. **12**(23): p. 4976-85.
161. Pirozzi, K.L., C.J. Long, C.W. McAleer, A.S. Smith, and J.J. Hickman, *Correlation of embryonic skeletal muscle myotube physical characteristics with contractile force generation on an atomic force microscope-based bio-microelectromechanical systems device*. *Appl Phys Lett*, 2013. **103**(8): p. 83108.
162. Bian, W., M. Juhas, T.W. Pfeiler, and N. Bursac, *Local tissue geometry determines contractile force generation of engineered muscle networks*. *Tissue Eng Part A*, 2012. **18**(9-10): p. 957-67.
163. van Rooij, E., A.L. Purcell, and A.A. Levin, *Developing microRNA therapeutics*. *Circ Res*, 2012. **110**(3): p. 496-507.
164. Duisters, R.F., A.J. Tijssen, B. Schroen, J.J. Leenders, V. Lentink, I. van der Made, V. Herias, R.E. van Leeuwen, M.W. Schellings, P. Barenbrug, J.G. Maessen, S. Heymans, Y.M. Pinto, and E.E. Creemers, *miR-133 and miR-30 regulate connective tissue growth factor: implications for a role of microRNAs in myocardial matrix remodeling*. *Circ Res*, 2009. **104**(2): p. 170-8, 6p following 178.
165. Stiehl, T., N. Baran, A.D. Ho, and A. Marciniak-Czochra, *Clonal selection and therapy resistance in acute leukaemias: mathematical modelling explains different proliferation patterns at diagnosis and relapse*. *J R Soc Interface*, 2014. **11**(94): p. 20140079.

166. Salimath, A.S. and A.J. Garcia, *Biofunctional hydrogels for skeletal muscle constructs*. J Tissue Eng Regen Med, 2014.
167. Olive, P.L., *Influence of cell crowding on toxicity of nitroheterocycles*. Chem Biol Interact, 1981. **35**(3): p. 285-96.
168. Colom, A., R. Galgoczy, I. Almendros, A. Xaubet, R. Farre, and J. Alcaraz, *Oxygen diffusion and consumption in extracellular matrix gels: Implications for designing three-dimensional cultures*. J Biomed Mater Res A, 2013.
169. Austin, S. and J. St-Pierre, *PGC1alpha and mitochondrial metabolism--emerging concepts and relevance in ageing and neurodegenerative disorders*. J Cell Sci, 2012. **125**(Pt 21): p. 4963-71.
170. Pillai, R.S., *MicroRNA function: multiple mechanisms for a tiny RNA?* RNA, 2005. **11**(12): p. 1753-61.
171. Cheema, U., R.A. Brown, B. Alp, and A.J. MacRobert, *Spatially defined oxygen gradients and vascular endothelial growth factor expression in an engineered 3D cell model*. Cell Mol Life Sci, 2008. **65**(1): p. 177-86.
172. Thorsteinsdottir, S., M. Deries, A.S. Cachaco, and F. Bajanca, *The extracellular matrix dimension of skeletal muscle development*. Dev Biol, 2011. **354**(2): p. 191-207.
173. Liu, N., S. Bezprozvannaya, J.M. Shelton, M.I. Frisard, M.W. Hulver, R.P. McMillan, Y. Wu, K.A. Voelker, R.W. Grange, J.A. Richardson, R. Bassel-Duby, and E.N. Olson, *Mice lacking microRNA 133a develop dynamin 2-dependent centronuclear myopathy*. J Clin Invest, 2011. **121**(8): p. 3258-68.
174. Wu, H., F.J. Naya, T.A. McKinsey, B. Mercer, J.M. Shelton, E.R. Chin, A.R. Simard, R.N. Michel, R. Bassel-Duby, E.N. Olson, and R.S. Williams, *MEF2 responds to multiple calcium-regulated signals in the control of skeletal muscle fiber type*. EMBO J, 2000. **19**(9): p. 1963-73.

175. Hennebry, A., C. Berry, V. Siriatt, P. O'Callaghan, L. Chau, T. Watson, M. Sharma, and R. Kambadur, *Myostatin regulates fiber-type composition of skeletal muscle by regulating MEF2 and MyoD gene expression*. *Am J Physiol Cell Physiol*, 2009. **296**(3): p. C525-34.
176. Rachagani, S., Y. Cheng, and J.M. Reecy, *Myostatin genotype regulates muscle-specific miRNA expression in mouse pectoralis muscle*. *BMC Res Notes*, 2010. **3**: p. 297.
177. Hitachi, K. and K. Tsuchida, *Role of microRNAs in skeletal muscle hypertrophy*. *Front Physiol*, 2013. **4**: p. 408.
178. Horie, T., K. Ono, H. Nishi, Y. Iwanaga, K. Nagao, M. Kinoshita, Y. Kuwabara, R. Takanabe, K. Hasegawa, T. Kita, and T. Kimura, *MicroRNA-133 regulates the expression of GLUT4 by targeting KLF15 and is involved in metabolic control in cardiac myocytes*. *Biochem Biophys Res Commun*, 2009. **389**(2): p. 315-20.
179. Haberland, M., M.A. Arnold, J. McAnally, D. Phan, Y. Kim, and E.N. Olson, *Regulation of HDAC9 gene expression by MEF2 establishes a negative-feedback loop in the transcriptional circuitry of muscle differentiation*. *Mol Cell Biol*, 2007. **27**(2): p. 518-25.
180. Mejat, A., F. Ramond, R. Bassel-Duby, S. Khochbin, E.N. Olson, and L. Schaeffer, *Histone deacetylase 9 couples neuronal activity to muscle chromatin acetylation and gene expression*. *Nat Neurosci*, 2005. **8**(3): p. 313-21.
181. Peters, E.B., N. Christoforou, K.W. Leong, and G.A. Truskey, *Comparison of mixed and lamellar coculture spatial arrangements for tissue engineering capillary networks in vitro*. *Tissue Eng Part A*, 2013. **19**(5-6): p. 697-706.
182. Ye, X., L. Lu, M.E. Kolewe, H. Park, B.L. Larson, E.S. Kim, and L.E. Freed, *A biodegradable microvessel scaffold as a framework to enable vascular support of engineered tissues*. *Biomaterials*, 2013. **34**(38): p. 10007-15.

183. Wallace, C.S., J.C. Champion, and G.A. Truskey, *Adhesion and function of human endothelial cells co-cultured on smooth muscle cells*. *Ann Biomed Eng*, 2007. **35**(3): p. 375-86.
184. Harimoto, M., M. Yamato, M. Hirose, C. Takahashi, Y. Isoi, A. Kikuchi, and T. Okano, *Novel approach for achieving double-layered cell sheets co-culture: overlaying endothelial cell sheets onto monolayer hepatocytes utilizing temperature-responsive culture dishes*. *J Biomed Mater Res*, 2002. **62**(3): p. 464-70.
185. Dietze, D., M. Koenen, K. Rohrig, H. Horikoshi, H. Hauner, and J. Eckel, *Impairment of insulin signaling in human skeletal muscle cells by co-culture with human adipocytes*. *Diabetes*, 2002. **51**(8): p. 2369-76.
186. Levenberg, S., J. Rouwkema, M. Macdonald, E.S. Garfein, D.S. Kohane, D.C. Darland, R. Marini, C.A. van Blitterswijk, R.C. Mulligan, P.A. D'Amore, and R. Langer, *Engineering vascularized skeletal muscle tissue*. *Nat Biotechnol*, 2005. **23**(7): p. 879-84.
187. Lavender, M.D., Z. Pang, C.S. Wallace, L.E. Niklason, and G.A. Truskey, *A system for the direct co-culture of endothelium on smooth muscle cells*. *Biomaterials*, 2005. **26**(22): p. 4642-53.
188. Fernandez, C.E., I.C. Obi-onuoha, C.S. Wallace, L.L. Satterwhite, G.A. Truskey, and W.M. Reichert, *Late-outgrowth endothelial progenitors from patients with coronary artery disease: endothelialization of confluent stromal cell layers*. *Acta Biomater*, 2014. **10**(2): p. 893-900.
189. Ingram, D.A., L.E. Mead, H. Tanaka, V. Meade, A. Fenoglio, K. Mortell, K. Pollok, M.J. Ferkowicz, D. Gilley, and M.C. Yoder, *Identification of a novel hierarchy of endothelial progenitor cells using human peripheral and umbilical cord blood*. *Blood*, 2004. **104**(9): p. 2752-60.
190. Wallace, C.S. and G.A. Truskey, *Direct-contact co-culture between smooth muscle and endothelial cells inhibits TNF-alpha-mediated endothelial cell activation*. *Am J Physiol Heart Circ Physiol*, 2010. **299**(2): p. H338-46.

191. Bogdanowicz, D.R. and H.H. Lu, *Studying cell-cell communication in co-culture*. Biotechnol J, 2013. **8**(4): p. 395-6.
192. Vanroose, G., A. Van Soom, and A. de Kruif, *From co-culture to defined medium: state of the art and practical considerations*. Reprod Domest Anim, 2001. **36**(1): p. 25-8.
193. Das, M., J.W. Rumsey, N. Bhargava, C. Gregory, L. Riedel, J.F. Kang, and J.J. Hickman, *Developing a novel serum-free cell culture model of skeletal muscle differentiation by systematically studying the role of different growth factors in myotube formation*. In Vitro Cell Dev Biol Anim, 2009. **45**(7): p. 378-87.
194. Kang, S.D., T.A. Carlon, A.E. Jantzen, F.H. Lin, M.M. Ley, J.D. Allen, T.V. Stabler, N.R. Haley, G.A. Truskey, and H.E. Achneck, *Isolation of functional human endothelial cells from small volumes of umbilical cord blood*. Ann Biomed Eng, 2013. **41**(10): p. 2181-92.
195. Cheung, T.M., M.P. Ganatra, E.B. Peters, and G.A. Truskey, *Effect of cellular senescence on the albumin permeability of blood-derived endothelial cells*. Am J Physiol Heart Circ Physiol, 2012. **303**(11): p. H1374-83.
196. van der Schaft, D.W., A.C. van Spreeuwel, H.C. van Assen, and F.P. Baaijens, *Mechanoregulation of vascularization in aligned tissue-engineered muscle: a role for vascular endothelial growth factor*. Tissue Eng Part A, 2011. **17**(21-22): p. 2857-65.
197. Eu, J.P., J.M. Hare, D.T. Hess, M. Skaf, J. Sun, I. Cardenas-Navina, Q.A. Sun, M. Dewhirst, G. Meissner, and J.S. Stamler, *Concerted regulation of skeletal muscle contractility by oxygen tension and endogenous nitric oxide*. Proc Natl Acad Sci U S A, 2003. **100**(25): p. 15229-34.
198. Stamler, J.S. and G. Meissner, *Physiology of nitric oxide in skeletal muscle*. Physiol Rev, 2001. **81**(1): p. 209-237.
199. Kobzik, L., B. Stringer, J.L. Balligand, M.B. Reid, and J.S. Stamler, *Endothelial type nitric oxide synthase in skeletal muscle fibers: mitochondrial relationships*. Biochem Biophys Res Commun, 1995. **211**(2): p. 375-81.

200. Kobzik, L., M.B. Reid, D.S. Bredt, and J.S. Stamler, *Nitric oxide in skeletal muscle*. *Nature*, 1994. **372**(6506): p. 546-8.
201. Cosentino, F., K. Hishikawa, Z.S. Katusic, and T.F. Luscher, *High glucose increases nitric oxide synthase expression and superoxide anion generation in human aortic endothelial cells*. *Circulation*, 1997. **96**(1): p. 25-8.
202. Green, D.J., G. O'Driscoll, B.A. Blanksby, and R.R. Taylor, *Control of skeletal muscle blood flow during dynamic exercise: contribution of endothelium-derived nitric oxide*. *Sports Med*, 1996. **21**(2): p. 119-46.
203. Truskey, G.A., *Endothelial Cell Vascular Smooth Muscle Cell Co-Culture Assay For High Throughput Screening Assays For Discovery of Anti-Angiogenesis Agents and Other Therapeutic Molecules*. *Int J High Throughput Screen*, 2010. **2010**(1): p. 171-181.
204. Ekert, J.E., K. Johnson, B. Strake, J. Pardinas, S. Jarantow, R. Perkinson, and D.C. Colter, *Three-dimensional lung tumor microenvironment modulates therapeutic compound responsiveness in vitro - implication for drug development*. *PLoS One*, 2014. **9**(3): p. e92248.
205. Yang, J., Y. Han, C. Chen, H. Sun, D. He, J. Guo, B. Jiang, L. Zhou, and C. Zeng, *EGCG attenuates high glucose-induced endothelial cell inflammation by suppression of PKC and NF-kappaB signaling in human umbilical vein endothelial cells*. *Life Sci*, 2013. **92**(10): p. 589-97.
206. van Rooij, E., J. Fielitz, L.B. Sutherland, V.L. Thijssen, H.J. Crijns, M.J. Dimairo, J. Shelton, L.J. De Windt, J.A. Hill, and E.N. Olson, *Myocyte enhancer factor 2 and class II histone deacetylases control a gender-specific pathway of cardioprotection mediated by the estrogen receptor*. *Circ Res*, 2010. **106**(1): p. 155-65.
207. Nobe, K., M. Miyatake, T. Sone, and K. Honda, *High-glucose-altered endothelial cell function involves both disruption of cell-to-cell connection and enhancement of force development*. *J Pharmacol Exp Ther*, 2006. **318**(2): p. 530-9.

208. Lee, P.H. and H.H. Vandeburgh, *Skeletal muscle atrophy in bioengineered skeletal muscle: a new model system*. *Tissue Eng Part A*, 2013. **19**(19-20): p. 2147-55.
209. McCarthy, J.J., *The MyomiR network in skeletal muscle plasticity*. *Exerc Sport Sci Rev*, 2011. **39**(3): p. 150-4.
210. Naguibneva, I., M. Ameyar-Zazoua, A. Polesskaya, S. Ait-Si-Ali, R. Groisman, M. Souidi, S. Cuvellier, and A. Harel-Bellan, *The microRNA miR-181 targets the homeobox protein Hox-A11 during mammalian myoblast differentiation*. *Nat Cell Biol*, 2006. **8**(3): p. 278-84.
211. Sun, Q., Y. Zhang, G. Yang, X. Chen, G. Cao, J. Wang, Y. Sun, P. Zhang, M. Fan, N. Shao, and X. Yang, *Transforming growth factor-beta-regulated miR-24 promotes skeletal muscle differentiation*. *Nucleic Acids Res*, 2008. **36**(8): p. 2690-9.
212. Rutkowski, J.M., N. Halberg, Q.A. Wang, W.L. Holland, J.Y. Xia, and P.E. Scherer, *Differential transendothelial transport of adiponectin complexes*. *Cardiovasc Diabetol*, 2014. **13**(1): p. 47.

BIOGRAPHY

CINDY SUE CHENG

Date of Birth: February 9th, 1986

Place of Birth: Downers Grove, Illinois

Academic Degrees

Duke University, Durham, North Carolina

- Ph.D. in Biomedical Engineering, May 2014
- M.S. in Biomedical Engineering, May 2011
- B.S.E. in Biomedical Engineering, May 2008

Publications

- Cheng C.S., Ran L., Kraus W.E., and Truskey G.A. "Joint microRNA-133a and microRNA-696 inhibition accelerates differentiation of human skeletal muscle and enhances peak specific force in vitro." Manuscript in preparation.
- Cheng C.S., Davis B.N.J., Madden L.R., Bursac N., and Truskey G.A., "Physiology of three-dimensional skeletal muscle tissue." Accepted.
- Cheng C.S., El-Abd Y., Bui K., Hyun Y.-E., Hughes R. H., Kraus W.E., and Truskey G.A. "Conditions that promote primary human skeletal myoblast culture and muscle differentiation in vitro." *Am J Physiol Cell Physiol* 206: C385-C395, 2014.
- Truskey G.A., Achneck H.E., Bursac N., Chan H.F., Cheng C.S., et al. "Design considerations for an integrated microphysiological muscle tissue for drug and tissue toxicity testing." *Stem cell research & therapy*. 2013.
- Rhim C., Cheng C.S., Kraus W.E., and Truskey G.A., "Effects of microRNA modulation on bioartificial muscle function." *Tissue Engineering Part A*. 2010.
- Brown M.A., Cheng C.S., and Truskey G.A., "Endothelial progenitor cells for vascular repair." *Stem Cell Engineering*. P. Kayser, ed. 293-316.

Awards

- Outstanding Teaching Assistant Award, Department of Biomedical Engineering, Duke University (2010)
- Center for Biomolecular and Tissue Engineering (CBTE) Fellow, Duke University (2008-2010)
- National Institutes of Health Predoctoral Training Grant (2008-2010)
- National Science Foundation Graduate Research Fellowship Program Honorable Mention (2009)